CASCADED PROXY-BASED SLIDING MODE CONTROL ENHANCED WITH DISTURBANCE OBSERVER FOR THE STABILIZATION AND CONTROL OF A GUN-TURRET PLATFORM

A THESIS SUBMITTED TO
THE GRADUATE SCHOOL OF NATURAL AND APPLIED SCIENCES
OF
MIDDLE EAST TECHNICAL UNIVERSITY

BY

ERCAN ÇANDIR

IN PARTIAL FULFILLMENT OF THE REQUIREMENTS
FOR
THE DEGREE OF MASTER OF SCIENCE
IN
ELECTRICAL AND ELECTRONICS ENGINEERING

JULY 2014

Approval of the thesis:

CASCADED PROXY-BASED SLIDING MODE CONTROL ENHANCED WITH DISTURBANCE OBSERVER FOR THE STABILIZATION AND CONTROL OF A GUN-TURRET PLATFORM

submitted by **ERCAN ÇANDIR** in partial fulfillment of the requirements for the degree of **Master of Science in Electrical and Electronics Engineering Department, Middle East Technical University** by,

Prof. Dr. Canan ÖZGEN
Dean, Graduate School of **Natural and Applied Sciences** _______________

Prof. Dr. Gönül Turhan SAYAN
Head of Department, **Electrical and Electronics Engineering** _______________

Prof. Dr. Aydan ERKMEN
Supervisor, **Electrical and Electronics Eng. Dept., METU** _______________

Examining Committee Members:

Prof. Dr. Kemal LEBLEBİCİOĞLU
Electrical and Electronics Engineering Department, METU _______________

Prof. Dr. Aydan ERKMEN
Electrical and Electronics Engineering Department, METU _______________

Assoc. Prof. Dr. Afşar SARANLI
Electrical and Electronics Engineering Department, METU _______________

Assoc. Prof. Dr. Umut ORGUNER
Electrical and Electronics Engineering Department, METU _______________

Mustafa Burak GÜRCAN, M.Sc.
Defense Systems Technologies Division, ASELSAN _______________

Date: _______________

I hereby declare that all information in this document has been obtained and presented in accordance with academic rules and ethical conduct. I also declare that, as required by these rules and conduct, I have fully cited and referenced all material and results that are not original to this work.

Name, Last Name: ERCAN ÇANDIR

Signature :

ABSTRACT

CASCADED PROXY-BASED SLIDING MODE CONTROL ENHANCED WITH DISTURBANCE OBSERVER FOR THE STABILIZATION AND CONTROL OF A GUN-TURRET PLATFORM

ÇANDIR, Ercan
M.S., Department of Electrical and Electronics Engineering
Supervisor : Prof. Dr. Aydan ERKMEN

July 2014, 168 pages

Stabilization and tracking is two of the most important properties of today's modern gun turret platforms mounted on the mobile land vehicles. Servo control of such gun-turret platforms is a very challenging issue due to the non-linearities of the system, the external disturbances resulting from the motion of the vehicle and varying operation conditions. In this thesis, a cascaded proxy-based controller with additional disturbance observer is developed as a solution to this control problem and to obtain high stabilization and tracking performance. A novel cascaded-proxy based sliding mode control architecture is used as the main controller. A reduced-order disturbance observer is also integrated to the controller to compensate the non-linearities in the system and to improve the disturbance rejection capability. Performance of this disturbance observer is enhanced by reducing noise in the feedback signal with an additional Kalman filter which fuses the measurements obtained from different sensor.

The proposed controller is tested with both simulations and experiments conducted

on the real gun-turret platform. Sensitivity and performance analysis are performed by using the mathematical model constructed for simulating the behaviours of the actual system and the hardware experimental setup.

Keywords: stabilization, tracking, proxy-based sliding mode control, disturbance observer, Kalman filter, gun-turret platform

ÖZ

SİLAH KULESİ DENETİMİ VE STABİLİZASYONU İÇİN BOZUCU ETKİ GÖZLEMCİSİ İLE GELİŞTİRİLMİŞ KADEMELİ VEKİL-TABANLI KAYAN KİPLİ DENETLEÇ

ÇANDIR, Ercan
Yüksek Lisans, Elektrik ve Elektronik Mühendisliği Bölümü
Tez Yöneticisi : Prof. Dr. Aydan ERKMEN

Temmuz 2014 , 168 sayfa

Hareketli kara araçlarında bulunan günümüz silah kulesi alt sistemlerinin en önemli iki özelliği istek takibi ve stabilizasyondur. Sistemdeki doğrusal olmayan etkiler, aracın hareketinden kaynaklı harici bozucu etkiler ve değişken çalışma koşulları nedeniyle bu silah kulesi alt sistemlerinin servo denetimi oldukça zorlu bir problemdir. Tez kapsamında, bu problemin çözümü ile yüksek stabilizasyon ve takip performansı elde etmek için bir bozucu etki gözlemleyicili kademeli vekil-tabanlı kayan kipli denetim yapısı geliştirilmiştir. Ana denetleç olarak bu tez ile literatüre katılan kademeli vekil-tabanlı kayan kipli denetim metodu kullanılmıştır. Ayrıca, sistemdeki doğrusal olmayan etkileri azaltmak ve sistemin bozucu etkilere karşı direnme yeteneğini artırmak amacı ile indirgenmiş dereceli bir bozucu etki gözlemcisi önerilen kontrolcü yapısına eklenmiştir. Sensör verilerini birleştirerek geri besleme sinyalindeki gürültü seviyesini azaltan ek bir Kalman filtre ile bu bozucu etki gözlemcisinin performansı iyileştirilmiştir.

Önerilen denetim yapısı, hem simülasyonlar ile hem de gerçek silah kulesi üzerinde yapılan deneyler ile test edilmiştir. Performans ve hassasiyet analizleri, gerçek sistemin davranışlarını simüle etmesi amacı ile oluşturulan metematiksel model ve deneyler için hazırlanan test düzeneği kullanılarak gerçekleştirilmiştir.

Anahtar Kelimeler: stabilizasyon, istek takibi, vekil tabanlı kayan kipli kontrol, bozucu etki gözlemcisi, Kalman filtre, silah kulesi

To my family and my love . . .

ACKNOWLEDGMENTS

I express my sincere appreciation to my thesis supervisor Prof.Dr.Aydan ERKMEN for her guidance, support and helpful critics throughout my thesis work. I am grateful for having the chance to work under her valuable supervision.

I would like to thank to Mustafa Burak GÜRCAN, Murat GÜLTEKİN, Evrim Onur ARI, Taha ÖZTÜRK and Uğur Doğan GÜL for sharing their experience and supporting me through the tough times. I would like to express my gratitude to Bülent BİLGİN and all my other administrators for granting me this valuable opportunity; to ASELSAN A.Ş for providing all the hardware and software requirements through out my thesis work.

I am grateful to my young, innovative and talented colleagues in Unmanned Systems Department in ASELSAN for their help and sincere friendship.

I acknowledge TUBİTAK for financially supporting me during my study.

I always feel lucky to have my parents, Hülya and Bülent, and my sister, Ece, with me. Like in all challenges in my life, I am thankful to them as they never leave me alone throughout the thesis work and they do their utmost to improve my power.

Finally, special thanks goes to my love, Fulden, for her endless support and for believing in my success more than I did.

TABLE OF CONTENTS

LIST OF TABLES

TABLES

LIST OF FIGURES

FIGURES

CHAPTER 1

INTRODUCTION

1.1 Motivation

Most of today's modern weapon systems have structures equipped with servo sub-systems for adjusting the aiming of their armaments towards a target. In general, such structures in weapon systems are also called platforms and provide a relative motion capability with respect to the base of the weapon system, for the components mounted on it. Various type of armaments can be mounted on these platforms which also denotes their types. Some common platform structures can be named as missile launcher platforms, electro-optic platforms and gun-turret platforms. With the developments in the servo system technologies and the integration of hydraulic and electric drives, these moving platforms become more important and commonly preferred in the battlefield with the evolution in their capabilities.

Gun-turret platforms are mounted on lots of different stationary and mobile weapon systems including armoured land vehicles. As it is in all other weapons systems, the main aim of the gun-turret platforms mounted on land vehicles is to provide the required movements for the gun mounted on it for maximizing its hitting probability. Required position or speed signals are determined directly by the user or by a fire control system which fuse different sensor measurements to calculate the optimal motion patterns. Servo sub-systems provide required torques to move the gun-turret platform according to these input signals and this forms critical controlled motion of tracking. Hitting probability is directly related to tracking the position or speed signals provided by an upper-level controller. Therefore, tracking performance is one of the most important criteria in evaluating the success of the servo sub-system of a gun-turret platform mounted on an armoured land vehicle or on any other stationary or mobile weapon system.

With the integration of the gun-turret platforms on armoured land vehicles, these platforms become mobile and new challenges with new performance measures come into the picture from control point of view. At the beginning, land vehicles especially with higher calibre guns needed to be halted and immobilized before aiming at targets and execute successful shots. However, such a need tampers their mobility and make them an easy target for their opponents on the battlefield. Such drawbacks of stopping for making shots increase the need for "fire on the move" capability which is the ability of making successful shots while the weapon system is moving on different terrains. Fire on the move becomes one of the most important capabilities of today's modern armoured land vehicles putting pressing needs on stabilization which can be simply defined as holding the orientation of the gun-turret platform stationary relative to earth despite all the random disturbances acting on the platform due to the motion of the vehicle and topography of the operation environment. So, for the gun-turret platforms mounted on moving land vehicles, stabilization performance is as crucial as tracking in order to increase the hitting probability of the gun mounted on the gun-turret platform.

In order to provide the required tracking and stabilization performance, proportion-derivative-integral(PID) type of controllers and their derivatives are used in most of gun-turret platforms. First of all, PID is a mature subject with lots of successful applications in its history which increase its reliability. When the literature is investigated and some state of art control applications are analysed, PID always holds its popularity over all other controllers although new controllers start to compete with it. There are also number of methods like Bode, Nyquist or Root-Locus available for analysis and design of the PID type controllers, which ease its implementation and makes it a desirable choice. Moreover, PID type of controllers do not need high computation power due to their simplicity which also makes it suitable for most of the applications.

On the other hand, PID type of controller structures also have important deficiencies especially for complex control applications as it is the case for the system investigated in this thesis work. There are effective non-linearities such as friction and backlash in gun-turret platforms and classical PID controllers are purely linear controllers with high susceptibility against such non-linearities. So, high precision tracking and stabilization even between manoeuvres and bowing motion of the vehicle are not possible using pure classical PID controllers. Due to the characteristic of classical PID, improving both local and global dynamics of the controller is also not possible by just tuning its parameters. Increasing the parameters of the controller can improve the tracking performance in situations like target tracking, in which tracking errors always stay within a limit. However, increments in the parameters can cause overshoots when strict changes occur in the desired speed or positions and large tracking errors originate. This trade-off in the PID controllers should be solved to yield an improvement in the overall tracking performance of the controller.

To sum up, obtaining a high tracking and stabilization performance with a gun-turret platform for better hit probability is a very tough control problem. Challenges generated from the non-ideal structures of the controlled system, operation conditions and variations in these conditions are making the controller design much more problematic and complex. Therefore, the core motivation of this thesis is to design a controller architecture for a gun-turret platform which handles all these challenges and provide an effective stabilization and tracking performance.

1.2 Problem Definition, Objectives and Goals

As it is explained in the motivations section, target tracking and stabilization are two of the most popular and challenging problem and investigation area in designing the servo controller for today's modern gun-turret platform systems. In these weapon systems, the main design goal is to obtain the ability of engaging targets while moving on rough terrains and under other disturbances coming from the nature of the mechanical system. Taking the above-mentioned cases into account, the problem in such an application can be summarized as the fusion of the tracking and stabilization under some challenging disturbances.

In general, such firing structures can be separated into two main sub-systems. These can be named as fire control sub-system and servo sub-system. Briefly, fire control sub-systems can be defined as the structure responsible for providing the correct angular position and velocity patterns for successful target tracking and shots. These systems include a variety of sensors(cameras, radars, laser range finders... etc.) and a fire control computer. On the other hand, servo systems are responsible for the motion of the gun according to the signals provided by fire control system or by the user directly. Servo systems consist of four main parts, which are sensors, motion generation part, motion transmission part and gun or load. As the main concern of the thesis, the controller in the motion generation part will be investigated in a detailed manner. As the performance and structure of the controller is closely related with the specifications of the other elements like motion generation part, sensors, transmission part, load and characteristics of the motion patterns provided by fire control system or user, properties of these elements are also taken into account throughout our studies.

The objective of the servo control system design from the controller point of view can be defined as supplying the torque demands that maintain a rapid and precise tracking of the desired angular position or velocity signals coming from the fire control computer or user and provide a stabilized gun-turret platform. However, there are some important facts that make this control problem much more challenging. These challenging facts can be grouped in four main categories namely non-linearities, unmodelled dynamics, parameter variations and external disturbances. There can be lots of other phenomenons affecting the system but these are the most effective ones on the controller performance so they are taken into account during the controller design, simulations and experiments of this thesis work.

The main non-linearities in the system are backlash, friction and servo limitations. Backlash in the system can be basically defined as the non-linearity in the transmission of the torque generated by the motor to the system through gearbox. During manoeuvres, where the direction of motion changes, none of the torque generated by the motor can be transmitted to the system due to the clearance between the mating gears until the contact between the gears is resumed. In the systems where motor is not directly driving the load, backlash is unavoidable due to the clearances in the transmission structure [1]. Friction is another source of non-linearity which affects the performance of the controller. As long as the moving parts in a mechanical system are in contact, friction is also unavoidable. Due to non-linear characteristics of friction, control problems like static errors, limit cycles and stick-slips can appear in the system [2]. These problems should be solved or reduced by some compensation precautions for a better controller performance. Another physical phenomena in addition to friction and backlash are servo limitations which also cause important non-linearities in the systems. These limitations are designated by the components chosen throughout servo system design. Most effective limitation can be named as the maximum torque that can be provided to the load by the motion generation and transmission parts.

In addition to non-linearities; unmodelled dynamics, parameter changes and external disturbances are also making the servo control problem in the gun-turret platforms much more complicated. Unmodelled dynamics are mainly coming from the mechanical design of the load such as gun barrel flexible modes which are directly affecting the performance of the controller. Some properties of the system may change in time or during operation. Therefore the controller should be also robust enough not to be corrupted by such parameter variations. Most effective parameter variations can be named as torsional stiffness and friction changes due to the variations in environmental conditions and life cycle of the components used in the servo system. There are also external disturbances like base motion and firing effects coming from the operation scenarios of the systems. These disturbances should also be analysed and the controller should withstand them to preserve its performance despite such external effects.

In the enlightenment of the given explanations about the challenges in the problem; a robust, stable and effective controller design for servo control of the gun-turret platform is required. Main design goals are enhancing the tracking performance of the servo system and providing a better stabilization accuracy despite all these challenges. From control point of view and by using the control jargon; high performance tracking can be defined as providing an output with minimum settling time, overshoot and steady state error while providing the maximum response bandwidth. In order to increase the response bandwidth and to reduce the settling time the controller must have stiff local dynamics as much as possible. On the other hand, its global dynamics should be over-damped for avoiding possible overshoots due to strict changes in the desired position or speed signals. Therefore, local and global dynamics of the controller need to be tuned separately. In order to obtain high stabilization accuracy, controller must also have exceptional disturbance rejection performance with maximum possible disturbance suppression and rejection bandwidth. So, additional precautions need to be taken for the compensation of non-linearities and suppression of the external disturbances. In addition to these performance goals, the proposed controller will be implemented on a digital signal processor in real-time so memory and computation power requirements should also be minimized as much as possible.

1.3 Methodology

In the enlightenment of the problem definition, challenges and goals given in Section 1.2, a detailed literature survey is conducted to analyse the problem better, to increase the knowledge about the challenges and to evaluate the possible control methods available in the literature. As an outcome of this detailed literature survey, a novel cascaded proxy-based sliding mode controller is designed for the servo control of the gun-turret platform and the control architecture is completed with an additional disturbance observer enhancement in order to satisfy the goals of the gun-turret platform in the thesis work.

Different from the proposed architecture, methods are offered and studied as the solution of similar problems in the literature. However, none of these alternative methods are fully compatible with our problem and goals. Alternative methods are either insufficient in meeting the performance goals, coping with various challenges in the problem and satisfying the reliability requirements or they are too complex to be implemented on a real time DSP available on the system due to high memory and computational power requirements. More detailed information about the alternative methods investigated throughout the literature survey, their advantages and disadvantages can be found in Chapter 2.

When advantages of the PID given in Section 1.1 is reviewed especially from reliability and compatibility to real time applications point of view, we thought that using a proved PID control architecture as the core structure and exploiting its advantages would be beneficial. On the other hand, some important modifications are needed to be brought into the structure of the PID control to solve the problematic correlation between its local an global dynamics. Also some additional structures are required in order to cope with the deficiencies of the classical PID control such as susceptibility to non-linearities and to enhance its disturbance rejection performance. As a result, a cascaded-proxy based sliding mode control architecture is constructed as the main controller and it is enhanced with an additional disturbance observer structure to finalize the proposed design.

Proxy-based sliding mode control is a modified version of sliding mode control with the ability of working with discrete-time controllers which can also be thought as an extension of force-limited PID control. Both sliding mode control and PID control are not perfect controllers for the systems with changing dynamics. Under ideal conditions, sliding mode control can be thought as an accurate controller for tracking (small errors) and as an over-damped (safe) controller for large error situations such as in instant input signal changes. But the problem with sliding mode controller is about the defined ideal conditions. Sliding mode control is based on the assumption that there are no time delays in the feedback loop; however, it is not possible in our real world. As we are using discrete-time controllers, delays occur during the switching between the sliding surfaces. These unavoidable switching delays cause high frequency oscillations, which is the most important problem in sliding mode control, namely chattering. This phenomenon decreases the performance of the controller and also makes the controller disadvantageous or even not applicable due to the negative effects of such oscillations on the systems. When PID controllers are taken into account, it is not possible to obtain both accurate tracking and over-damped response for large errors all together by only adjusting the parameters of the controller. In order to obtain reasonable speeds and avoid overshoots, the response of the system to big errors should be over-damped and moderate. In order to obtain such responses, the gains of the controller should be limited or its velocity feedback gain should be increased. But such an adjustment in parameters will result in increased reaction time and decreased accuracy in tracking, which is a highly undesired condition. So due to problems explained above for each single control approach; proxy-based sliding mode control(PBSMC) idea, a combination of the PID and sliding mode control is used to exploit the advantages of both strategies while eliminating their drawbacks [3–5].

Setting out from the PBSMC idea, we offer a new cascaded proxy-based sliding mode controller concept as the core control structure for the solution of the problem. In our new concept, there are two PBSMCs connected to each other in a cascaded manner such that one PBSMC is used for tracking desired position signals and acts as a position controller (outer loop), while other proxy is used as a speed controller (inner loop) for stabilizing the platform and tracking the desired speed signals created by the outer loop or directly by another upper-level controller. Proxies in PBSMCs are following the desired speed or position signals with a sliding mode controller. The position and the speed of these proxies are compared with the actual speed and position of the system coming from the sensors mounted on the system. The differences between the proxies and measurements are fed to stiff PID controllers to make the system follow the proxies.

In addition to the core cascaded proxy based controller structure, a reduced-order disturbance observer with an additional Kalman filter enhancement is integrated to the proposed controller architecture to improve the tracking and stabilization performance of the core controller. The main objective of the disturbance observer is to reduce the effect of non-linearities coming from the nature of the servo system, especially friction and to increase disturbance rejection capability of the controller. A Luenberger observer with a basic single mass system model is used as a disturbance observer. It takes the torque applied to the system as input and compares the angular velocity calculated by using the system model with the angular velocity measurements taken from the gyroscope mounted on the gun-turret platform. The observer is designed to have closed loop characteristics and tries to drive the difference between measured speed and calculated speed towards zero. Such an observer is chosen as for the compensation of internal non-linearities and external disturbances due to its effectiveness and insensitivity to parameter changes [6]. This disturbance observer is also enhanced with an additional Kalman filter used for reducing the noise on the gyroscopes measurements used by the observer. Such a Kalman filter is added to the disturbance observer in order to reduce the amount of gyroscope noise coupled to the torque applied to the system through the observer. This Kalman filter structure is providing the angular velocity of the gun-turret with reduced noise by fusing the measurements taken from the feedback gyroscope, feed-forward gyroscope and encoder available on the system. The feed-back gyroscope is measuring the velocity of the gun-turret platform in the inertial frame, the feed-forward gyroscope is measuring the angular velocity of the armoured vehicle's base (base motion) in the inertial frame and the encoder is measuring the relative position of the gun-turret with respect to the vehicle base.

1.4 Contributions

Several control methods are offered in the literature for the stabilization of a moving platform and for tracking applications. Most of the solutions offered in the literature are using traditional control methods. However, due to their deficiencies in coping with non-linearities and insufficiencies in disturbance rejection, pure classical control methods are not preferred for the control of the system concern of the thesis. There are also few solutions based on advanced control techniques like neural networks and fuzzy logic available in the literature and used for the stabilization and tracking applications. We disregarded such approaches due to their lack of analytical methods for analysing their stability and robustness, difficulties in their design and tuning, high computational power and memory requirements in their implementation. Investigations about some other control methods and their lack of compatibility analysis for the problem in our thesis work are mentioned in literature survey chapter.

Different from the solutions offered in the literature, a novel controller architecture needed to be generated and is designed for the stabilization and tracking problem in the thesis work. As it is explained in Section 1.3, the proposed controller architecture is the composition of a cascaded PBSMC controller with an additional disturbance observer enhanced with a Kalman filter. Proxy-based sliding mode control(PBSMC) is a recently introduced control technique and has only two up-to-date leading applications in the literature. In one application PBSMC is used for the position control of a robotic arm [3–5] and in the other application it is used for stabilization of a two-axis gimbal [7]. So, gun-turret platforms are a new application area for PBSMC with their size, their dynamics, different challenges and performance requirements. In addition to implementation in a new application area, cascaded use of the PBSMC is also a completely novel idea in the literature. PBSMC applications in the literature are focused on use of a single PBSMC; however, two PBSMCs are used together and assembled in a cascaded manner in our proposed controller architecture. This new cascaded PBSMC architecture is verified with simulations and experiments throughout the balance of this thesis. The performance of our new approach is also compared with the force-limited PID with anti-wind up enhancement already being in use on a prototype gun turret platform.

There are different model based and non-model based methods offered and used in the literature for the compensation of the non-linearities in the systems. A non-model based reduced order Luenberger disturbance observer is implemented in our proposed architecture for the compensation of the non-linearities resulting from the characteristics of the system and to improve the disturbance rejection performance simultaneously. Some applications with reduced order disturbance observer can be found in the literature [7]; however, it is not used with a PBSMC in any of these studies and so neither with a cascaded PBSMC since it is a novel concept. So, PBSMC and disturbance observer combination implemented in the proposed controller is also a new controller and enhancement pair in the literature.

Kalman filters are commonly used in the literature for the sensor fusion applications and for reducing the noise in the sensor measurements. Kalman filter added to the disturbance observer is also used for reducing the noise in the angular velocity measurements fed to the observer by fusing two gyroscope and one encoder outputs. In the literature, Kalman filters are generally used for fusing the sensor measurements obtained at same reference frame such as measurements only in inertial frame or only in reference frame. However, the Kalman filter in the proposed architecture is fusing encoder measurements obtained in the reference frame and gyroscope measurements obtained in the inertial frame and provide an angular velocity data in inertial frame. Using Kalman filters for enhancing the disturbance observer performance is also not a common practice in the literature.

1.5 Outline Of The Thesis

In this first chapter of the thesis, the motivations for the studies in the thesis are given and problem investigated throughout the thesis is explained with the objectives and goals. Methodology and contributions to the literature are also included in this chapter.

In the second chapter, a detailed literature survey conducted before deciding on the proposed controller architecture is presented. The literature survey in second chapter includes information about general gun-turret platforms, servo systems used for stabilization and tracking applications of gun-turret platforms, challenges in stabilization and tracking from the controller point of view, servo control techniques used for stabilization and tracking, enhancement methods for non-linearities in the system and enhancement techniques for reducing noise in the gyroscope measurements.

In the third chapter, the hardware system which is a gun-turret platform prototype providing the engineering motivation of our thesis work is described. Detailed information is given about its main components, namely motor controller, actuator, gyroscopes, encoder and current sensor. Stewart platform, data acquisition and monitoring systems used throughout the experiments are explained in this chapter. Our proposed controller architecture is introduced in a detailed manner in the forth chapter. First the general controller architecture is explained and then each sub-component of the controller, its derivation and implementation are introduced in explicit details.

In the fifth chapter, modelling, simulation results and discussions are given. The chapter starts with a construction of a mathematical model. Then possible parameters of the proposed controller are tuned for the constructed model. And the chapter is finalized by proposing the results obtained in the different simulations conducted by using the constructed mathematical model and the proposed controller.

In the sixth chapter, experimental results obtained from the hardware are discussed. This chapter starts with off-line tuning of the possible parameters of the proposed controller according to the original gun-turret platform using simulation results obtained in the previous chapter and data collected from the real system. And the chapter is finalized by results obtained from the experiments made on the real system and comments about these results.

The thesis is finalized with concluding remarks and future works given in the seventh chapter. Detailed information about the references used throughout the thesis work can be found in the references part at the end of the thesis.

CHAPTER 2

LITERATURE SURVEY

2.1 Gun-Turret Systems

Turrets are the moving platforms made for integrating different type of guns and target detecting components to warfare systems. By using these structures, crews have the opportunity of firing while protecting themselves behind armours. Moreover, with rotational motion around different axes, turret structures provide a movement capability for the instruments mounted on them. Throughout the history, turrets are mounted on lots of different systems with different dynamics. Some of the most common systems can be listed as fortified units, military air crafts, naval ships and combat vehicles. The instruments mounted on the turret is also changing according to the application and the requirements of the main warfare system. Turrets can be armed with rocket launchers, heavy cannons, simple machine guns, large-caliber guns and even with some target seeking components. Servo control solutions investigated as the subject of this thesis will be for turrets armed with large-caliber guns and target seeking instruments, mounted on mobile combat vehicles.

The idea of integrating turret platforms to the land combat vehicles was started with armoured cars, namely Lanchester and Rolls-Royce Armoured Cars in 1914. Photos of these two cars can be seen in Fig.2.1. These vehicles were first manufactured for World War I and had turret platforms armed with a regular water cooled machine gun [8].

During the World War I, a serious fundamental problem appears in the field. Armies were able to use their fire-power in static defence but they cannot use them offensively

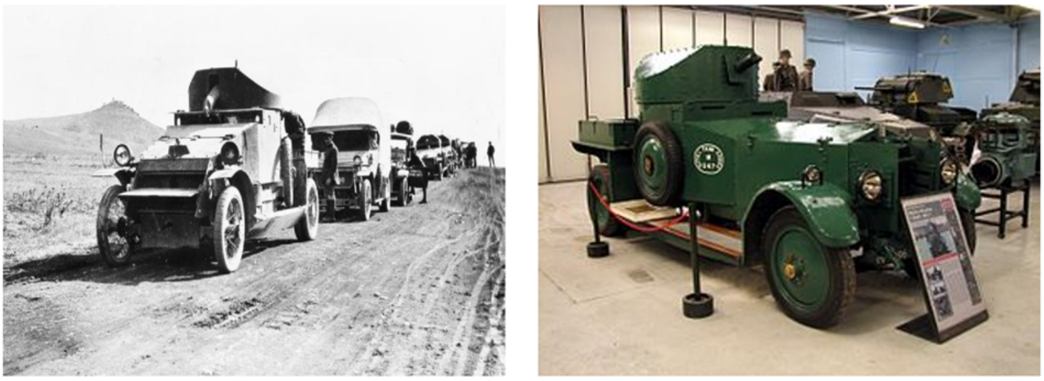

(a) (b)

Figure 2.1: (a)Lancaster Armoured Car (from [9]) (b) Rolls-Royce Armoured Car (from [10])

as their heavy weapons are not mobile. This problem made the tracked vehicles carrying heavier guns take their part in the history of the land combats. Although there were some early trials of tracked vehicles all around the world, Renault FT with its rotating turret can be taken as the pioneer of the modern tanks. It was completed in April 1917 and either a single machine gun or a short 37 mm gun can be mounted on its turret. Photo of a sample Renault FT can be seen in Fig.2.2. The capabilities and successes of Renault FT increase the popularity of the armoured land vehicles with heavy guns and also raise the interest towards the technology of turrets mounted on them [8].

Figure 2.2: A sample Renault FT with 37 mm gun (from [11])

In addition to mobility, probability of hitting target is also another very important performance criteria for the gun turret systems. In order to increase the hitting performance, better positioning and precise tracking is required. But with the increase in mobility, tracking performance decrease as the motion of the base disturbs the turret. Especially for the early turrets with higher calibre guns, making shots under the base motion disturbance is impossible as the manual targeting requires remarkable amount of time. Due to this fact, such mobile combat vehicles needed to stand still for making successful shots with high hitting ratios. However, standing still means not only increasing the hitting ratio but also becoming an open target for the opponents on the field.

Today's modern armoured land vehicles have to successfully detect and fight targets even while in motion on rugged terrain. Due to this requirement, in addition to precise tracking, stabilization becomes an indispensable property for the gun turret platforms mounted on the moving warfare. The use of electrically and hydraulically powered systems for the motion of the turret structures make the stabilization concept applicable to the land vehicles. Nowadays, stabilization is a common phenomenon, implemented in most of the turret platforms on moving systems in order to increase the performance of the instrument mounted on the turrets.

2.2 Servo Systems for Stabilization and Precise Tracking of Gun-Turret Platform

Tracking for platforms like turrets can be defined as obtaining the required speed and position values provided by an upper level controller like fire control system or directly by the operator. For the systems with gun-turret, precise tracking is essential for higher probability of hitting target. On the other hand, stabilization can be explained as holding the orientation of the platform stationary relative to a reference on the ground despite movements of the base on which platform or turret is mounted. In most of the mobile combat vehicles, for achieving stabilization and precise tracking, two-axis inertially stabilized turret platforms with high performance servo systems are used. A simple two-axis turret model with its motion axes can be seen in Fig.2.3. Servo systems used in turret platforms composed of sensors (gyroscopes, encoders, resolvers etc.), actuators (motors, transmission elements, power electronics etc.), controller and load.

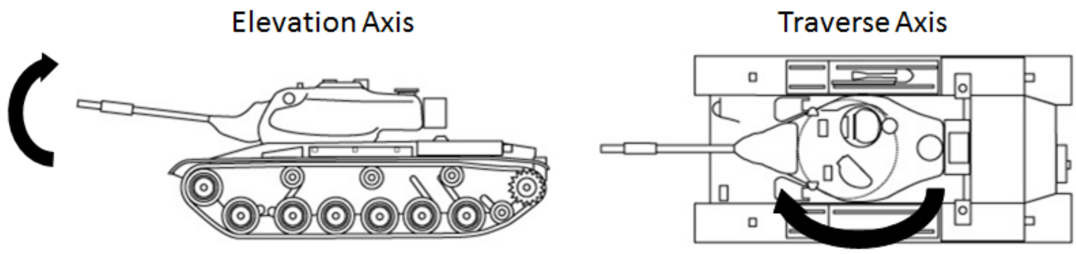

Figure 2.3: Simple two-axis turret model with its motion axes

In order to form a two-axis inertially stabilized platform, first requirement is measuring the relative movement of the platform with respect to the earth. Inertial sensors like gyroscopes are used for such measurements and according to the mounting method of these sensors stabilization techniques are separated into two main categories, namely direct and indirect stabilization. In direct stabilization, inertial sensors are mounted directly on the moving platform so sensing axes overlap with the gimbal's movement axes and changing with the movement of the gimbal. This technique offers a simpler solution with only one two-axis rate sensor which provides direct measurement of the effects due to the motion in the base and other disturbances acting on the platform's coordinate frame [12]. This direct measurement issue provides an opportunity for better performance as no manipulation is made on the sensor measurement, inertial movement of the platform in both axis is directly measured and precision is preserved. On the other hand, as the gyroscope must be mounted on the platform in this technique, the size of the platform enlarges. However, with the new technological developments in fiberoptic and MEMS technologies, gyroscopes becomes smaller and smaller which makes their effect on the size of the gimbals less. Also, for the gun-turret systems, in general, that much increment in the size is not very effective when the total size of the systems taken into account. But a much more serious and unavoidable problem about direct stabilization is kinematic coupling and gimbal lock problem. In most of the systems' moving platform, as in the systems concern of the thesis, elevation axis is mounted on the traverse axis and gyroscope is mounted on the elevation with the gun as an outcome of direct stabilization concept. Due to such configuration, movements in traverse axis can be obtained by multiplying the gyroscope measurements with cosine of the elevation axis angle. This phenomenon is called kinematic coupling. With the increase of the elevation angle, coupling becomes more effective and at ninety degrees no measurement about traverse axis motion can be obtained from gyroscope. Kinematic coupling problem can be much more serious for the systems designed for the fields like air defence which require high elevation angles. However, for the systems with limited elevation angle requirement, such a disadvantage of the direct stabilization can be tolerated compared to its advantages.

In indirect stabilization, inertial sensor is placed on the base of the moving structure which prevents the kinematic coupling problem and makes the solution of the mounting problems easier compared to the direct stabilization. But, as stabilized platform is also moving relative to the base, x-y-z orientation of the base is not same as the orientation of the stabilized platform in action. So, for an indirect stabilization application, a three-axis gyroscope and precise knowledge about the rotation of the platform relative to the base is required. With these informations or measurements and using Euler transformations, inertial rotational movements of the stabilized platform can be obtained [13]. But the performance of such an estimation is closely related with the properties of the system and its elements like gimbal geometry, structural rigidity, resolver accuracy, encoder accuracy and processing efficiency. So, when these relationships are taken into account, it can be said that beyond its advantages, fusion of the additional sensors and transformations in indirect stabilization brings much error and it becomes more complex compared to the direct stabilization from control point of view [12, 14].

Another indispensable component of the gun-turret platforms are actuators. In early gun turret platforms, actuation is provided manually through transmission elements with high transfer ratios. But manual operation has serious problems especially about the rendered rotation speed. Transfer ratios must be increased for moving the heavier armaments with limited human power; however, with the increase in the ratios, maximum rotation speed of the turrets decrease again due to the limitations of human. In order to solve such problems, hydraulic and electric drives were put into action. The main idea of the hydraulic drive is delivering fluid under pressure to a hydraulic motor connected to the gears by using a hydraulic pump. Hydraulic drive has some important advantages like being able to hold large out-of-balance loads and acting as break easily due to its nature. Nevertheless, due to the flammability of the hydraulic fluids, possibility of explosion and fire is unavoidable especially after a damage in the battlefield. Also hydraulic fluids' viscosity inevitably depends on the temperature of the fluid and so performance of the hydraulic servo system is changing during the operation [15]. Due to such disadvantages of hydraulic drive, electric drive becomes prominent in the servo control of the gun-turret platforms as in the systems concern of the thesis.

Electric drives can be separated into two basic parts, namely motion generation and transmission. Motion generation part is mainly composed of power electronics and motors. In today's modern servo systems usually permanent magnet synchronous motors (PMSMs) are used for motion generation. Power electronics are used for generating required voltages for motor commutation by using special PWM patterns. Field-orientation and vector control based techniques are usually used for the torque control of the PMSMs but they are out of the scope of the thesis. Transmission part is used for adapting the output of the motor to the speed and torque requirements of the turret and manipulating the shape of the motion. In general, PBSM motors used in the gun turret systems has high rotational speed but low torque output. However, turrets usually require less speed and higher torque output for most of the applications. In order to solve such inconsistencies, transmission elements are integrated into the systems. According to the requirements and size of the armament mounted on the turret, gun-turret platforms have various transmission mechanisms like rack-pinions, lead-screws, gear stages and ring gear-bearing couples. These transmission mechanisms introduce non-linearities and disturbances like friction and backlash to the servo system. These effects will be discussed in a detailed manner in the "Challenges In Stabilization and Tracking" part.

As it can be understood from its name, main load of the gun turret systems are guns. There are various type of guns mounted on the turret platforms with different calibres, size and weight. In addition to guns, other instruments like target seeking components and sensors are usually mounted on the gun turret. Some of the most common components can be listed as different type of cameras, Radars, Ladars and laser range finders. The performance requirements of a servo system is directly determined by the loads mounted on the turret platforms. In addition to determining requirements, loads also directly affecting the performance of a servo system with their inertia, stiffness and shocks or vibrations appear during their operation.

Servo controller can be thought as the brain of a servo system. It collects the required information from the sensors, get the desired motion patterns from upper level controllers and calculates the required torques for obtaining the best tracking and stabilization performance. Different electronic components like PICs, FPGAs and DSPs are being used for implementing the control algorithms according to their complexity and calculation power requirement. For tracking and stabilization, lots of different servo control algorithms and techniques are studied and used in the literature. These techniques and algorithms will be investigated in a detailed manner.

2.3 Challenges In Stabilization and Tracking From Controller's Point of View

As it is explained, main aim of a gun turret platform controller is providing a rapid and precise tracking with high stabilization performance by using sensors and controlling the actuation sub-system. However, achieving such a performance goal is a very challenging issue as controller must cope with lots difficulties like non-linearities, disturbances and uncertainties in addition to classical control problems. Some challenges in a gun-turret platform control can be listed as below:

- External disturbances and safety limits,
- Backlash between contacting bodies,
- Friction between the moving structures,
- Limited torque output and non-linearities in the magnetic structure of the motor,
- Uncertainties or variations in the system and sensor noise.

External disturbances and safety limits are resulted from the operational requirements of the system and needs to be handled by the controller. Two of the most common external disturbances are base motion and firing effects. Base motion compensation is the core of the stabilization idea and the consequence of the fire during the motion concept. Firing effects can be defined as shocks and vibrations with different amplitudes and characteristics that can be induced on the servo system of a gun-turret during a fire which needs to be compensated for avoiding a reduction in the performance. Therefore, a gun-turret platform controller must have an excellent disturbance rejection capability in order to satisfy performance requirements despite external disturbances. Gun-turret platforms can also have some pre-defined limits like maximum speed and acceleration for the safety of the operation. Such non-linear limitations violate the linear characteristic of the problem and also needs to be handled by the controller.

Different from external disturbances and safety limits; friction, backlash, limited torque output, non-linearities in motion generation subsystem, uncertainties or variations in the model and sensor noises are resulted from the structure of the gun-turret platform or from characteristics of its components. Noise coupled to the measurement data is a common and unavoidable phenomenon in all sensors as in the sensors of a gun-turret platform namely resolvers, encoders and gyroscopes. As the controller use sensor feedbacks while calculating the controlling signal, performance of the controller highly depends on the accuracy of the measurements and the handling of the noise. Also, there are many uncertainties about the system model as some of the parameters are hard to measure and changing during the operation like the variations in the mass moment of inertia and center of mass with the change in the elevation angle and number of stored ammunition. Hence, controller must be highly robust against the model uncertainties and sensor noise in order to satisfy the performance requirements.

Backlash and especially friction are the most effective non-linearities limiting the performance of a gun turret platform and arising from the structure of the servo system. Backlash can be defined as varying gap between adjacent movable parts and it is an unavoidable phenomenon in the systems with transmission elements between motion generation part and load, as in the system concern of the thesis. During the drive of the systems with backlash, backlash gap can become open and the contact between motor and load can be lost in some instances like when the motor rotation direction is reversed compared to the load's moving direction, or when the load is moved by an active disturbance. When the contact between motor and load get lost, torque generated by the motor only drives itself and torque cannot be transferred to the load; which means control over the load is also got lost momentarily and load is moving autonomously [1]. Due to such contact losses, precise control of a system with a load behind a backlash can be a very challenging issue. There are lots of different studies available about the various modelling approaches of the backlash [16–18]. A simple sketch of backlash with contact loss modelling can be found in Fig.2.4. In the figure, $2xb_s$ shows the backlash between teeth before meshing, R is the radius of the gears, k_s is the stiffness of the gear mesh, δ_s is the distance between two gears and f_s is the torque transferred to the second gear [19].

Figure 2.4: Contact loss modelling of backlash [19]

Like every mechanical system, gun-turret platforms also have friction. Friction appears at the physical interface of two adjacent in contact surfaces with relative motion. There are some mechanical precautions like adding lubricants such as grease or oil; but, all the mechanical solutions just reduce the friction to some extent. Friction is a highly nonlinear phenomena which can cause lots of different problems like limit cycles, steady state errors in tracking and performance reduction in stabilization due to the stick-slip motions. Especially when gun turret platform is making low frequency motions or velocity reversals most commonly while target tracking and stabilization, system exposed to stick-slip conditions frequently which reduces the performance of the servo control dramatically. There are lots of investigations and experiments in the literature for the modelling of the friction; however, it is a very complicated phenomenon arise from complex interactions between surfaces so no complete model is available [20,21]. In gun-turret platforms, lubricant exists in the contacts between the structures with relative motion so models derived for such structures are investigated within the scope of the thesis. From servo control point of view, friction models can be divided in to two main categories namely static and dynamic models.

Static friction models are single state models which only use velocity to calculate the friction force. Most common components of a static friction model from simple to complex can be listed as; coulomb friction, viscous friction, stiction friction and Stribeck friction which is a continuous version of stiction. In coulomb friction, friction force just opposes the motion with constant amplitude independent of velocity. With viscous friction, viscosity of the lubricants also taken into account and effect of velocity is also added to the model. Stiction friction is added to the static models for describing the friction force at rest which should be higher than coulomb friction. Stribeck friction is a more complex model for defining the stiction effect in a continuous manner, different from discontinuous stiction friction model [20]. According to the characteristics of the system and required precision, different combinations of the components can be used to obtain a static friction model. A static friction model with coulomb and viscous friction components will be used in the system model constructed for the simulations, as Stribeck effect is very weak and even not seen in the system compared to the dominant coulomb and viscous components. In Fig.2.5a a sample static friction model with only coulomb and viscous components can be seen. Also, for a comparison, a total static model with Stribeck effect can be seen in Fig.2.5b.

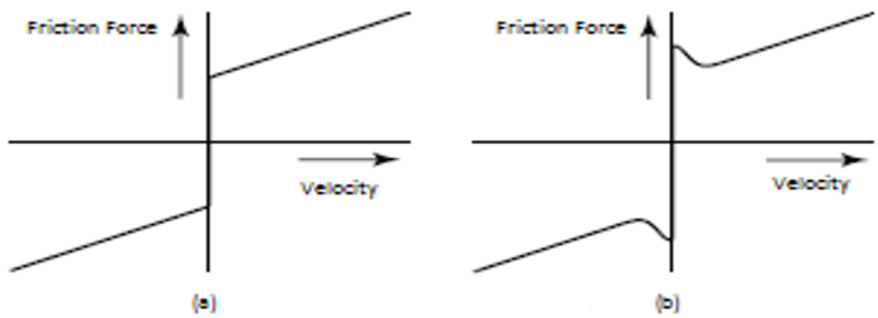

Figure 2.5: Sample static friction models. (a) Static friction model with coulomb and viscous friction (b) Complete static friction model with Stribeck effect(Adapted from [22])

Dynamic friction models, or state variable models, are more complex and complicated compared to static models. Different from static models, in dynamic models, extra state variables are added for determination of the friction torque and friction characteristics are introduced by several differential equations [22]. Due to the additional internal states and parameters, identification procedure of the dynamic models are longer and harder. There are various dynamic friction model approaches with different complexity levels, details of the most common dynamic model approaches will be investigated in Part 2.5.

2.4 Servo Control for Stabilization and Tracking

Stabilization and tracking are general and widely used concepts. In addition to gun-turret platforms, these concepts can be found in many other applications in the fields like consumer electronics, robotics and automation. For example, stabilization is implemented in digital cameras for obtaining images with higher quality and in lots of different platforms for civil applications in order to increase the performance of the instruments mounted on the platform similar to the idea in stabilized gun-turret platforms. Despite the changes in the type of the input signal, tracking is also a very common phenomenon and the tracking performance is the main goal for most of the controllers in many systems. Control of pick and place robot arms, target tracking electro-optic platforms, or automatic micro-machining tools can be given as instances for tracking applications. In order to satisfy the stabilization and tracking performance requirements of the servo systems, various control techniques and enhanced derivatives of these techniques are developed and used by control engineers. Throughout the literature survey, in addition to gun-turret platforms, stabilization and tracking applications from different fields are investigated and analysed in order to get an intuition and improve the knowledge about developed approaches.

Model Predictive Control (MPC) is a common control technique used especially for the large multi-variable constrained control problems. The main idea in MPC is using a well-defined plant model for predicting the plants future states and making optimal control actions according to these predictions while respecting the pre-defined constraints of the plant. For deciding on the optimal control actions in each time step, an online optimization problem is solved by using the sensor measurements taken at that time step. In [23] authors used MPC for the control of a gun-turret platform in an armoured tank in motion. The aim of the application is providing a stabilized platform with precise pointing performance under large disturbances due the movement of vehicle along rough terrain while accounting for the constraints posed by obstacles present on the vehicle. According to the simulation results given for linear system model, MPC control can be a good alternative for weapon stabilization problem with constrain avoidance. However, stabilization and pointing performance of MPC degrades gradually for the model modified with non-linearities namely coulomb friction. In [24] MPC is applied for the control of an elastic three-mass drive system with torque constraints. The purpose of the implementation is to obtain high-performance speed control and torsional vibration suppression in the elastic three-mass drive system. Different form [23], in this application MPC laws are computed offline in a different form and implemented as a look-up table for reducing the complexity by disregarding online optimization. MPC's performance is compared with a 2-DOF PI controller and it is shown that MPC improve the performance of the drive system. When the applications and their results are investigated, MPC can be seen as a promising alternative. However, key point for the performance of MPC is obtaining a precise model of the system and for the system concern of the thesis it is not possible due to non-linearities with varying dynamics. Also, due to the high sampling rate of our system and limited available memory size, it is not possible to make online optimization or using pre-prepared look up tables either.

Linear Quadratic Gaussian control with Loop Transfer Recovery (LQG/LTR) is another very effective technique for linear multi-variable feedback systems. LQG/LTR is a derivative of LQG and the main idea is approximating optimal full-state filters integrated to plants by specific choice of free parameters. LQG/LTR have the same compensator structure as LQG, namely model based compensator, but they differ in methods used for selecting design parameters. While LQG is using least square error, LQG/LTR use loop-shaping [25–27]. In [26] author used LQG/LTR for a stabilization loop design for a two-axis gimbaled system under base disturbance and compare its performance with lead-PI controller. According to the test results, LQG/LTR satisfy the stabilization performance and provide a better relative stability compared to Lead-PI. The performance of LQG/LTR appeared to be promising for the applications with linear system characteristics; however, for the systems with higher complexity and under harsher non-linear disturbances like the one in concern with thesis, using LQG/LTR is not that feasible. First of all, LQG/LTR needs a system model with known or estimated uncertainties but it is not that easy to obtain the quadratic system model for complex systems and especially systems containing non-linearities which should be linearized for this technique. Also applying LQG/LTR technique to a control problem requires great effort, especially some parts of design like designation of reasonable performance trade-offs and stability-robustness constraints [25].

H-infinity is still another robust linear control technique like LQG/LTR that can be used for stabilization and precise tracking. The main idea of H-infinity is converting the control problem to a mathematical optimization problem and find an optimal controller that solves this optimization. By using H-infinity, a unified solution valid in both time and frequency domain can be obtained and different performance requirements can be included to the design of optimal controller [28]. In [29] author applied H-infinity techniques to a flexible satellite attitude control system and compare its robustness and performance with LQG approach. Sensibility function associated with performance and complementary sensibility functions associated with robustness and energy limit were used. From the results it can be seen that H-infinity approach has a better combined performance when three criteria evaluated together but it is more sensitive to unmodelled dynamics of the plant and the designed controller has higher order than the plant. The high order solution concept is one of the biggest problem of the H-infinity approach and makes it impossible to apply the approach in real systems with limited processing capability, like the system concern of the thesis, due to requirement of high computational power. H-infinity control concept is also a linear concept and needs a system model like LQG/LTR so the same problems explained in the previous paragraph need to be considered for H-infinity too.

Different from classical approaches, intelligent and more advanced control techniques like fuzzy logic control and artificial neural networks(ANN) are also being used for stabilization and precise tracking control for different type of systems including gun-turret platforms. Fuzzy logic control do not use an analytic model like classical control so complex, high order or nonlinear systems can be handled by fuzzy logic. In the design of a fuzzy logic controller, input-output measurements are used and the system is thought as a black box. By this way, fuzzy control system can provide a satisfactory, stable non-optimal behavior despite variations in the system parameters or uncertainties [30, 31]. In [32] fuzzy logic is used for position control and current stabilization of a robot manipulator under the influence of non-linear loads, viscous and Coulomb's friction torque. Mamdani type fuzzy logic controller with position error and armature current inputs is used for generating the motor control signals. A satisfactory tracking performance is achieved with the help of the non-linear character of the proposed fuzzy controller.

In addition to pure fuzzy logic controllers, fuzzy logic is being combined with classical controllers especially to cope with the non-linearities. For example, in [30] fuzzy logic is applied to a weapon control design for improving the transient response and steady state error performance. Instead of pure fuzzy control which is also possible, a cascaded structure with robust inner loop and fuzzy outer loop controller was used in order to simplify the fuzzy logic design. As a result, fuzzy logic control improved the tracking performance by reducing the rise time in transient period without any negative effect on stability. Despite the promising results obtained with pure and combined fuzzy logic controllers as in given examples, fuzzy logic concept have important problems about reliability and lack of systematic design methods. As fuzzy logic do not depends on an analytic model, it is not possible to make the analysis of the structural properties of a fuzzy logic control system like stability, controllability and robustness [33]. Although there are some studies about the stability and sensitivity analysis of fuzzy logic controllers as in [33], they are not commonly accepted as the analytic methods available for classical controllers. Lack of such analysis makes the fuzzy control unsuitable especially for the systems in the areas with high reliability requirements like military applications as the system concern of the thesis. Moreover, as the fuzzy logic controllers' performance highly depend on control rules and there is no well-defined systematic way to specify them, fuzzy logic control design become complicated especially for the systems with high performance requirements.

ANN is a computational model based on the structure of biological nervous systems and can be described as a group of nodes (neurons) interconnected with adaptive weighted links tuned by a learning algorithm. ANN controllers do not have an analytic model and input-output relationships are constructed by a training procedure so with a proper neural network architecture they can provide characteristics of a non-linear controller [34, 35]. In [36] artificial neural network approach is implemented for robust speed control of a servo drive with varying moment inertia and stator magnetic flux. A cascaded structure, with PI (proportional integral) approach at the inner loop as a current controller and ANN approach at the outer loop as a speed controller, was constructed for the control of the system. Experimental results showed that with the nonlinear characteristics provided by ANN, speed controller has a higher robustness against the variations of moment of inertia and torque constant. But as the author implies in [36], in design procedure of ANN controller, user need to decide on architecture or size of neural network which directly affects the generalization and duration of the training process. There is no commonly accepted systematic way for the choice of neural network structure for a particular control problem and a prior information about the complexity of the system is required also with some trial and errors for some cases. Oversize neural networks over-fit the training data which means poor generalization; on the other hand, under-size neural networks have difficulties in learning the samples [37]. Although some studies like [38] have been carried on the verification and validation of neural network based controllers; there is an important gap about the reliability validation of ANN especially for the safety critical applications as traditional methods cannot be applied. Similar to the reasons in fuzzy control, ANN control is not chosen as an alternative controller for the system concern of the thesis due to reliability concerns and problems in the design procedure. Computational power requirement of ANN should also be investigated and analysed especially for the complicated systems for which size of the ANN needs to be increased.

In addition to linear and intelligent control techniques, optimal non-linear control approaches like sliding mode is also investigated and applied in literature. Sliding mode is a very powerful optimal non-linear control technique which does not require a precise mathematical model of the plant. The design of a sliding mode controller is composed of two main stages. First, sliding surface is defined such that closed loop system motion on this surface exhibit a desired behaviour. Then, in order to guarantee the system motion stick to pre-defined sliding surface and make the system reach the surface in finite time, a control function is specified. Various successful applications of sliding mode control can be found for different control problems in theory and simulation [39–41]. For example, in [41] sliding mode control approach is applied for the control of two-axis gimbal system. According to simulation results, sliding mode provide excellent tracking performance despite the unknown disturbances and uncertainties in the system model. In real life applications, using sliding mode can be problematic due to non-ideal dynamics of actuators or sensors and discrete-time processing. Such non-idealities cause delays during the switching between the sliding surfaces and result in high frequency oscillations, namely chattering. Chattering is strongly undesirable due to its negative effects like exciting the unmodeled high frequency dynamics of the system, additional power loss and reduction in available torque [42, 43]. Introducing boundary layer around the switching surface [43], observer-based chattering suppression [42], time-varying switching gain and multi-phase sliding mode control [44] are some methods offered for the solution of the chattering problem. However, in general, such solution methods decrease the robustness and simplicity of the sliding mode control. So, instead of pure sliding mode control approach, a compound technique including sliding mode concept is used in the offered solution in the thesis.

Despite the availability of various control techniques explained till now, linear proportional - integral - derivative (PID) control is certainly the most popular and widely used control approach in today's modern world. In [45], Knospe reported that "It is estimated that over 90% of control loops employ PID control, quite often with the derivative gain set to zero (PI control)" [45]. PID control is mature concept and has a very long history with lots of successful applications in many areas. As a part of linear control theory, it has systematic design and analysis methods like Root-locus, Nyquist and Bode plots. These advantages make the PID approach such popular despite its limitations about non-linearities and uncertainties.

As it is explained for gun-turret platform concern of the thesis, motion platform control has lots of challenges like non-linearities, servo limitations and uncertainties. In order to cope with such problems over the capacity of classical PID, lots of enhancement methods studied and implemented for PID after the introduction of digital control. One of the most common enhancement method in motion platform applications is cascading multiple PID controllers [46]. In this method, inner loop is used as velocity controller with high bandwidth which handles rapidly changing desired speed signals and provide a resistance to high frequency load disturbances. Outer loop is used as a position controller, generally single proportional control, with lower bandwidth and generates velocity demands [47]. Cascaded controller idea is also implemented in proposed control structure as the solution for the problem concern of the thesis. Another widely used enhancement method is gain scheduling or adaptive PID. Gain scheduling or adaptive PID can be basically defined as changing the parameters of a PID controller during operation according to a pre-determined procedure in order to add PID approach some non-linear characteristic and adaptability. There are different scheduling procedures some of which are listed as; conventional gain-scheduling, fuzzy gain-scheduling [48] and gain scheduling with adaptive learning [49]. Conventional gain-scheduling can provide a very limited performance enhancement especially for the non-linearities resulted from the system itself. On the other hand, same problems, like design burden and lack of analysis methods, about intelligent control techniques can be stated for adaptive learning and fuzzy gain scheduling.

There are also some PID enhancement techniques that improves the performance by enlarging or compounding the PID controller with some additional structures like feed-forward loops, different type of filters, observers and non-linear compensators. The main idea of feed-forward approach is measuring disturbances and accounting for before affecting the system in order to reduce the effect of that disturbance. Feed-forward loops make the independent tuning of disturbance rejection characteristic available if the model of the system can be estimated with not big differences [50–52]. For example, in [50] author used feed-forward technique in main battle tank stabilization in order to increase the stabilization performance by using the hull rate. Results obtained in the simulations are promising and an important improvement was observed in the stabilization accuracy.

Different type of filters are being used in various control problems for manipulating the plant's or system's response characteristics and for noise or vibration suppression [53–55]. For instance, in [53] authors are concentrated on a first order noise filter in series with a PID controller and its tuning. Also in [56] a notch filter is implemented to the controller's feedback path to reduce the torsional oscillations in the motor and load velocities of a dual inertial system. Although the realization method is different, the idea of integrating notch filter to feedback path is used in the controller structure offered as the subject of thesis. In addition to feed-forward and filters, observers and non-linear compensators are used for enhancing the classical PID approach and a detailed literature survey about observers and non-linear compensators will be given in part 2.5.

There are also some controller structures constructed as a fusion of the investigated approaches. Proxy-based sliding mode control (PBSMC) is a newly offered control method, by Kikuuwe and Fujimoto in 2006, for the position control of a robot arm. PBSMC can be thought as a modified version of sliding mode control with the ability of working on discrete-time controllers and an extension of force-limited PID [3–5]. The main goal of this new approach is providing a precise tracking performance and over-damped response for large errors together, by the separation of the local and global dynamics. Small error cases occur during the tracking, namely local dynamics, are handled by PID-type virtual coupling; whereas SMC copes with big error situations due to step input signals or unexpected effects during tracking, namely global dynamics. A physical interpretation of the PBSMC can be seen in Fig.2.6 [3].

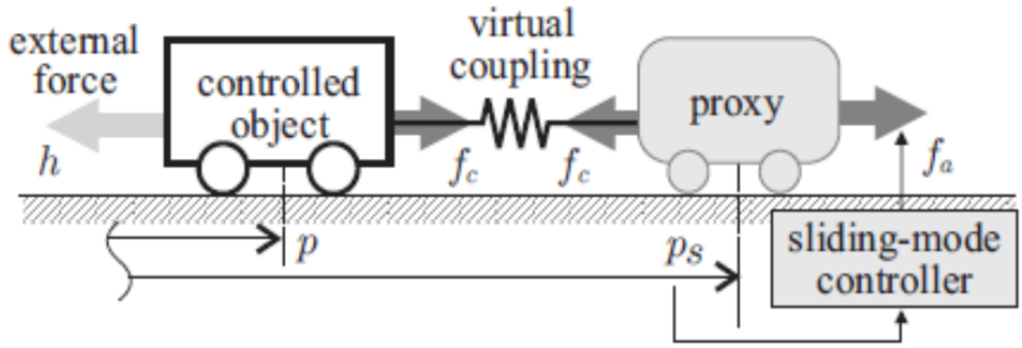

Figure 2.6: Physical representation of proxy-based sliding mode control [3]

In the idea of PBSMC, proxy is a massless particle that can be thought as a point in a virtual world representing the virtual end effector position. Real end-effector is connected to proxy thru a virtual coupling and this virtual coupling is acting as a spring which tries to make its length zero. In general, virtual coupling is taken as a stiff PID controller used to make the real end-effector track the virtual proxy. By using such virtual proxy, an ideal environment with no time delays is provided for sliding mode control which avoids possible chattering [4]. A more detailed information about the PBSMC structure and derivation of the controller will be given in Chapter 4.

In literature, as a comparably recent approach, PBSMC structure has been implemented into two separate systems with different performance goals. In [3–5] PBSMC is used for the precise position control of an industrial robot. The aim is to obtain a stiff controller which provides an accurate and safe position control; however, the recovery problem from large positional errors needs to be solved. The experiment results showed that an over-damped recovery from large positional errors without sacrificing the tracking accuracy during normal operation can be ensured by PBSMC. On the other hand, in [7], PBSMC is applied to line-of-sight stabilization problem of a two-axis gimbal system. Tracking performance and disturbance rejection capability of the method is compared with conventional PID control. According to the experiments, it was found out that the rise time and steady state accuracy of the PID controller can be greatly improved with tuning; however, PBSMC is still superior compared to tuned PID in both tracking performance and disturbance rejection capability. The problems and goals in these two applications are very similar to the application concern of the thesis, also results are promising. So the PBSMC idea is taken as the base control structure of the total solution constructed throughout the thesis.

2.5 Enhancement Methods for Non-linearities In The System

As it is explained, despite their important advantages, linear controllers can have serious problems in dealing with non-linearities. By fusing linear controllers with non-linear control approaches, as in PBSMC, some of the non-linearities like limited available torque and maximum speed limit can be compensated completely. However, methods specifically used for compensating non-linearities such as friction and backlash can provide additional improvements in the performance. In this part, compensation methods for backlash and especially for friction will be investigated, as they are two of the most dominant non-linearities disturbing the tracking and stabilization performance of a gun turret platform.

As backlash is a common problem of the mechanical systems, there are various compensation methods offered in the literature some of which includes state variable observers [57], fuzzy compensators [58], nonlinear controller with soft switching [59] and self-learning time-optimal control methods [60]. In [57] authors offered a state variable observer as an addition to the state feedback technique for the speed control of a motor drive system having torsional loads and containing gear backlash. When the experiment results analysed, it can be seen that oscillations and limit cycle due to backlash are eliminated with offered backlash compensator, but load speed has higher overshoot and longer settling time as a drawback of the compensator. In [58] fuzzy logic is used for the compensation of output backlash in tracking problem with PI based controller. An adaptive fuzzy logic is used for modelling the dynamic inversion of the output backlash and output of the fuzzy backlash inverse block is directly feed-forwarded to the system. Simulation results have improvements in the performance but challenges in the design and problems about application in real-time system makes such compensator structures not feasible for the application concern of the thesis.

Different from [57] and [58], in [59] and [60] authors are offering methods based on the switching of the controller when the backlash gap is open. In [59] two linear speed controllers, one with high performance but causing limit cycles and other with reduced performance, are designed for the speed control of an elastic system with backlash. The goal of the proposed method is reducing the effects of backlash by a soft switching from high performance controller to low performance controller when backlash gap is open and such improvements are shown on a real life drive system. But, for applying this type of control, two controllers must be tuned separately according to the related situations and that could be a very challenging issue especially for the complicated controller structures. Also detection of switching point can be trivial at the systems with more than one gear, as in the system concern of the thesis. On the other hand, in [59] no output position sensor is used for the detection of switching point different from the technique in [58]. First, amount of backlash is measured by the proposed identification methods. Then based on the pre-measured backlash, angular error of the output shaft is reduced by a self-learning time optimal control method. This method also requires a switching from PID to a deadbeat algorithm in which motor is accelerated by its rated current for a time and then decelerated by the negative rated current for a pre-defined specific time when the velocity sign changes. Applying this method to a gun-turret system can be very problematic as the amount of backlash or pre-defined times can change during the operation and the proposed method has also same switching point decision problems as in [58].

Compensation methods for friction can be classified into two main groups, namely model-based and model-free compensation. Main idea in the model-based compensation techniques is estimating the torque created by the friction directly by using a predefined friction model and feed-forwarding the calculated torque to the system. A sample block diagram for model-based friction compensation can be seen in Fig.2.7 [20].

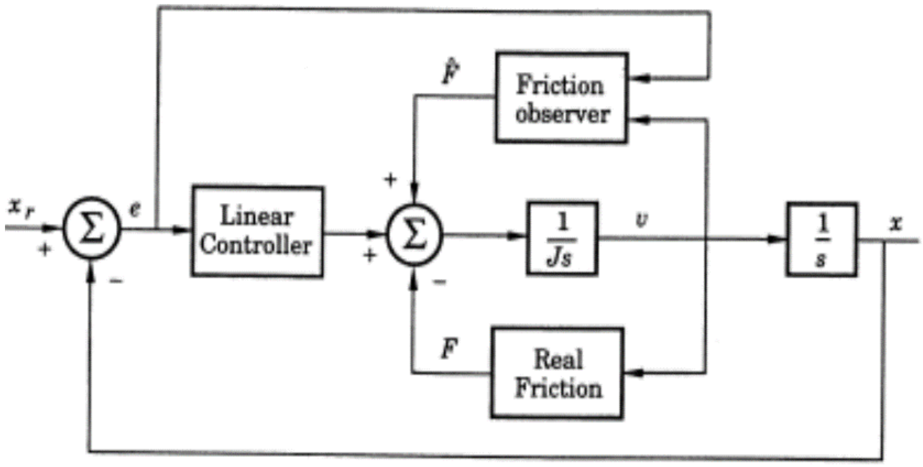

Figure 2.7: A sample block diagram for model-based friction compensation [20]

Most important component of a model-based compensator is the friction model used for estimating the actual friction acting on the system. Brief information about friction models is given in part 2.3 for describing the nonlinear behavior of the system due to friction. As it is mentioned in part 2.3, static and dynamic friction models are available in the literature but more recent studies about model-based friction compensation have focused more on dynamic friction models. The main reason for this tendency is the discontinuity of static models at zero velocity. Due to such discontinuity, infinite number of values can be assigned to the friction at that point and instabilities can arise in the algorithms. For a friction model used in compensation; complexity, number of required parameters and easiness of these parameters' identification is also very important for the feasibility of the model in a real application in addition to its success in imitating the actual friction. Most common dynamic models used in the friction compensators can be listed as; Dahl friction model, LuGre friction model, Leuven friction model and Generalized Maxwell-slip (GMS) friction model.

From simplicity point of view Dahl is the best dynamic friction model without any switching function, but it cannot represents stick-slip motion and Stribeck effect which means a poor imitating performance [61]. On the other hand, Leuven model is more complete model and it is very strong from imitation point of view; however, as it is using a hybrid hysteresis model, a model-based friction compensator implementation with Leuven is not feasible due to the number of parameters and complexity in the identification of parameters [22]. As an extension of Leuven, GMS friction model is also a complete model with great estimation capability but it also have serious problems about implementation in real-time discrete systems due to requirement of two different switching functions used to pass through friction regions in addition to excessive number of parameters with hard identification methods [62]. Although LuGre model have problems about representing the hysteresis behavior in pre-sliding, it provides a sufficient estimation with a smooth transition from pre-sliding to sliding regime and it has reasonable number of parameters compared to its performance with acceptable identification difficulty. Therefore, LuGre model is used in various model-based friction compensation applications including [63–65]. Details about the implementation of the LuGre model can be obtained from these studies.

Despite the feasibility of the LuGre friction model, model-based control is not preferred as the friction compensation method in the proposed solution due to the characteristic of the application taken as the subject of the thesis. For the success of model-based compensation methods; friction model should be accurate, actuator bandwidth should be enough and stiffness from actuator to load should be high [66]. For the system concern of the thesis, actuator bandwidth and stiffness requirements can be satisfied to some extent. However, as the system needs to work under different environmental conditions, friction characteristics of the system can change in time according to the operation conditions. Some mechanical specifications, like performance of the lubricants and surface precision, can also change in time and effects the behaviour of the friction in the system. So, although LuGre model can provide sufficient estimate of the friction for a specific configuration of the system and environment, it cannot provide required adaptation to the variations in the friction characteristics as a model-based friction compensation method.

For such systems with dynamic friction characteristics, model-free friction compensation approach can offer more effective alternatives, as they do not depend on a pre-defined friction model and can cope with the variations in the friction behaviour. Although lots of different model-free compensation techniques are available in the literature, some of the most common methods can be listed as torque feedback compensation, dither injection, learning compensators and disturbance observers or estimators.

Torque feedback compensation technique can also be stated as a measurement-based friction compensation method. In this method, a torque sensor is directly mounted on the transmission output in order to measure the net torque transmitted to the load. By using the measurements of this torque sensor as feedback signal, a close torque control loop can be constructed. Such a torque control loop with enough bandwidth can provide the required friction rejection capability without affecting the main controller [67]. Successful applications for precise position control of robot arms can be seen in [67] and [68]. The most important disadvantage of this method is the need of a torque sensor for direct measurement of the net torque applied to the load; such a substructure is not available and hard to insert in most of the servo systems as in the system concern of the thesis.

As an alternative model-free compensation, dither injection method is used for eliminating the friction in some applications [69, 70]. In this method, a high frequency signal, called "dither", with amplitude higher than the stick friction force is applied to the system. With the addition of such high frequency signal to the main control signal, system always kept in non-zero velocities which provides the avoidance of stick-slip friction. So, dither signal introduced to the system manipulates the behaviour of the friction and provides a smoother reaction rather than the discontinuous effects especially at low velocities. On the other hand, implementation of such a high frequency signal to the system means additional power consumption, possible excitation of natural frequencies and fatigue problems due to the additional vibration. Although some of these effects can be acceptable or resolvable with pneumatic or hydraulic servo systems as it is stated in [71], they are very undesirable for electro-mechanic servo systems and make the dither injection method very impractical for the system concern of the thesis.

There are also intelligent friction compensator applications with neural network structures available in the literature [72–74]. The main idea in intelligent friction compensators is obtaining the dynamic friction model by using a model-free neural network structure with on-line learning capability. There are intelligent algorithms without on-line learning concept, but they have similar deficiencies as in model-based methods. Because in such intelligent methods intelligence is only used in defining the friction characteristic without using a pre-defined model and learned characteristic is used throughout the operation which means no additional improvement is made to solve the adaptability problem [75]. With the implementation of on-line learning concept, intelligent controllers come up as a possible solution for the systems with varying friction behaviour. A sample block diagram for adaptive intelligent friction compensator can be seen in Fig.2.8 [72].However; with the real time application of on-line learning neural network concept; classical problems, like challenge in the decision of optimal radial basis function or high computation power requirement, also arise in adaptive intelligent friction compensation approach and detracts from its feasibility for complex systems, like the system concern of the thesis.

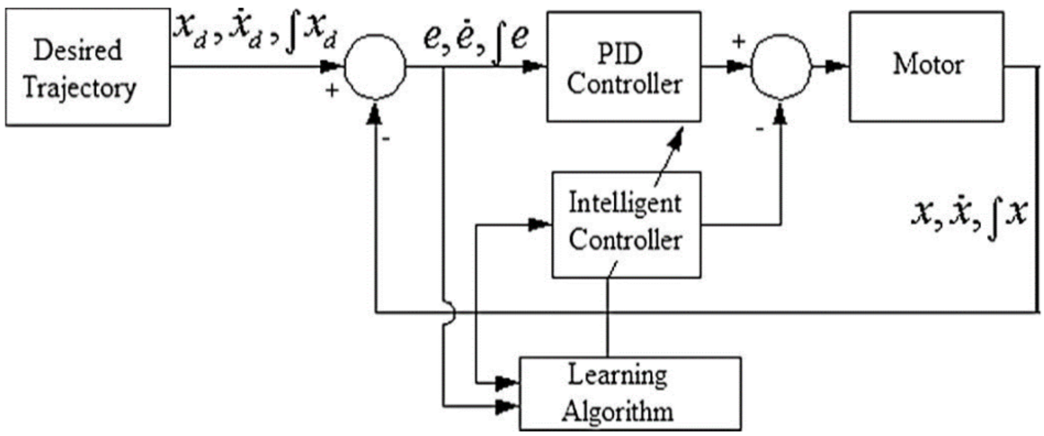

Figure 2.8: A sample block diagram for adaptive intelligent friction compensator

Disturbance observers are also another commonly used model-free friction compensation technique especially in recent studies and they are classified as a model-free method as no specific friction model is used in its architecture. Disturbance observers are used not only for friction compensation but also for the elimination of other disturbances. In this type of compensators, observer structures are implemented to estimate the disturbance torque acting on the system by using some system parameters, like inertia or viscous friction, and some sensor measurements, like position or speed of the system. Estimated disturbance torque directly introduced to the controlling signal in order to compensate the effect of friction and other disturbances. Required system parameters and sensor measurements are changing with the corresponding observer structure used for the estimation. Extended Kalman-Bucy filters (EKBF) [76, 77] and reduced-order observers [6, 78] are common examples in the literature used for the friction torque estimation needed for the compensation. A sample disturbance observer based friction compensation representation can be seen in Figure Fig.2.9 [61].

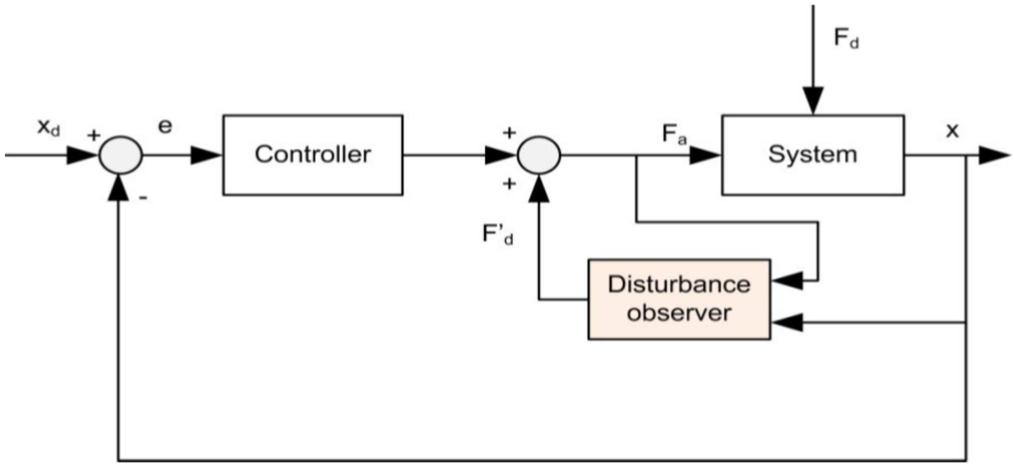

Figure 2.9: A sample disturbance observer based friction compensation representation [61]

In EKBF type of friction estimators, friction torque is taken as an unknown state and augmented state is estimated. For such filters, an accurate dynamic system model needs to be constructed by known system parameters while actual torque applied to the system and motion of the load should be measured to be used as inputs. By fusing these information and measurements, EKBF structures provide a real-time friction torque estimation required for the compensation with optimal noise filtering [76]. In [77] authors treated friction torque as a random constant and used EKBF for estimating the friction torque in a well-defined test apparatus specially made for friction tests and used a system consists of a heavy disk with known inertia and a DC-motor driving it. As a result of the experiments, it is reported that a robust compensation can be obtained by using EKBF-based techniques, but plant dynamics should be known precisely which is not that possible for the complex systems. Difficulties present in the parameter tuning and computational power requirements also reduce the practicality of the technique with increments in the order of the filter for better performance.

On the other hand, reduced order disturbance observer structures provide a simpler non-model based approach relatively insensitive to the possible imperfections in the system model [6]. Similar to EKBF approach, reduced order disturbance observers also use a system model, actual torque and system motion measurements. With all these information, such observer structures provide a closed-loop behaviour that drives the state variable estimated from the system model towards the actual measurement. In [6] a single-state reduced order disturbance observer is offered for increasing the disturbance rejection capability of an inertially stabilized line-of-sight control and its effectiveness is investigated from both performance and robustness points of view. Simulations and analysis showed that such a single state observer can be a promising enhancement method for stabilized systems with its practicality and insensitivity to model errors; despite the gyro noise coupled to the output. The given advantages of single state reduced order observer and its compliance with the requirements of the application make it a strong candidate for the friction compensation in the thesis work.

2.6 Enhancement Techniques for Gyroscope Measurements

Gyroscopes are very popular sensors that are extensively used in many applications for measuring the angular velocity of a system in inertial reference frame. Various gyroscopes with different structure and working principle can be found in the market. Some commonly used gyroscope types can be listed as; mechanical gyroscopes, fiber-optic gyroscopes (FOGs), MEMS (Micro Electronic Mechanical System) gyroscopes and ring laser gyroscopes. In the system consent of the thesis, a fiber-optic gyroscope is used due to its ruggedness and high performance specifications compared to its cost and size. Measurement techniques in fiber-optic gyroscope are based on Sagna effect phenomenon. In fiber optic type gyroscopes, there is a fiber-optic coil and two lights send from the different ends of this coil in opposite directions. With the rotation of the coil, these two lights in the coil experience different coil lengths; which results in a phase difference between the lights due to different travel times. From the phase difference between optical waves, the angular velocity of the coil is derived [79]. Like all other types, FOGs also have some measurement errors and limitations originated from the components and idea used in it.

Most important specifications defining the errors and limitations of a FOG are bias offset, bias drift, scale factor, bandwidth and angle random walk. Bias offset, which can be also named as long-term bias, is the average angular velocity measured at the output when gyroscope's actual angular velocity is zero in inertial frame. This type of bias does not change throughout the operation so bias offset can be easily detected by taking a long-term average of the measurement at each initialization of the gyroscope and can be compensated by subtracting the detected bias offset directly from the sensor measurements. Bias drift is the dynamic version of the bias offset which can be defined as bias fluctuations during the operation; detection of bias drift is not as easy as bias offset due to its varying characteristic and poses a challenge for compensation. Scale factor is also another specification of FOGs used for designating the error in the angular velocity measurement while the gyroscope is turning [80]. For the navigation applications, bias drift and scale factor non-linearity can be very important properties of the gyroscope as the integral of the measurements are used in position calculations. However, from stabilization and tracking point of view, bias drift and scale factor non-linearities in tactical grade FOGs are small enough for the sake of stabilization and not very effective on the tracking performance of the system investigated in the thesis as the outer position loop in the offered solution compensates the possible effects of these errors inherently. On the other hand, bandwidth and angular random walk (ARW) are very effective in the stabilization and tracking performance of a servo system. ARW can be defined as the noise in the rotation rate measurement provided by gyroscope and limits gyroscopes' fundamental accuracy by reducing the signal to noise ratio (SNR) [79]. Such a noise can couple to the output signal of the controller and cause flickers in the torque provided by the actuators, which is also given as the disadvantage of the reduced order disturbance observer. Therefore, noise in the gyroscope measurements needs to be reduced and noise suppression techniques used in the literature are investigated and compared for evaluating their possible integration to the solution proposed in the thesis.

Although the amplitude of the ARW vary among the different types, it is a common problem existing in all gyroscopes. Hence, various investigations on ARW compensation are available and different type of solutions are proposed in the literature. ARW compensation is a tough problem due to its white noise type of characteristic. Kalman filters and its derivatives, like extended and unscented Kalman filters, are mostly used for the suppression of the noise especially by fusing gyroscope measurements with some other sensor outputs available in the system. Wavelet type of filters are also another common structures used for the compensation of ARW and enhancing the SNR performance of the gyroscopes.

Wavelet de-noising filters are comparably recent approach in ARW compensation based on different wavelet transforms. Main idea in wavelet de-noising is manipulating wavelet coefficients by some threshold algorithm after obtaining a wavelet decomposition of the noisy measurement output and recovering the filtered measurement by using manipulated coefficients in reconstruction [81, 82]. The performance of a wavelet filter is closely related with the decomposition level. By increasing the decomposition level more precise and efficient wavelet filters can be obtained; however, increasing decomposition level also means computational burden for a real time system. Such a burden cause longer data processing time and delays in the output, which makes the use of wavelet filters impractical despite the promising results obtained in de-noising applications as in [81]. Other flexible wavelet construction methods with simple structures like second generation wavelet transform are also offered in the literature for faster and computationally less expensive noise filtering [83]. In [83] a second generation wavelet transform is used to improve performance of a MEMS gyroscope by suppressing the noise in the measurement output. The results obtained in the experiments showed that second generation wavelet transform provide an improvement in calculation speed without deterioration in the filtering performance compared to the classical wavelet transform schemes. However, despite faster response obtained by second generation wavelet transform, decomposition level capacity for real-time application is yet not enough for thresholding and reconstructing the actual rotation data with such a little information loss required for the compensation of noise in the output of the FOGs.

Kalman filter is a powerful and widely used Bayesian estimation approach for estimating states of a system with uncertain dynamics by fusing noisy sensor measurements. By incorporating statistical information about the model uncertainties and sensor measurement noise in addition to the deterministic system model, Kalman filters can provide optimal estimations for the states of a system starting from set of initial estimates [84]. Statistical information about the system uncertainties and measurement noise are injected to the KF as process noise covariance and measurement noise covariance matrix, respectively. An estimation process with KF has two stages namely prediction stage and correction stage. In each sample time, first current state and error covariance is predicted by using previous state estimate, system model and process noise covariance. In second stage, these predicted values are corrected by using recent measurements and measurement noise covariance [85]. For instance, in [86] authors use Kalman filter approach first for fusing the measurements obtained from three identical gyroscopes to construct a virtual gyroscope output with higher accuracy and secondly for improving the attitude estimation performance more by combining the derived virtual gyroscope output with additional sensors like magnetometers and accelerometers. Performance of the Kalman filter is verified by the experiments and promising results are obtained. Also a sample method for deciding the process and measurement noise covariance matrices for a real-time gyroscope output filtering example is proposed in [87].

For the optimality of KF, process and measurement noise must be Gaussian, zero-mean, uncorrelated, and white. Also classical KF can be only applied to the linear systems or systems close enough to linear; for applications with non-linear system characteristics its variants have been evaluated in the literature. Two of the most common variants of KF used for sensor fusion applications with non-linear system model can be stated as extended Kalman filter (EKF) and unscented Kalman filter (UKF). EKF is a non-linear extension of KF which depends on the linearisation of the non-linear system in each time step around the state estimated by KF. State estimations are calculated by using conventional KF rules and linearised system model [88]. EKF approach is offered as a solution for many sensor fusion problems in the literature. For instance, EKF is successfully used in [89] for accurate localization of a mobile robot by sensor fusion and in [90] for attitude estimation of an airship by again fusing different type of sensors. Despite its applicability to the non-linear systems, EKF cannot guarantee the stability and convergence due to the possible errors resulted from linear approximation of a non-linear system which should be taken into account during implementation of it especially for highly non-linear systems. There are also some other higher order extensions of Kalman Filter with a better linearisation performance like second-order Kalman filter, sum-based Kalman filter and grid-based Kalman filter. However, with the increase in the complexity, computational power requirements also step up gradually which makes such approaches infeasible for real-time applications.

In order to cope with the approximation error problem in EKF approach, other variants of KF are investigated in the literature for the non-linear systems and UKF is one of the most popular method among the alternatives as stated. UKF is a sigma point KF which directly focused on improving the approximation method in the EKF. Rather than linearised transformation of covariance and mean in EKF, unscented filters use a set of deterministic points called sigma points for transformation. In UKF, the sigma points are transformed by applying known non-linear function, true mean and covariance are taken as the mean and covariance of these transformed sigma points [88]. In UKF approximation, performance is specified by the number of sigma points used in the calculations and small number of sigma points can insufficient to represent highly non-linear distributions. However, rise in the number of sigma points also means increase in the computational power requirement which is a very important trade of in UKF. Like EKF, UKF also used in many sensor fusion application as in [91] for mobile robot localization and in [92] for alignment of IMUs while moving. Lots of comparative studies including EKF and UKF can be found in the literature [93, 94]. Most of the investigation like [93] and [94] showed that UKF outperforms conventional EKF from accuracy point of view; however, as it is stated in [93] UKF algorithms may need more computational power especially for higher number of sigma points.

CHAPTER 3

HARDWARE SYSTEM

The system used for the experiments throughout the thesis work is a gun-turret platform prototype used for continuing research and development activities in ASELSAN Inc. This prototype system is reflecting all the properties of an ordinary gun-turret platform and includes all the challenges explained in Section 2.3. The servo system of the prototype gun-turret platform is composed of a motor controller, an actuator sub-system, gyroscopes, an encoder and current sensors. A schematic representation of the gun-turret platform used in the experiments can be seen in Fig.3.1.

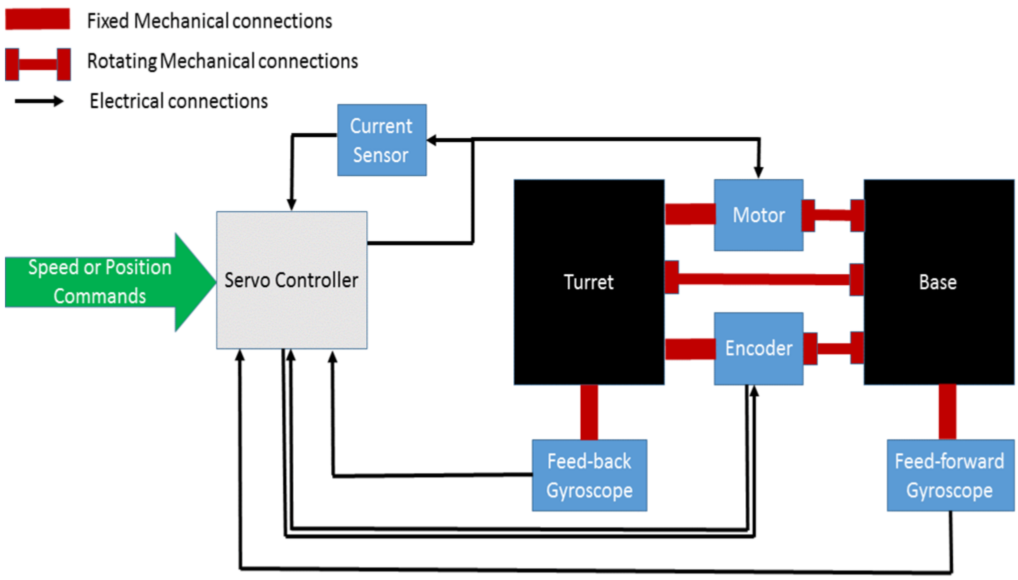

Figure 3.1: Schematic representation of the gun-turret platform and its components used in the experiments

The entire gun-turret platform is mounted on a 6-DOF motion simulator for all the stabilization performance tests. This simulator is used to create different base motion disturbances and imitate the base motions that can occur during a real operation on the field. There is also a data acquisition and monitoring system for recording the required data for analysis and performance evaluation. The entire test setup used for the experiments in the thesis can be seen in Fig.3.2.

Figure 3.2: Test setup used in the experiments

The required information about modelling the mechanics of the gun-turret platform is based upon some tests introduced in Chapter 4, so we will not deal with the mechanical properties of the system in this chapter. In the rest of this chapter, a brief explanation about the components of the servo system is given and the chapter is concluded with the properties of the additional equipments used specifically for the experiments.

3.1 Motor Controller

A Herkul-10D is chosen as the motor controller of the gun-turret platform used in the experiments. It is developed by ASELSAN for the servo control of the systems with brushless servo DC motors and high current requirements. It can drive two brushless servo DC motors simultaneously and can supply peak current up to 900 A for each motor with high efficiency. With its DSP infrastructure, it provides the required digital environment for the implementation of different controller architectures and algorithms. Throughout the experiments, all the algorithms and controller structures are implemented in this DSP module. Some simulation parameters like solver's sampling time is also determined according to the properties of this DSP module. Herkul-10D also supports different communication protocols like CANBus, RS-232/422, SSI and EnDat to communicate with the external units like different type of sensors and data acquisitions equipments. Communication abilities of the servo controller is used in the experiments to acquire required measurements from gyroscopes, encoder and current sensor mounted on the gun-turret platform. Herkul-10D also transmits the required information for analyses and performance evaluations into the data acquisition and monitoring system directly through its RS422 communication channels in real-time. In addition to its abilities for servo control applications, Herkul-10D is a very rugged servo controller so it is suitable for military applications and can work in harsh environmental conditions. An ASELSAN Herkul-10D servo controller can be seen in Fig.3.3.

Figure 3.3: ASELSAN Herkul-10D motor controller used in the hardware system

3.2 Actuator

Actuators are used to generate and transmit the required torque for the control of the system according to the motor controlling signals created by the motor driver inside the servo controller. The actuator in the hardware system is composed of a brushless servo DC motor which can be classified as a permanent magnet synchronous motor and transmission structure. Some important specifications of the brushless servo motor used in the hardware system are given in Table 3.1.

The transmission structure used in the gun-turret platform includes a gear stage, a ring gear and a ring bearing. Gear stage is directly connected to the output shaft of the motor. The torque obtained at the output of this gear stage is transmitted to the turret via a ring gear fixed to the base. The turret is also connected to the base with a ring bearing that can freely rotate about its center. The total transfer ratio from motor to turret obtained by complete transmission structure can be calculated as 388:1.

Table3.1: Specifications of the brushless servo DC motor used in the hardware system

Specification	**Unit**	**Value**
Bus Voltage	Volts	21
Continuous Stall Torque	Nm	18,54
Continuous Stall Current	Arms	236,48
Peak Stall Torque	Nm	21,7
Peak Stall Current	Arms	282
Rated Torque	Nm	13,73
Rated Current	Arms	175,2
Rated Power	W	4099
Rated Speed	rpm	2850
Torque Constant	Nm/Arms	0,078
Terminal to Terminal Resistance	Ohm	0,002
Terminal to Terminal Inductance	mH	0,018
Inertia	$kgcm^2$	16,8
Mass	kg	14,6

3.3 Gyroscopes

As explained in Section 2.2, gyroscopes are one of the most important component of the servo system in gun-turret platform since they are used to obtain angular velocity measurements in inertial frame and so their quality is directly affecting the performance of the complete system. There are two gyroscopes in the gun-turret platform, one is mounted on the turret to provide the required speed feedback and the other is mounted on the base to provide angular velocity of the base. Both of the gyroscopes are chosen as DSP3000 tactical grade high precision single-axis gyroscopes manufactured by KVH Industries. A KVH DSP3000 single-axis gyroscope can be seen in Fig.3.4.

Such tactical grade high precision fiber optic gyroscopes are used in the hardware system especially due to their low noise characteristics and their relatively high bandwidth which makes them a suitable alternative for high performance control and stabilization applications like the one in this thesis work. These gyroscopes are providing measurement data through RS232 interface so measurements are directly read and

Figure 3.4: KVH DSP3000 single-axis gyroscope used in the hardware system

processed by the motor controller in the hardware system and are directly used in the control algorithms by minimizing the possible delays during the transmission of the information. Some important properties of the DSP3000 gyroscopes used in the hardware system are summarized in Table 3.2.

Table3.2: Properties of the gyroscopes used in the hardware system

Attribute	**Rating**
Maximum Input Rate	$\pm 375 \quad deg/sec$
Scale Factor Linearity (room temp.)	$1000 \quad ppm, 1\sigma$
Scale Factor Temperature Sensitivity	$500 \quad ppm, 1\sigma$
Bias Offset (room temp.)	$\pm 20 \quad deg/hr$
Bias Stability (room temp.)	$\pm 1 \quad deg/hr, 1\sigma$
Bias Temperature Sensitivity	$\pm 6 \quad deg/hr, 1\sigma$
Angle Random Walk	$0.0667\ ^{o}/\sqrt{hr}$
Bandwidth (3 dB)	400 Hz
RS-232 Output Baud Rate	115,200 Baud rate RS232 1000 Hz asynchronous
Power Consumption	3 W

3.4 Encoder

A precise single turn absolute encoder with high resolution capability is used to measure the relative angular position of the turret with respect to base which is used as the angular position feedback and as Kalman estimator input in the control algorithm. The encoder used in the hardware system is a product of Posital Fraba Inc. designed especially for military applications and can work in harsh environment conditions. The encoder is mounted on the turret and its shaft is connected to the ring gear on the base so it directly measures the angular position of the turret independent of the transmission structure. It provides 16-bit resolution for one turn which means one step of the encoder corresponds to 0.0055 degrees angular position variation between turret and base. Like gyroscopes, the encoder is also directly connected to the servo controller and sends the angular position measurement data according to Synchronous Serial Interface(SSI) transmission protocol based on the clock provided by the controller with 1 kHz data rate. A Posital Fraba 16-bit single turn absolute encoder can be seen in Fig.3.5.

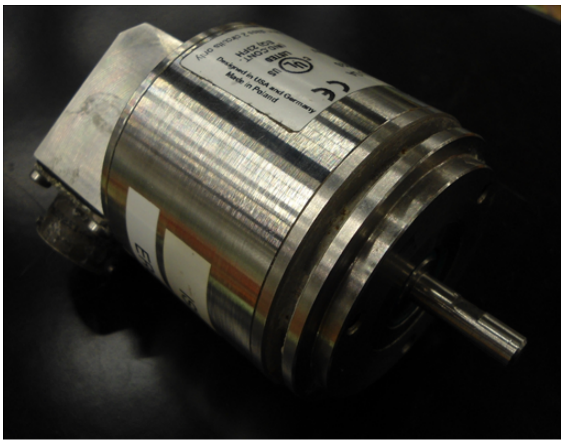

Figure 3.5: Posital Fraba 16-bit single turn absolute encoder used in the hardware system

3.5 Current Sensor

LEM's LTC 350-S current transducers are used to measure the current supplied to each coil of the brushless DC motor using Hall effect phenomenon. These transducers are providing current measurements with high accuracy, good linearity, low temperature drift and wide frequency bandwidth. The torque created by the motor is calculated from these current measurements using the torque constant of the motor. Torque control is also made according to these measurements to drive the motor efficiently but that part of the servo system is out of the scope of the thesis. Some important properties of the LTC 350-S current transducers used in the hardware system are summarized in Table 3.3.

Table3.3: Properties of current sensor used in the hardware system

Specification	**Unit**	**Rating**
Primary nominal r.m.s current	Ampere	350
Primary current measuring range @ 24V	Ampere	±1200
Overall accuracy at nominal current	%	±0.5
Linearity error	%	0.1
Maximum offset Current	Miliampere	±0.5
Maximum thermal drift of offset current	Miliampere	±0.8
Maximum Response time	Microsecond	1
Frequency bandwidth (-1 dB)	kHz	100

3.6 Data Acquisition and Monitoring System

A data acquisition hardware, a real time computer and a real time model developed in MATLAB Simulink is used for recording and monitoring the required data provided by the servo controller while manipulating the parameters used in the controller architecture implemented in the DSP of the servo controller. All of these two sided communication is made through RS422 serial interface with 1 kHz data rate and 921600 bit/seconds baud rate.

Data acquisition hardware is an electronic card designed and manufactured by ASELSAN to be used on real time computers for establishing different communication interfaces. It has a field programmable gate array(FPGA) chip on board to handle different communcation interfaces and is used to establish the communication between the real time computer and the servo controller through RS422 serial interface in the experimental setup.

Real time computer used in the experimental setup is a PC with Intel Core i7 2.8 Ghz processor, 16 GB RAM and Windows 7 operation system. A kernel is created on the computer for real time communication with the servo controller by constructing a model using Real Time Windows Target(RTWT) toolbox of MATLAB Simulink software. Matlab Simulink version 2011b with Real Time Workshop and Real Time Windows Target toolboxes are used in the experimental setup. By using the RTWT model created in MATLAB Simulink, parameters of the controller are easily altered on-line while monitoring and recording the desired information by processing the data collected by the data acquisition hardware in the performance evaluations and other analyses. Such a real time parameter tuning, monitoring and recording capability speeds up and eases the development and testing process.

3.7 Stewart Platform

In order to evaluate the stabilization performance of the system with different controller structures, controllable disturbances have to be applied as the base motion. A 6-DOF motion simulator, which can be also called a Stewart platform, is used to create such base motions. This 6-DOF motion simulator has six linear actuators to realize different motion profiles. The weight of the platform mounted on the motion simulator is held by pneumatic actuators while the required torques for realizing the desired motion profile is created by electric drives. The simulator has a control computer to calculate the required motion of each actuator to create the desired motion profile so the user only loads the motion profile as a combination of three translational and three rotational motions in the platform coordinate frame within the limits of the simulator and the simulator realizes it. For the experiments, a sinusoidal acceleration profile with different frequencies are loaded to the simulator and tests are conducted for each controller architecture alternative for all the frequencies of the base motion disturbance created by the simulator. The feed-forward gyroscope mounted on the base is also used to verify the characteristics of the base motion created by the simulator. Details about the stabilization performance experiments can be found in Section 6.2.3. Some important properties of the Stewart platform can be found in Table 3.4.

Table3.4: Properties of Stewart Platform used in the Experiments

Specifications	**Unit**	**Ratings**
Maximum Gross Moving Load(GML)	kg	21000
GML moment of inertia about X-axis	kgm^2	35000
GML moment of inertia about Y-axis	kgm^2	62000
GML moment of inertia about Z-axis	kgm^2	57000
Maximum Roll Angle	degree	± 20
Maximum Pitch Angle	degree	+19/-18
Maximum Yaw Angle	degree	± 20
Maximum Roll Angular Velocity	degree/s	± 44
Maximum Pitch Angular Velocity	degree/s	± 40
Maximum Yaw Angular Velocity	degree/s	± 43
Maximum Roll Angular Acceleration	$degree/s^2$	± 135
Maximum Pitch Angular Acceleration	$degree/s^2$	± 130
Maximum Yaw Angular Acceleration	$degree/s^2$	± 185
Attenuation for Acceleration Commands with Frequencies between 0.1 Hz to 10 Hz	dB	$\leq \pm 3$
Phase-shift for Acceleration Commands with Frequencies between 0.1 Hz to 10 Hz	degrees	$\leq \pm 90$
Latency	second	0.04

CHAPTER 4

PROPOSED APPROACH

4.1 Proposed Controller Architecture

In this chapter, the controller structure proposed for the control of the gun-turret system will be explained in a detailed manner. The aim of the proposed controller structure is to provide a precise tracking and high stabilization performance with better disturbance rejection capability despite the challenges explained in Part 2.3. The controller we design for satisfying the performance expectations is composed of two cascaded proxy-based controller, a notch filter and a reduced-order disturbance observer with additional Kalman filter. The proposed controller architecture can be seen in Fig.4.1

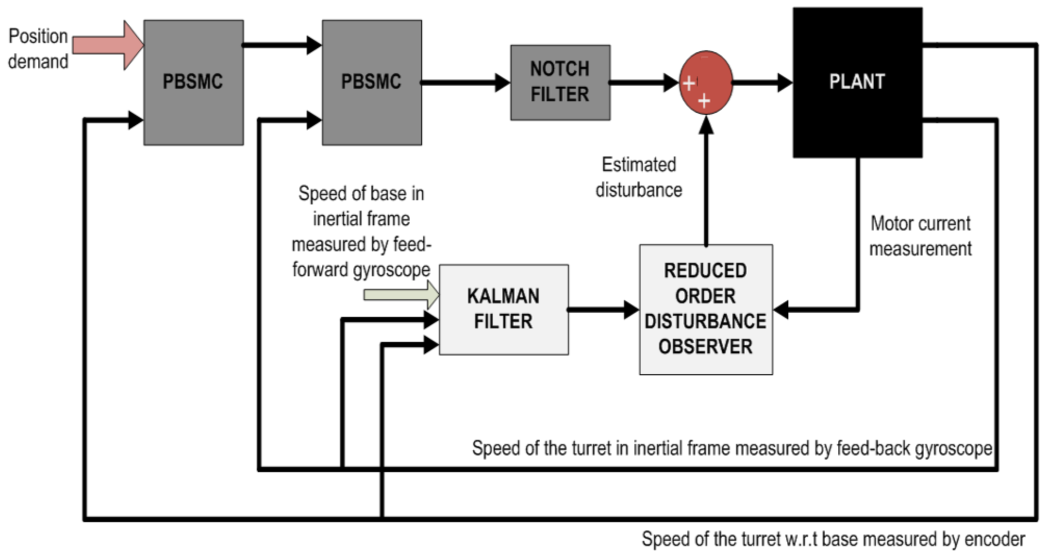

Figure 4.1: Proposed Controller Architecture

The proposed controller can be separated into two main parts, namely the main controller and enhancement subsystems. In Fig.4.1 components of the main controller are designated with dark grey while components of the enhancement subsystems are shown with lighter grey boxes. The main controller is a cascaded proxy-based sliding mode structure with a notch filter added to its output. The goal of the main controller is to provide the required tracking while enabling stabilization abilities with the support of enhancement sub-systems. The inner-loop in the cascaded PBSMC is working as a speed controller with torque limitation by using the FOG measurements as speed feedback. On the other hand, the outer loop is working as a position controller with a speed limit by using the encoder measurements as position feedback.

Enhancement subsystems are added to the controller architecture in order to increase the performance of the main controller. They are composed of a reduced-order disturbance observer and an additional Kalman filter. Reduced-order disturbance observer is integrated to the controller architecture for compensating the internal nonlinearities of the system such as friction and for increasing the proposed controller's disturbance rejection capability against the base motion or base disturbance. This reduced order observer is improved by an additional Kalman filter which is used for estimating the actual velocity of the system by fusing measurements taken from encoders, feed-back and feed-forward gyroscopes mounted on the gun-turret platform and base for measuring their motion in inertial frame.

In the rest of this chapter, details of the proxy-based sliding mode controller and notch filter addition will be explained first. Then, information about the architecture of the disturbance observer and some mathematical details and derivations about its effects on the main controller's performance will be given and evaluated analytically. Finally, this chapter will end by introducing the adaptation of a Kalman filter to our enhancement problem. For the rest of this chapter, gun-turret platform consent of the thesis will be denoted as turret system and controller architecture designed for the control of the turret system will be called as proposed controller.

4.2 Cascaded Proxy-Based Sliding Mode Controller(PBSMC) with Notch Filter

The main controller of the proposed architecture is composed of two PBSMC which are used in a cascade structure with a notch filter at the output path of the inner PBSMC: this is one of the most important novelty in the proposed controller. As a newly offered method, PBSMC has few applications in the literature and in all these applications a single PBSMC is used. Therefore, cascaded use of the PBSMC method is first introduced with the proposed controller offered as a solution in this thesis work. The outer PBSMC is taking the desired position signal from the user or automatic fire control system, position feedback from the encoder mounted on the turret system and is computing the speed signal required for tracking the desired position without exceeding the speed limits. On the other hand, the inner PBSMC is generating the torque signal required for both stabilization and tracking the desired speed signals without exceeding the torque limits. It uses the speed signals created by the outer PBSMC as desired speed input and measurements taken from the FOG mounted on the turret system as speed feedback. Also, a notch filter is integrated to output path of the inner controller for suppressing the first resonance in the open-loop frequency response function(FRF) between the torque applied to the system and speed of the system.

As it is explained in the Chapter 2, PBSMC is a comparably new control approach first offered by Kikuuwe and Fujimoto in [4], to be utilized in the position control of an industrial robot. Proxy-based sliding mode control is a modified version of sliding mode control with the ability of working with discrete-time controllers which can also be thought as an extension of force-limited PID control. Under ideal conditions, sliding mode control can be thought as an accurate controller for tracking, also acting as an over-damped controller minimizing large errors like drastic changes in the desired position signals. But the problem with sliding mode controller is about the ideal conditions defined. Optimality of the sliding mode control is only attained based on the assumption of instantaneous switching and on the existence of no time delays in the controlled system which are not possible in real world. Since we are using discrete-time controllers, delays occur at least during the switching between the sliding surfaces. These unavoidable switching delays cause high frequency oscillations, which is the most important problem of chattering in sliding mode control. This phenomenon decreases the performance of the controller due to the negative effects of such oscillations on systems. If we compare PBSMC with PID controllers, we see that it is not possible to obtain both accurate tracking and over-damped response for large errors by just effectively tuning a conventional PID. In order to obtain over-damped response for all type of error signals, the gains of the controller should be reduced. But such an adjustment of parameters results in increased reaction time and decreased accuracy in tracking, which is a highly undesired condition. So due to the problems and performance constraints explained above and also in Chapter 2 in more details, proxy-based sliding mode control which is a combination of the PID and sliding mode control, is chosen as the main control technique to get rid of such flaws and use advantages of both control methods.

The main idea in PBSMC is creating a virtual proxy which tracks the input signals generated by sliding mode control(SMC) to yield an ideal virtual world without any delay to be used optimally by SMC avoiding chattering. The actual plant to be controlled is connected to this proxy with a virtual coupling which behaves like a stiff PID to annihilate itself, difference between proxy and real system [3]. For the PB-SMC control used in the inner speed loop, the free-body diagrams of proxy and turret can be represented as in Fig.4.2. The figures and derivations will be given only for the inner loop since outer loop has a very similar structure except for the derivations and explanations of notch filter.

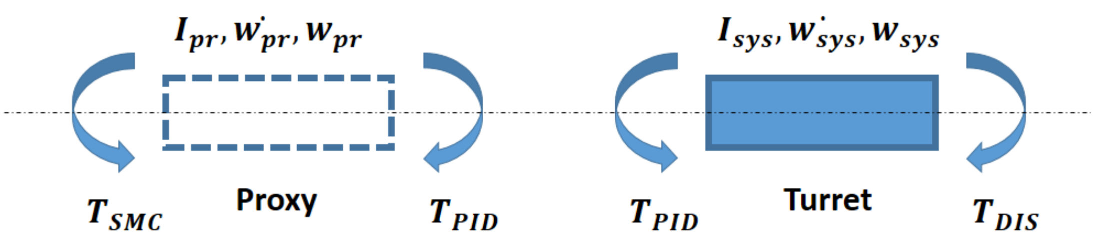

Figure 4.2: Free body diagram of proxy of the turret and the actual turret for PBSMC in inner speed loop

According to the body diagram for proxy of the turret in Fig.4.2, equation of motion for the proxy can be written as:

$$I_{pr}\dot{w}_{pr} = T_{SMC} - T_{PID} \tag{4.1}$$

where

I_{pr}	is inertia of the proxy of the turret
$\dot{w}_p$	is angular acceleration of the proxy of the turret
T_{SMC}	is torque applied by sliding mode controller to proxy of the turret
T_{PID}	is torque applied by virtual coupling (PID controller)

Torque applied by SMC to proxy of the turret for tracking the desired speed signal can be calculated as below by using conventional SMC formulation and sliding surface structure:

$$T_{SMC} = T sgn(S) \tag{4.2}$$

$$S = (w_{cmd} - w_{pr}) + H(\dot{w}_{cmd} - \dot{w}_{pr}) \tag{4.3}$$

where

T	is control gain of sliding mode control
H	is SMC time constant
w_{cmd}	is desired angular speed signal needs to be tracked
w_{pr}	is angular speed of the proxy of the turret

Torque applied by the virtual coupling, based on classical PID structure, for reducing the angular velocity difference between proxy and turret can be also stated as:

$$T_{PID} = K_i \int (w_{pr} - w_{sys}) + K_p(w_{pr} - w_{sys}) + K_d(\dot{w}_{pr} - \dot{w}_{sys}) \tag{4.4}$$

where

K_i is integral gain of the PID control
K_p is proportional gain of the PID control
K_d is derivative gain of the PID control
w_{sys} is angular velocity of the actual gun-turret platform

For the easiness of notation and further manipulations, we can use “e” as "$\int(w_{pr} - w_{sys})$" and restate the (4.4) as:

$$T_{PID} = K_i e + K_p \dot{e} + K_a \ddot{e} \tag{4.5}$$

When (4.1), (4.2), (4.3) and (4.5) are put together; the block diagram of the proposed structure for the inner loop speed control with additional notch filter can be illustrated in s-domain as in Fig.4.3

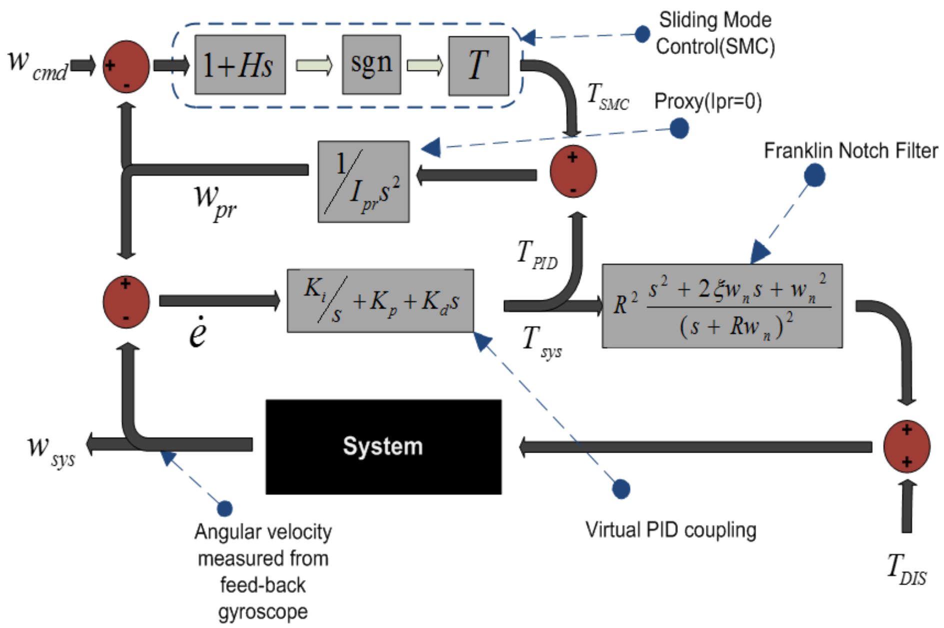

Figure 4.3: Block diagram of PBSMC control structure designed for inner speed loop with notch filter addition

Inertia of the proxy is taken as zero in the PBSMC structure constructed as a part of the proposed controller. This is the general trend in the literature [3–5,7]. We can also adopt this trend because there is no need for a mass to reflect the effect of the SMC and an additional mass can cause undesired delays. When the inertia of the proxy is taken as zero, the equation of motion of the proxy can be reconstructed as below by integrating equations (4.2),(4.3) and (4.5) into equation (4.1):

$$0 = T_{sgn}(w_{cmd} - w_{pr} + H(\dot{w}_{cmd} - \dot{w}_{pr})) - (K_i e + K_p \dot{e} + K_d \ddot{e}) \tag{4.6}$$

By applying the mathematical transformation given in equation (4.7) to (4.6), the formulation of the PBSMC structure in continuous time can be obtained as in (4.8),(4.9) and (4.10):

$$y = sgn(z - y) \Longleftrightarrow y = sat(z) \quad \forall y \in \quad R \forall z \quad \in R \tag{4.7}$$

$$s = w_{cmd} - w_{sys} + H(\dot{w}_{cmd} - \dot{w}_{sys}) \tag{4.8}$$

$$\ddot{e} = -\frac{K_p \dot{e} + K_i e}{K_d} + \frac{T}{K_d} sat(\frac{K_d}{T}(\frac{s - \dot{e}}{H} + \frac{K_p \dot{e} + K_i e}{K_d})) \tag{4.9}$$

$$T_{sys} = T_{PID} = T sat(\frac{K_d}{T}(\frac{s - e}{H} + \frac{K e \dot{+} L e}{K_d})) \tag{4.10}$$

PBSMC structure needs to be realized in discrete time in order to be used in real-time applications using digital processors. Therefore, continuous time formulation obtained in (4.8),(4.9) and (4.10) should be transformed into a discrete time model. If "Backward Euler" method is used for discretization, which is especially practical for discretization of such complicated continuous time models [95], a discrete time model of PBSMC control structure can be obtained as in the following set of equations that we use in our proposed control solution:

$$s(k) = w_{cmd}(k) - w_{sys}(k) + H(\frac{w_{cmd}(k) - w_{cmd}(k-1)}{T_s} - \frac{w_{sys}(k) - w_{sys}(k-1)}{T_s}) \tag{4.11}$$

$$T_{usys}(k) = \frac{K_d + K_pT_s + K_iT_s^2}{H + T_s}s(k) + \frac{K_pH - K_d + K_iT_s(2H + T_s)}{(H + T_s)T_s}e(k-1) - \frac{K_pH - K_d + K_iT_sH}{(H + T_s)T_s}e(k-2) \tag{4.12}$$

$$T_{sys}(k) = T\,sat(\frac{T_{usys}(k)}{T}) \tag{4.13}$$

$$e(k) = \frac{(2K_d + K_pT_s)e(k-1) - K_de(k-2) + T_s^2T_{sys}(k)}{K_d + K_pT_s + K_iT_s^2} \tag{4.14}$$

where

T_s is sampling time of the discrete-time controller

As it can be seen from the discrete time model of the PBSMC in (4.11), (4.12), (4.13) and (4.14), five parameters need to be tuned to obtain an optimal performance from the controller in an application. In PBSMC, SMC is responsible from the global dynamics which can be alternatively defined as respose of the controller to large errors. Therefore, H and T parameters of SMC are used to adjust the response of the controller to large amount of changes in the desired speed signal that cause large errors. In the proposed controller for turret system, maximum available torque output of the actuators are used as “T” parameter and H is adjusted online by observing the step response of the controller. On the other hand, virtual coupling in the PBSMC is responsible for local dynamics which can be also defined as respond of the controller to small errors. So Kp, Ki and Kd parameters of PID type virtual coupling are specifying the tracking and stabilization performance which corresponds to small error dynamics. In general, gains of the PID in PBSMC can be tuned by conventional PID tuning rules. We use frequency domain tuning with Bode Diagram in the proposed solution as the frequency response functions (FRFs) of the plant can be obtained through experiments and it is a commonly accepted analytical method in the literature.

In the main controller, an additional Franklin type notch filter is also integrated into the feedback path of the inner speed loop for shaping the open-loop frequency response function(FRF) between input torque and actual speed of the turret system by suppressing the first resonance. A continuous time Laplace formulation of a conventional Franklin (asymmetric) notch filter is given below:

$$G_f(s) = R^2 \frac{s^2 + 2\varepsilon w_n s + {w_n}^2}{(s + R w_n)^2} \tag{4.15}$$

where

R is asymmetric gain of the notch filter

ε is damping ratio of the notch filter

w_n is center frequency of the notch filter

To be used in the real-time application, the continuous time Laplace representation of the notch filter in (4.15) is discretized by the Tustin method which uses the transformation given in (4.16). This type of discretization does not disturb the gain and phase characteristics of the filter up to 1/10 of the sampling rate [95].

$$s = \frac{2}{T_s} \frac{1 - z^{-1}}{1 + z^{-1}} \tag{4.16}$$

here:

T_s is sampling frequency of the digital processor

When the transformation in (4.16) is integrated to (4.15) and the result is rearranged, the discrete time Franklin notch we use in our proposed solution is formulated as:

$$G_f = \frac{(T_s^2 w_n^2 + 4sT_s w_n + 4) + (2T_s^2 w_n^2 - 8)z^{-1} + (T_s^2 w_n^2 - 4sT_s w_n + 4)z^{-2}}{(R^2 T_s^2 w_n^2 + 4RT_s w_n + 4) + (2R^2 T_s^2 w_n^2 - 8)z^{-1} + (R^2 T_s^2 w_n^2 - 4RT_s w_n + 4)z^{-2}} \tag{4.17}$$

The main goal in suppressing the first resonance of the system by implementing a notch filter is to provide a possible increase in the gains of PID without violating the stability of the system. With the increment in the PID gains, bandwidth of the controller is also increased and better disturbance rejection capability is obtained which directly means an enhancement in the stabilization performance.

4.3 Reduced Order Disturbance Observer

As it is explained in Chapter 2, there are effective non-linearities and disturbances in the turret system which decrease the tracking and stabilization performance of the plant. It is not possible to cope with such non-linearities and disturbances by only adjusting the parameters of the main controller so a reduced order single state disturbance observer is implemented for the compensation of these detrimental effects. We adopt the structure used in [6] for the construction of the disturbance observer subsystem. A Kalman filter is also integrated to improve its performance as a part of our contribution.

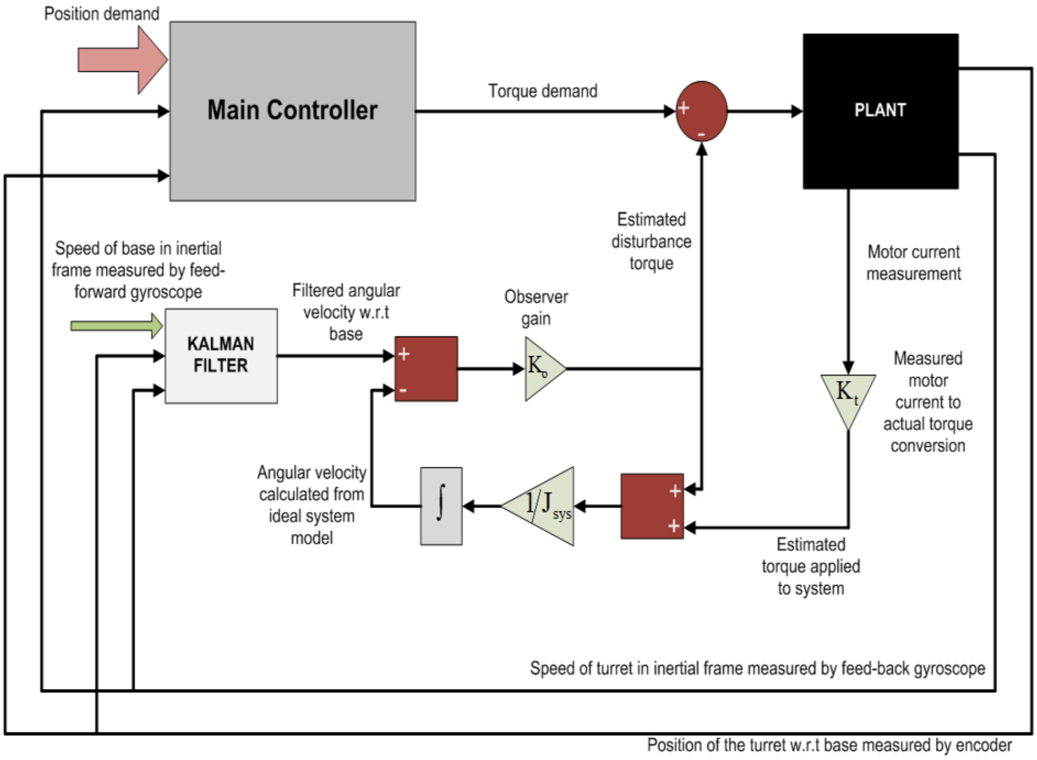

Figure 4.4: Block diagram of the disturbance observer subsystem

A Luenberger type of state estimator is used as the single state disturbance observer. The observer includes a basic single mass system model and it only uses the estimated inertia of the turret as the model parameter which makes it very practical. A disturbance torque estimation is obtained by using this system model, the torque demand signal generated by the whole proposed controller and the speed of the turret calculated by the Kalman filter. By adding the inverse of the estimated disturbance torque to the torque demand calculated by the main controller, disturbance rejection capability of the main controller is increased. The block diagram of the disturbance observer is illustrated in Fig.4.4.

One of the most important property of the proposed observer is its closed loop configuration which drives the estimation error to zero through an observer gain and reduces the sensitivity of the observer against possible uncertainties. Moreover, as it can be seen from Fig.4.4, that the proposed observer structure does not have any effect on the dynamics of the main controller so it is easily integrated to the main controller without any concern about possible interactions. Such a convenience in integration also makes the disturbance observer approach a preferred enhancement method for the proposed approach.

By using Fig.4.4, the transfer function representing the relation between disturbance torque estimation, the angular velocity of the system and the measured motor torque can be derived as:

$$T_{Dest}(s) = \left(\frac{\frac{K_0}{J_{sys}}}{s + \frac{K_0}{J_{sys}}} \right) \left(J_{sys} s w_k(s) - T_a(s) \right) \tag{4.18}$$

where:

T_{Dest} is the disturbance torque estimated by the observer
K_0 is the observer gain
J_{sys} is the pre-estimated inertia of the system
w_k is the angular velocity of the system estimated by Kalman
T_a is the torque applied to the system by actuators

When Newton's second law of motion is thought for the turret with given inertia, it can be said that the second term of the transfer function in (4.18) is just the calculation of the disturbance torque from the angular velocity provided by the Kalman filter and the torque applied to the system by actuators. So, the transfer function in (4.18) shows that the observer structure provides a filtered disturbance calculation by fusing available information and measurements about the system.

In order to make analytical evaluations about the proposed observer's contribution to the disturbance rejection capability and effect on the noise coupling characteristics; all the measurements are taken as ideal, the Kalman filter is not included and the actual system model is thought to be equal to a single mass model used in the observer. Also, the main controller is assumed to be linear and its transfer function is denoted as Gmc(s). With these assumptions, the disturbance rejection characteristics of the system shown in Fig.4.4 can be simply obtained as:

$$\frac{w_s(s)}{T_D(s)} = \left(\frac{\frac{1}{J_{sys}}}{s+\frac{G_{mc}(s)}{J_{sys}}}\right)\left(\frac{s}{s+\frac{K_0}{J_{sys}}}\right) \tag{4.19}$$

where:

w_s is the angular velocity of the turret

T_D is the torque exerted on the turret by disturbances

G_{mc} is assumed to be the linear model for the main controller

And noise coupling characteristics can be obtained as:

$$\frac{w_s(s)}{n_w(s)} = -\left(\frac{\frac{G_{mc}}{J_{sys}}}{s+\frac{G_{mc}}{J_{sys}}}\right) - \left(\frac{\frac{K_0}{J_{sys}}}{s+\frac{K_0}{J_{sys}}}\right)\left(\frac{s}{s+\frac{G_{mc}}{J_{sys}}}\right) \tag{4.20}$$

where:

n_w is the noise in the angular velocity measurements without Kalman filter

In both of the equations (4.19) and (4.20), second terms of the transfer functions are due to the existence of disturbance observer and show respectively its effects in disturbance rejection capability and noise coupling characteristics. As it can be seen from (4.19), the observer structure has a high-pass type of effect on the disturbance rejection characteristic and improve the rejection capability for the low frequency disturbances inside its bandwidth. This bandwidth is proportional to the ratio between the observer gain and the inertia of the system so it can be increased by using higher observer gains. On the other hand, disturbance observer cause additional noise coupling to the angular velocity of the turret as it is shown by the second term of (4.20). Such a noise can be tolerated up to a point, but increase in the observer gain yields a noise with higher magnitude which can cause serious problems in the control of the system. This contradiction between disturbance rejection capability and magnitude of the coupled noise is the main tradeoff in the disturbance observer structure. So, a Kalman filter is implemented to reduce the noise in the gyroscope measurements used in the disturbance observer and provides an opportunity to an additional increment in the observer gain which is essential for enlarging the disturbance rejection bandwidth of the observer. In addition to these observations and comments made for ideal conditions and ideal single mass system model, detailed analysis about sensitivity of the offered disturbance observer structure against non-idealities and different system models are carried out in our simulations explained in Chapter 5 and they are also tested in the experiments with real turret system as explained in Chapter 6.

4.4 Additional Kalman Filter

Without using a Kalman filter, the angular velocity of the system in inertial frame is directly obtained from the measurements provided by feed-back fiber-optic gyroscope(FOG). However, angular velocity obtained from these measurements includes all the angular random walk(ARW) noise in the gyroscope and this noise limits the performance of the disturbance observer. The main goal of the conventional discrete-time Kalman filter integrated to the angular velocity input of the disturbance observer is to obtain an estimate of this angular velocity input with minimized noise by fusing redundant and uncorrelated FOGs and encoder measurements.

The operation principle of discrete-time Kalman filters' (DTKF) is based on the propagation of the state mean and covariance with each time-step. The aim of these filters is to estimate the states of a linear system by using the knowledge about the dynamics of the system and available noisy sensor measurements. Operation of DTKF in one time step can be separated into two main stage, estimation and correction. At the beginning of each iteration, Kalman Filter receives the expected value and covariance of the states obtained at the end of the previous time step. Each iteration starts with the calculation of new state estimation and derivation of new error covariance estimate by using the information about the system dynamics. These calculations constitute the estimation part of the DTKF and is called time update. Then, by using the measurements taken at that time step and predefined measurement noise covariance, state estimations and error covariance values are regenerated. This regeneration procedure constitutes the correction stage of the DTKF and is called measurement update [88].

DTKF implemented in the proposed controller depends on constant acceleration kinematic model for time update stage and measurements used in the measurement update stage are taken from the feed-back gyroscope mounted on the turret, hull gyroscope mounted on the base and the encoder. The main idea in the constructed Kalman filter is combining the inertial and reference frame equations by using the feed-forward gyroscope measurements. So set of kinematic equations are implemented for each frame by using the constant acceleration assumption and variations in the acceleration are defined as the modelling noise. State space representation of the implemented system model is illustrated as:

$$x(k) = \begin{bmatrix} \theta_{tr}(k) \\ w_{tr}(k) \\ w_b(k) \\ \alpha_{tr}(k) \\ \alpha_b(k) \end{bmatrix} = \begin{bmatrix} 1 & T_s & -T_s & \frac{T_s^2}{2} & 0 \\ 0 & 1 & 0 & T_s & T_s \\ 0 & 0 & 1 & 0 & T_s \\ 0 & 0 & 0 & 1 & 0 \\ 0 & 0 & 0 & 0 & 1 \end{bmatrix} \begin{bmatrix} \theta_{tr}(k-1) \\ w_{tr}(k-1) \\ w_b(k-1) \\ \alpha_{tr}(k-1) \\ \alpha_b(k-1) \end{bmatrix} + \begin{bmatrix} 0 \\ 0 \\ 0 \\ Q_m \\ Q_m \end{bmatrix} \tag{4.21}$$

$$y(k) = \begin{bmatrix} \theta_e(k) \\ w_{fb}(k) \\ w_{ff}(k) \end{bmatrix} = \begin{bmatrix} \theta_{tr}(k) \\ w_{tr}(k) \\ w_b(k) \end{bmatrix} = \begin{bmatrix} 1 & 0 & 0 & 0 & 0 \\ 0 & 1 & 0 & 0 & 0 \\ 0 & 0 & 1 & 0 & 0 \end{bmatrix} \begin{bmatrix} \theta_{tr}(k) \\ w_{tr}(k) \\ w_b(k) \\ \alpha_{tr}(k) \\ \alpha_b(k) \end{bmatrix} + \begin{bmatrix} R_e \\ R_{fbg} \\ R_{ffg} \end{bmatrix} \tag{4.22}$$

where:

$x(k)$	is the state vector
$y(k)$	is the output vector
$\Theta_{tr}(k)$	is the angle of the turret with respect to base
$w_{tr}(k)$	is the angular velocity of the turret in inertial frame
$w_b(k)$	is the angular velocity of the base in inertial frame
$\alpha_{tr}(k)$	is the angular acceleration of the turret with respect to base
$\alpha_b(k)$	is the angular acceleration of the base in inertial frame
Q_m	is the acceleration modelling noise covariance
R_e	is the encoder measurement noise covariance
R_{fbg}	is the feed-back gyroscope measurement noise covariance
R_{ffg}	is the feed-forward gyroscope measurement noise covariance
$\Theta_e(k)$	is the angle measured by the encoder
$w_{fb}(k)$	is the angular velocity measured by the feed-back gyroscope
$w_{ff}(k)$	is the angular velocity measured by the feed-forward gyroscope

According to the state space system model defined by (4.21) and (4.22), formulation of a priori state and error covariance estimations by using the system model in the time update stage is defined as:

$$\hat{x}_k^- = A\hat{x}_{k-1}^+ + Bu_{k-1} \tag{4.23}$$

$$P_k^- = AP_{k-1}^+ A + Q \tag{4.24}$$

$$A = \begin{bmatrix} 1 & T_s & -T_s & \frac{T_s{}^2}{2} & 0 \\ 0 & 1 & 0 & T_s & T_s \\ 0 & 0 & 1 & 0 & T_s \\ 0 & 0 & 0 & 1 & 0 \\ 0 & 0 & 0 & 0 & 1 \end{bmatrix}, Q = \begin{bmatrix} 0 \\ 0 \\ 0 \\ Q_m \\ Q_m \end{bmatrix} \tag{4.25}$$

where:

$\hat{x}_k^-$ is the priori state estimation after time update stage

$\hat{x}_{k-1}^+$ is the posteriori state estimation of the previous time step

P_k^- is the priori error covariance matrix estimation after time update stage

P_{k-1}^+ is the posteriori error covariance matrix estimation of the previous time step

Q is the modelling noise covariance matrix

By using the priori state and error covariance matrix calculated in time update stage, posteriori state and error covariance matrix is computed by using the measurement update equations. There are some alternative formulations for the covariance measurement update equation, but Joseph stabilized version is used in the proposed controller structure due to its stability and robustness [88]. Measurement update equations used in the proposed Kalman filter are listed as follow:

$$K_k = P_k^- C^T \left(C P_k^- C^T + R\right)^{-1} \tag{4.26}$$

$$\hat{x}_k^+ = \hat{x}_k^- + K_k(y_k - C\hat{x}_k^-) \tag{4.27}$$

$$P_k^+ = (I - K_k C) P_k^- (I - K_k C)^T + K_k R K_k^T \tag{4.28}$$

$$C = \begin{bmatrix} 1 & 0 & 0 & 0 & 0 \\ 0 & 1 & 0 & 0 & 0 \\ 0 & 0 & 1 & 0 & 0 \end{bmatrix}, R = \begin{bmatrix} R_e \\ R_{fbg} \\ R_{ffg} \end{bmatrix} \tag{4.29}$$

where:

K_k is the Kalman filter gain

$\hat{x}_k^+$ is the posteriori state estimation after measurement update stage

P_k^+ is the posteriori error covariance matrix estimation after measurement update

R is the measurement noise covariance matrix

In order to finalize the Kalman filter design, three noise covariance values also need to be determined. Gyroscope and encoder measurement noise covariance parameters can be specified numerically by using the specifications given in their datasheets and analyzing the measurements taken from the sensors mounted on the real system. However, it is not that easy to decide analytically on acceleration modelling noise covariance as it is very hard to estimate the modelling error done with the constant acceleration assumption. So, tuning of the modelling noise covariance is made empirically by fixing the two measurement noise covariance and evaluating the effect of different modelling noise covariance values on the characteristics of the filter. Details about the analytical tuning of the measurement noise covariance and empirical tuning of the modelling noise covariance are provided under the tuning topic in Chapter 5.

CHAPTER 5

MODELLING, SIMULATION RESULTS AND DISCUSSIONS

Before the implementation on our real system, we decided to run some simulations in order to perform an exhaustive analysis of the proposed controller structure. In order to approximate the characteristics of the real system to use in this analysis, a non-linear mathematical model is constructed and its parameters are adjusted according to the data taken from the real system. This chapter mainly focuses upon the construction procedure of this mathematical system model, the tuning of the proposed controller architecture for the control of the constructed model and on the performance analysis of the controller sub-structures. In addition to performance analysis, sensitivity analysis for critical parameters are also presented in this chapter.

5.1 Construction of a Mathematical System Model

For simulating the characteristics of the real system, a mathematical system model of the real gun-turret platform is constructed and validated in MATLAB Simulink software. This model is composed of three main structures; namely the linear model, the non-linear extensions and the sensor noise components. First a linear model is created in order to reflect the response of the system in frequency domain according to the results obtained from frequency sweep tests made on the real system. Then friction and backlash models are inserted to the linear model for simulating the non-linearities. At last, simulation of the noise in the measurements taken from the sensors on the system is added to the outputs of the mathematical model to acquire more realistic analysis results.

5.1.1 Linear Model

The system considered as a main source of this thesis work is a gun-turret platform in which torque is supplied by a motor, transmitted by a gear-box and acting on a flexible load. In this system, angular speed measurements are taken from the gyroscope mounted on the load but closer to the transmission elements and angular position measurements are taken from the encoder mounted just output of the transmission elements. Due to such configuration of the real system, a flexible lumped three-mass model is used in order to simulate the linear characteristics of the real system as in [96], [97] and [98]. In this model first mass is representing the moment of inertia of the motor, the second mass is representing the moment of inertia of the gear series and the third mass is representing the moment of inertia of the load. Also the angular speed of the second-mass corresponds to gyroscope measurements and the angular position of the second mass corresponds to encoder measurements. A schematic diagram of the three-mass model can be seen in Fig.5.1.

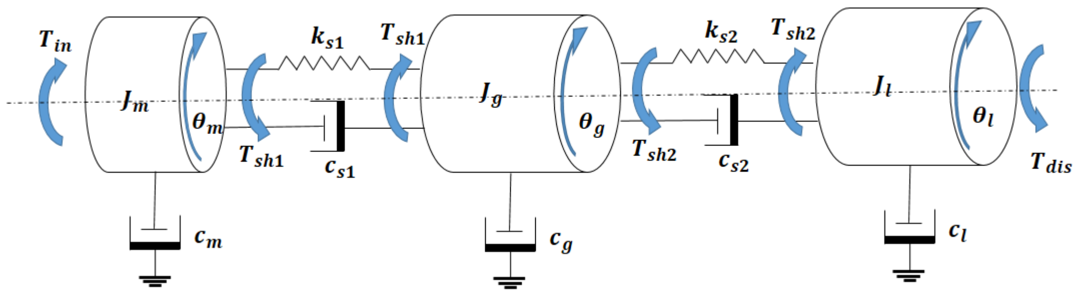

Figure 5.1: Schematic diagram of the three-mass model

According to Fig.5.1, equations of motion for each mass can be stated as follows;

$$J_m\ddot{\theta}_m = T_{in} - T_{sh1} - c_m\dot{\theta}_m \tag{5.1}$$

$$J_g\ddot{\theta}_g = T_{sh1} - T_{sh2} - c_g\dot{\theta}_g \tag{5.2}$$

$$J_l\ddot{\theta}_l = T_{sh2} - T_{dis} - c_l\dot{\theta}_l \tag{5.3}$$

$$T_{sh1} = k_{s1}\left(\theta_m - \theta_g\right) + c_{s1}\left(\dot{\theta}_m - \dot{\theta}_g\right) \tag{5.4}$$

$$T_{sh2} = k_{s2}\left(\theta_g - \theta_l\right) + c_{s2}\left(\dot{\theta}_g - \dot{\theta}_l\right) \tag{5.5}$$

where

J_m is the motor moment of inertia

J_g is the gear series moment of inertia

J_l is the load moment of inertia

θ_m is angle of the motor

θ_g is angle of the gear series

θ_l is angle of the load

T_{in} is input torque applied by the motor

T_{sh1} is transmitted torque between motor and gear series

T_{sh2} is transmitted torque between gear series and load

T_{dis} is disturbance torque acting on the load

k_{s1} is the elasticity between motor and gear series

k_{s2} is the elasticity between gear series and load

c_{s1} is the damping coefficient between motor and gear series

c_{s2} is the damping coefficient between gear series and load

c_m is the damping coefficient of the motor

c_g is the damping coefficient of the gear series

c_l is the damping coefficient of the load

As the damping coefficients are very small compared to stifness values in our real system, they are omitted for the simplicity of the calculations and analysis. By using the equations of motion given in (5.1), (5.2), (5.3), (5.4) and (5.5), we found the transfer function between input torque and gear series angular speed in frequency domain as follows:

$$\frac{J_l k_{s1} s^2 + k_{s1} k_{s2}}{s\left\{J_m J_g J_l s^4 + \left[\left(J_m + J_g\right) J_l k_{s1} + \left(J_g + J_l\right) J_m k_{s2}\right] s^2 + \left(J_m + J_g + J_l\right) k_{s1} k_{s2}\right\}} \tag{5.6}$$

In order to have a linear model with response characteristics similar to the real system, especially in the low frequencies, resonance and anti-resonance frequencies of the model is matched with the first two resonance and first anti-resonance frequencies of the real system. By observing the poles and zeros of the transfer function given in equation (5.6); formulation of the resonance and anti-resonance frequencies of the three-mass system model can be calculated as:

$$\omega_{ares} = \sqrt{\frac{k_{s2}}{J_l}} \tag{5.7}$$

$$\omega_{res1} = \sqrt{\frac{C - \sqrt{C^2 - 4J_mJ_gJ_l\left(J_m + J_g + J_l\right)k_{s1}k_{s2}}}{2J_mJ_gJ_l}} \tag{5.8}$$

$$\omega_{res2} = \sqrt{\frac{C + \sqrt{C^2 - 4J_mJ_gJ_l\left(J_m + J_g + J_l\right)k_{s1}k_{s2}}}{2J_mJ_gJ_l}} \tag{5.9}$$

$$C = \left[\left(J_m + J_g\right)J_lk_{s1} + \left(J_g + J_l\right)J_mk_{s2}\right] \tag{5.10}$$

where

ω_{ares} is the first anti-resonance frequency of the two-mass model

ω_{res1} is the first resonance frequency of the three-mass model

ω_{res2} is the second resonance frequency of the three-mass model

For determining the resonance and anti-resonance frequencies of the real system, open loop frequency response functions(FRFs) between torque applied to the system and angular velocity measurements are investigated. Open loop FRFs of the real system is obtained by applying sinusoidal motor torques with different frequencies and observing the corresponding gyroscope measurements. For the consistency, experiments are repeated for different amplitudes of the sinusoidal torque inputs. Bode plots of the open loop system FRFs acquired as a result of the experiments can be seen in Fig.5.2.

By observing Fig.5.2, the first resonance, the second resonance and the anti-resonance frequencies can be approximated as 14.25 Hz, 19.5 Hz and 16.75 Hz respectively. In addition to open loop FRFs, another experiment is made for estimating the total inertia of the system at load side($J_m + J_g + J_l$). In this experiment, torque input which is a square wave with amplitude of 6578 Nm is applied to the system and angular acceleration is calculated from slope of the angular velocity measurements taken from gyroscope mounted on the system. The angular velocity measurement obtained from the system can be seen in Fig.5.3.

If the system under the constant torque input is taken as a single mass and friction or disturbance torque is assumed to be constant, the simplified system equations of motion for acceleration and deceleration cases can be written as:

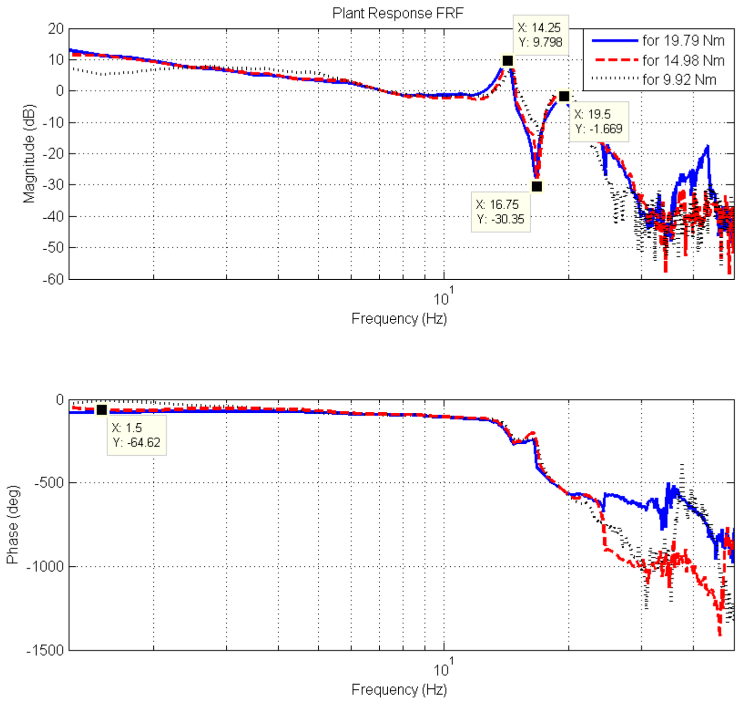

Figure 5.2: Open Loop Real System FRF for different amplitudes of the sinusoidal torque input

$$J_{sys}\alpha_{acc} = T_{in} - T_{dis} \tag{5.11}$$

$$J_{sys}\alpha_{dec} = T_{in} + T_{dis} \tag{5.12}$$

where,

J_{sys}	is the total inertia of the system
θ_{acc}	is the acceleration of the system
ω_{dec}	is the deceleration of the system

Using equations (5.11) and (5.12), the derivation of total inertia of the system based on acceleration and deceleration values obtained from Fig.5.3 can be formulated as follows:

$$J_{sys} = \frac{2T_{in}}{\alpha_{acc} + \alpha_{dec}} \tag{5.13}$$

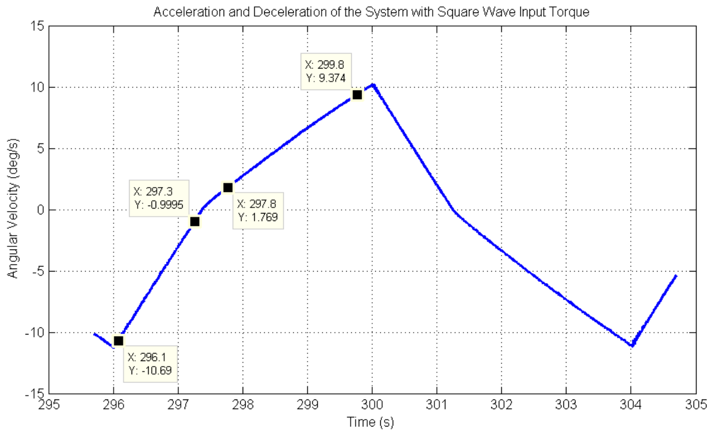

Figure 5.3: Acceleration of the system with 6578 Nm constant torque input

When the angular acceleration and deceleration measurements in Fig.5.3 are inserted into equation (5.13), the total inertia of the system is approximated as 31730 kgm^2. Also the motor inertia at the load side can be calculated as 280 kgm^2 by using the inertia specification of the motor and gear ratio given in Chapter 3. If the resonance frequencies, anti-resonance frequency, total system inertia and motor inertia acquired from the experiments and system specifications are combined with equations (5.7), (5.8), (5.9) and (5.10); unknown model parameters J_g, J_l, k_{s1} and k_{s2} can be calculated as 23750 kgm^2 , 7700 kgm^2, $2.25 \times 10^6 \quad Nm/rad$ and $8.5 \times 10^7 \quad Nm/rad$ respectively. Such a high gear series inertia can be thought as abnormal at first; however, it shows that turret is also acting as a part of the second mass and the third mass or load represents only the inertia of the gun. In such a configuration, the second stiffness coefficient stands for the elasticity of the gun which can be thought as a beam mounted to the turret from one end. The frequency response characteristics of the finalized system model is obtained as in Fig.5.4.

In addition to inertia and stiffness values, damping coefficients are also added to the system model and are tuned manually in order to adjust the amplitudes of the resonance and anti-resonance peaks similar to the real systems plant response. With the addition of the damping coefficients peaks are suppressed and especially amplitude of the second resonance peak is reduced below the first resonance peak by increasing the c_{s2} more compared to c_m. Damping coefficients c_m, c_g, c_{s1} and c_{s2} are chosen in

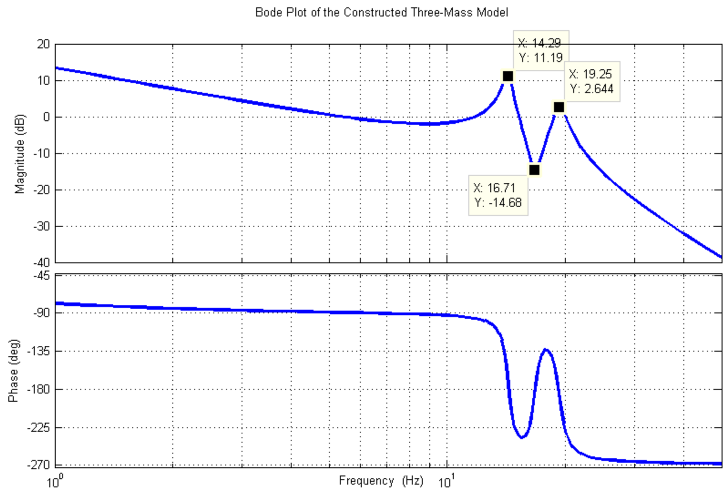

Figure 5.4: Frequency characteristics of the approximate three-mass system model

the system model as 1400,40000, 100 and 50000 $Nm \cdot s/rad$.

5.1.2 Friction and Backlash

Three-mass linear model represents the linear characteristics of the real system independent of non-linearities; however, non-linearities are also very effective in the performance of the controllers so they should be implemented in the model used for simulations. As it is explained in Chapter 2, backlash and especially friction are the most effective non-linearities in the system considered. A simple dead zone backlash model is implemented to represent the effects of the backlash and a static friction model is constructed to represent the friction in the real system. A static friction model is chosen to represent the friction in the system as dynamic models are much more complex and the dynamic components are not as dominant as the static components in the friction measurements taken from the real system as it can be seen in Fig.5.7.

For the system model derived, dead-zone or physical backlash model do not make a difference, since the damping and stiffness of the shafts are already modelled as a part of the linear three-mass model. So, we decided to adopt a dead-zone model to represent backlash. Stiffness in the dead-zone model is chosen to be the pre-calculated stiffness obtained for the linear model. Dead-zone model can be physically represented as in Fig.5.5 [1].

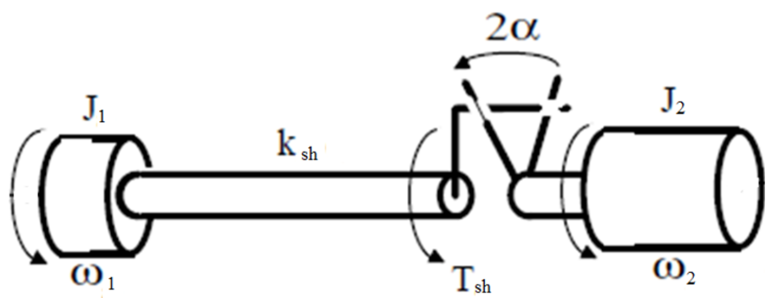

Figure 5.5: Physical representation of the dead-zone backlash model (Adapted from [1])

Dead zone model is a static model and uses only the angle difference, namely the shaft twist, between two inertias mounted on two sides of the shaft. The calculation of the shaft torque in the dead zone model is carried out as follows:

$$T_{sh} = \begin{cases} k_{sh}(\theta_{sh} - \alpha) & \theta_{sh} > \alpha \\ 0 & |\theta_{sh}| < \alpha \\ k_{sh}(\theta_{sh} + \alpha) & \theta_{sh} < -\alpha \end{cases} \quad (5.14)$$

$$\theta_{sh} = \theta_1 - \theta_2 \quad (5.15)$$

where,

T_{sh}	is the torque of the shaft
θ_{sh}	is the twist angle of the shaft
θ_1	is the angle of the first inertia
θ_2	is the angle of the second inertia
k_s	is the elasticity of the shaft
α	is the angle of the backlash gap

On the other hand, for simulating friction in the system, a static friction model with coulomb and viscous components is used. In order to detect the effects of the friction in the real system, gun-turret platform is rotated with different constant speeds by using the speed controller and average torque applied to the system is calculated from the motor current measurements. A sample experiment result obtained for 1 deg/s constant speed can be seen in Fig.5.6.

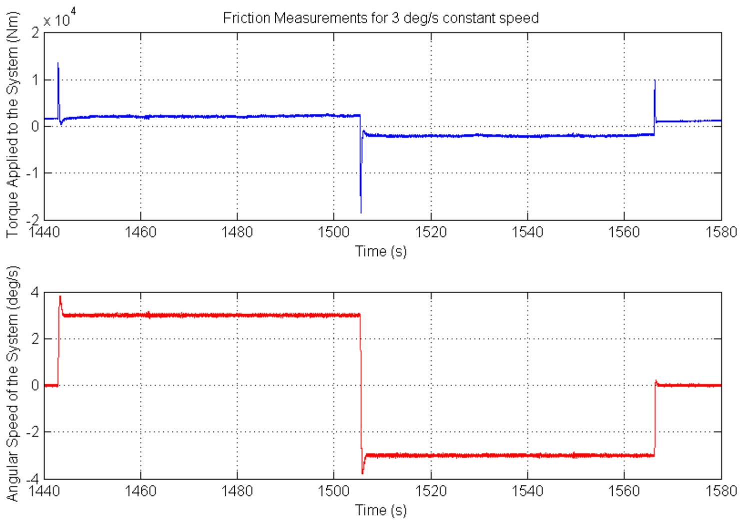

Figure 5.6: Friction measurement for 3 deg/s constant angular speed

The friction value for each specific angular speed is calculated by taking the average of absolute values of the applied torque after the oscillations in the system speed settles down in both directions and system reaches to the desired speed. The same experiment is repeated for different angular speeds ranging from 0.2 deg/s to 30 deg/s to find out the variation of friction according to the changes in the angular speed of the system. Results show that coulomb and viscous components are sufficient to represent the friction in the real system because the Stribeck type components are not distinguishable and effective in the friction calculations obtained for lower speeds. Optimal coulomb and viscous friction coefficients are calculated by comparing the derived model with measurements taken from the real system, also using mean square error(MSE) method. Comparison of the friction characteristics obtained from real system and that of the friction model obtained after optimization can be seen in Fig.5.7.

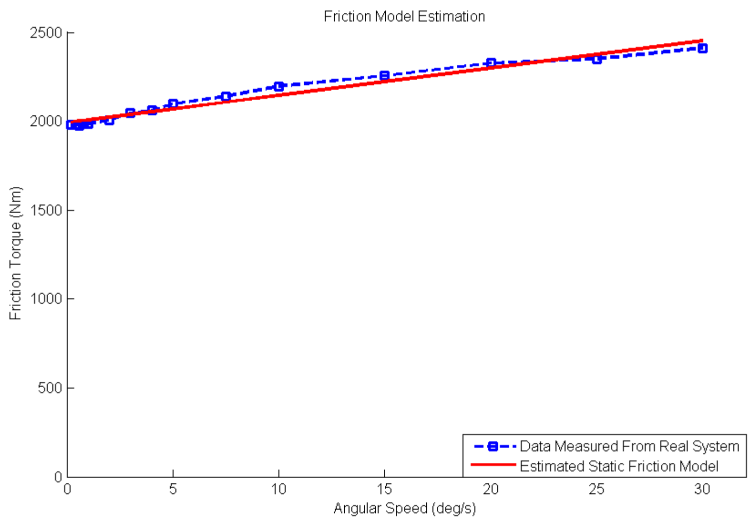

Figure 5.7: Comparison of the friction characteristics obtained from the real system and the friction model

5.1.3 Imperfections of the Sensors

There are four main sensors that are used as the input in the proposed controller, namely the current sensor, the feedback gyroscope, the feed-forward gyroscope and the encoder. As it is explained, none of these sensors can provide a perfect measurement and these imperfections in the sensor measurements deteriorate the performance of the controller. In order to approximate sensor flaws and insert them into the proposed model, data are collected from the real system and have been analysed.

Current sensor is used for measuring the phase currents of the motors. By multiplying its current measurements with torque constant of the motor, torques applied to the system are estimated. A sample current sensor measurement collected from the real system at rest can be seen in Fig.5.8.

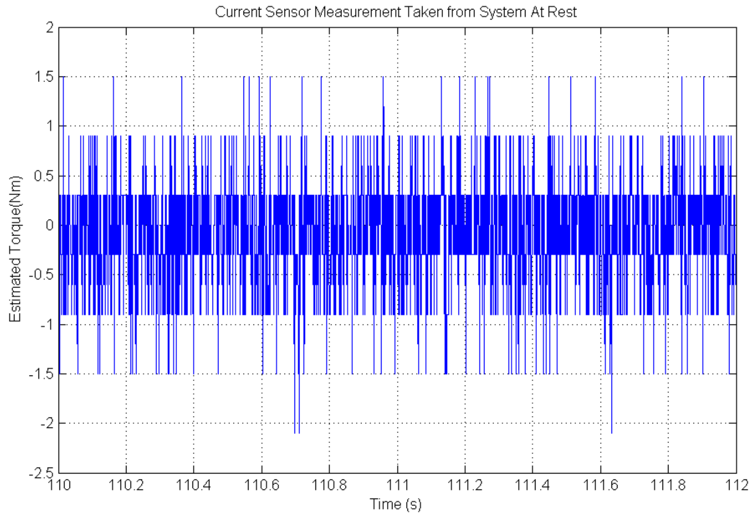

Figure 5.8: Current sensor measurement collected from the real system at rest

In addition to 2 seconds measurement given in Fig.5.8, a 140 second long current sensor measurement is taken to calculate the variance and analyse the power spectral density of the signal. The variance of the current sensor noise for the stationary system is found as 0.3355 and a periodogram power spectral density is evaluated as in Fig.5.9.

When the power spectral density in Fig.5.9 is analysed, it can be said that power density stays flat for nearly all frequencies and showing a white noise signal characteristic. Therefore, such a signal with variance of 0.3355 is added to torque measurements used in the simulation model to represent the noise in the real sensor measurements.

As it is explained in Section 2.6, gyroscopes have different type of imperfections like bias offset, bias drift and scale factor faults but the most critical one is angular random walk. Therefore, only the angular random walk or short-term noise characteristics of

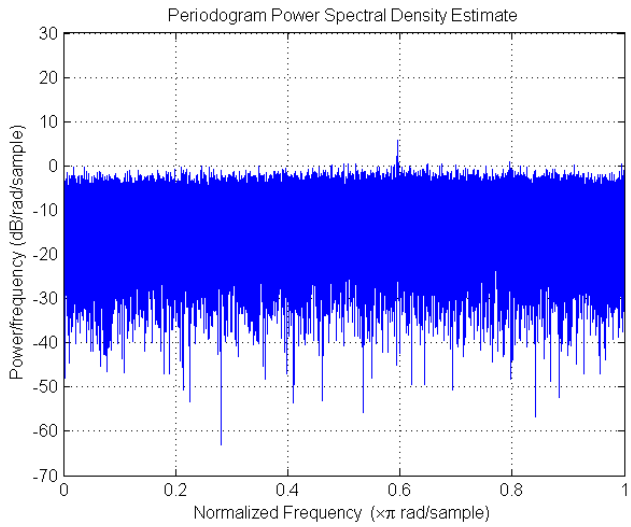

Figure 5.9: Periodogram power spectral density analysis of current sensor noise

the gyroscope is measured and analysed. Also since the feed-forward and feed-back gyroscopes are identical, the analysis are carried out for only feed-back gyroscope and are taken as valid for both of them. A sample gyroscope measurement collected from the real system at rest can be seen in Fig.5.10.

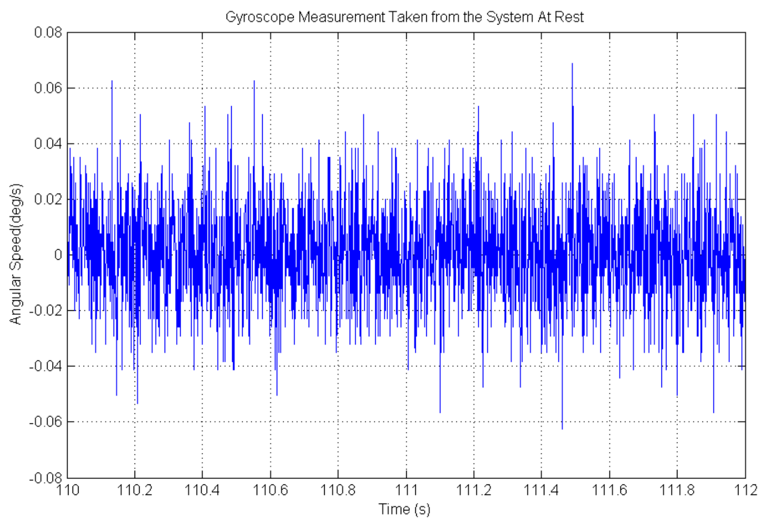

Figure 5.10: Gyroscope measurement collected from the real system at rest

In addition to 2 second measurements given in Fig.5.10, a 140 second long gyroscope measurement sample is also taken to calculate the variance and analyse the power spectral density of the signal. The variance of the gyroscope noise for the stationary system is found as 3.0197×10^{-4} and a periodogram power spectral density is found as in Fig.5.11.

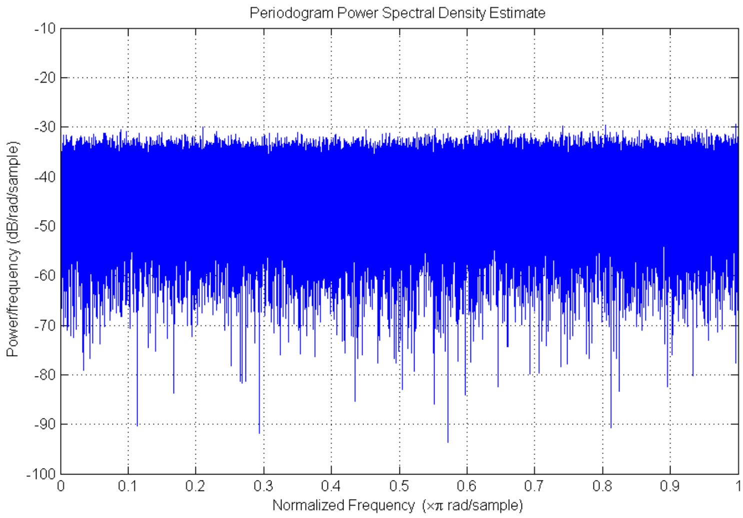

Figure 5.11: Periodogram power spectral density analysis of gyroscope noise

When the power spectral density in Fig.5.11 is analysed, it can be said that the power density of gyroscope measurements remains the same for nearly all frequencies similar to the current sensor measurements. Therefore, a white noise signal with variance of 3.0197×10^{-4} is also added to the angular speed measurements used in the simulation model to represent the noise in the real gyroscope measurements.

Different from current sensor and gyroscopes,the critical flaw in the encoders is quantization error more than measurement noise. As it is explained in Chapter 3, encoders used in the system to measure the angle of the load have 16-bit resolution for one full rotation. So, resolution of encoders can be stated as 0.0055 in degrees. A sample encoder measurement collected from the real system in motion can be seen in Fig.5.12.

As it can be observed from Fig.5.12, encoder measurement shows a stepwise characteristic as expected. So, in order to represent such characteristics, a quantizer with 0.0055 degree step-size is integrated into the angle measurement taken from the system in the constructed model. Also, the variance of the encoder in the Kalman filter is taken to be 0.00225 degrees which is the half of its step-size.

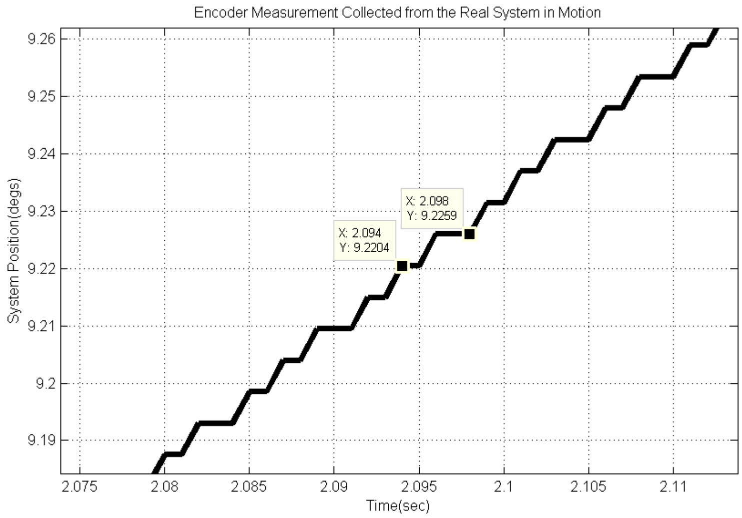

Figure 5.12: Encoder measurement collected from the real system in motion

5.2 Off-line Tuning of the Controller Parameters

Parameter tuning is one of the most important part of controller design. Tuning can be made off-line using the measurements and running the analysis; or it can be made on-line observing the real output of the system and applying trial-error type of procedures. PID parameters of the PBSMC sub-structures and that of the notch filter are tuned off-line based on commonly accepted and applicable analytical tuning tools. The measurement noise covariance matrix of the Kalman filter is directly determined by the analysis made on sensor measurements which are explained in the sub-section 5.1.3. On the other hand; the time constant in the PBSMC sub-structure, modelling noise covariance in the Kalman Filter and observer gain in the disturbance observer sub-structure are all tuned on-line by manipulating the corresponding parameter and observing the resulting performance. In this sub-section, the off-line tuning of the PID parameters for both, the inner and the outer PBSMC sub-structures in the main controller will be explained in a detailed manner.

Tuning of the PID parameters in both PBSMC sub-structures and notch filter are made in the frequency domain using Bode plots. For inner PBSMC, the plant is directly the three-mass system model derived from the real system measurements with additional notch filter. However, the plant for the outer PBSMC controller is the combination of both inner PBSMC and three-mass system model with additional notch filter. Such plant configurations can be described by a simplified block diagram as in Fig.5.13.

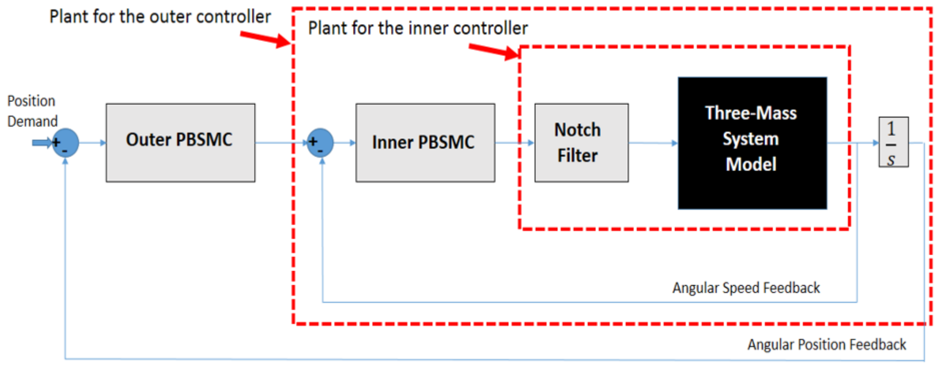

Figure 5.13: Simplified block diagram representation of the plants for inner and outer PBSMCs

According to the configuration given in Fig.5.13, the parameter tuning procedure starts with notch filter sub-structure, which is used to enhance the frequency response characteristic of the system by suppressing its lower resonance frequencies. The center frequency of the notch filter is determined as the first resonance frequency of the system, 14.3 Hz. Since the damping ratio of the notch filter determines the suppression amount of the filter and is inversely proportional to the depth of the notch, it is chosen small enough to flatten the resonance and as big as possible to avoid the possible problems at the phase response of the plant in the lower frequencies with the decrease in damping. By taking these fact into consideration, the damping ratio is chosen as 0.04 and the asymmetric gain is chosen as 1. Also a double notch filter structure is tried in which one more additional notch filter is added in series to the first filter in order to compensate the second resonance of the system. The center frequency, damping ratio and asymmetric gains of the second notch filter are chosen as 19.2, 0.1 and 2.3 respectively based on the same principles used in the tuning of the first notch filter. Resultant plant responses after the addition of single and double notch filter sub-structures are given in Fig.5.14.

Fig.5.14 shows that with the additional single notch filter sub-structure, phase and gain margins are modified to 69 degrees and 12.5 dB, respectively. On the other hand, the phase and gain margins of the plant with additional double notch filter structure can be found as 60 degrees and 15 dB. So, in order to obtain a smoother

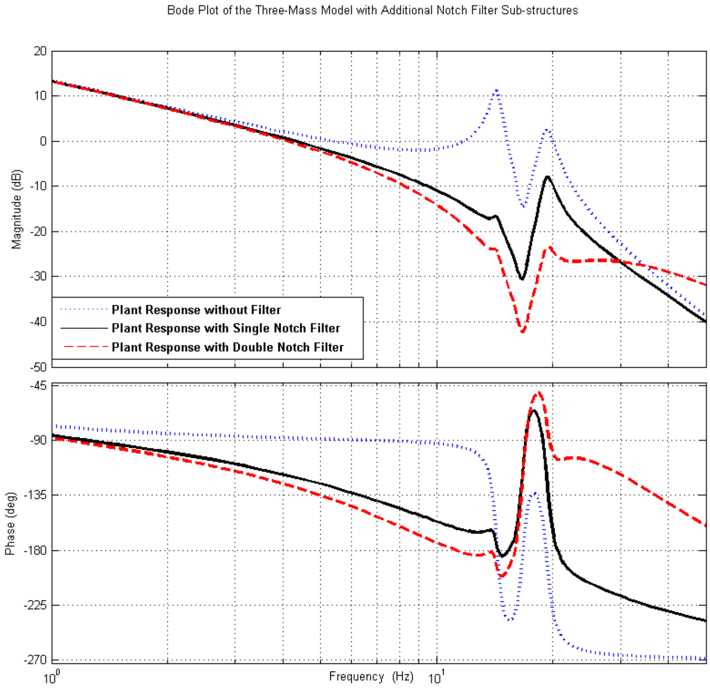

Figure 5.14: Plant responses with the additional notch filter sub-structures

plant response, a double notch filter is used in the proposed control architecture.

By using the obtained plant response with double notch filter as in Fig.5.14, off-line tuning proceeds with PID parameters of the inner PBSMC. During the tuning of the PID parameters, the main purpose is to increase the gains as much as possible to have a better closed loop controller performance with respect to two constraints on phase and gain margins.Since these two margins are very critical for the stability of the system, a boundary is designated to be on the safe side by avoiding the possible instabilities due to non-linearities and other effects that cannot be seen in the linear model. As a rule of thumb, the minimum limits of gain and phase margins are specified as 6 dB and 30 degrees. According to the procedure explained, the proportional and integral gains of the inner PBSMC are determined as 1.7 and 9.35 while the derivative gain is not used since it amplifies the feedback sensor noise coupled to the actual system velocity due to the derivation operation which is highly undesirable. Final open loop frequency response function(FRF) between desired angular speed and actual angular speed of the system obtained with the inner PBSMC controller is given in Fig.5.15.

By using the open loop characteristics, closed loop frequency response function(FRF)

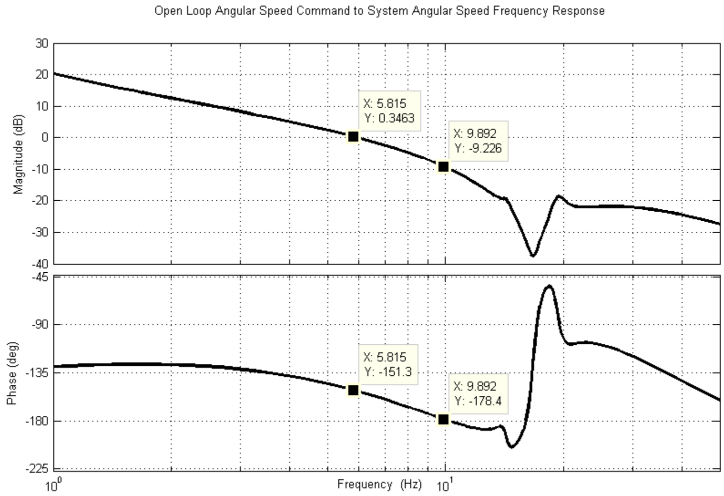

Figure 5.15: Open loop frequency response function(FRF) between desired angular speed and actual angular speed of the system

between desired angular speed and actual angular speed of the system can also be estimated as in Fig.5.16. The bandwidth or 3 dB cut-off frequency of the controller can be found as 9.27 Hz.

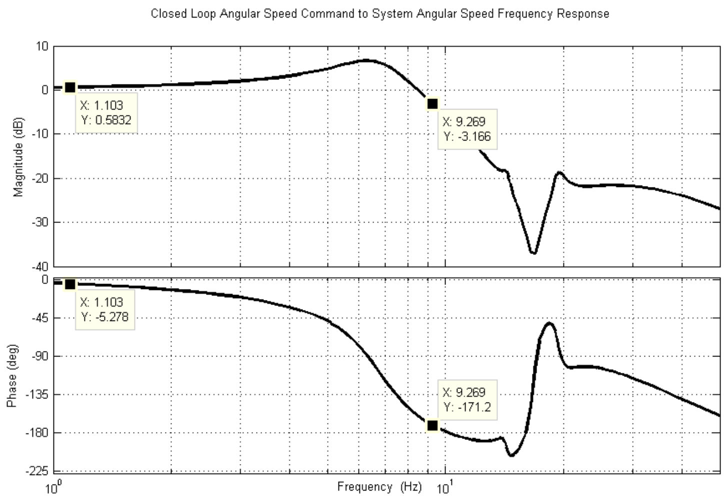

Figure 5.16: Closed loop frequency response function(FRF) between desired angular speed and actual angular speed of the system

After the inner PBSMC is tuned and the frequency response characteristics of the speed loop is obtained, the PID parameters of the outer PBSMC are also tuned by applying the same procedure using the same minimum margin limits as for the inner PBSMC. As a result of the tuning procedure, the proportional gain of the outer PBSMC is determined as 8.5 while the derivative and integral gains are not used.

The decision on elimination of the integral gain is made due to its negative effect on the phase margin at low frequencies. Also derivative gain is not used since it amplifies the encoder quantization error coupled to the actual system position due to the derivation operation which is highly undesirable. Final open loop frequency response function(FRF) between desired position and actual position of the system obtained with the outer PBSMC controller is given in Fig.5.17.

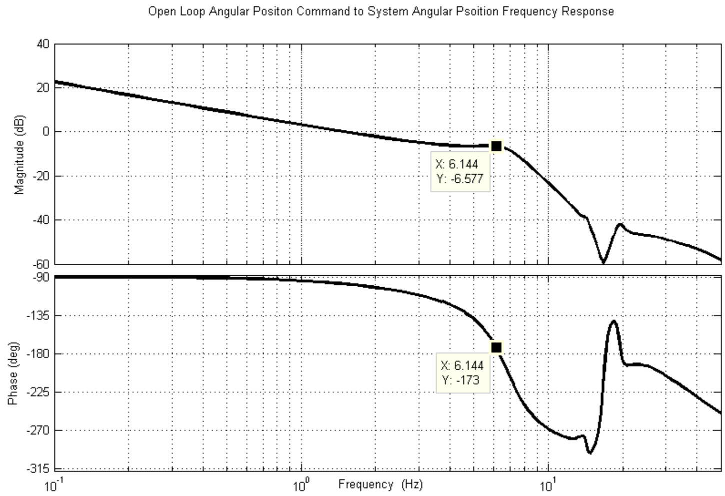

Figure 5.17: Open loop frequency response function(FRF) between desired position and actual position of the system

By using the open loop characteristics, closed loop frequency response function(FRF) between desired position and actual position of the system can also be estimated as in Fig.5.18. The bandwidth or 3 dB cut-off frequency of the controller can be found as 1.8 Hz.

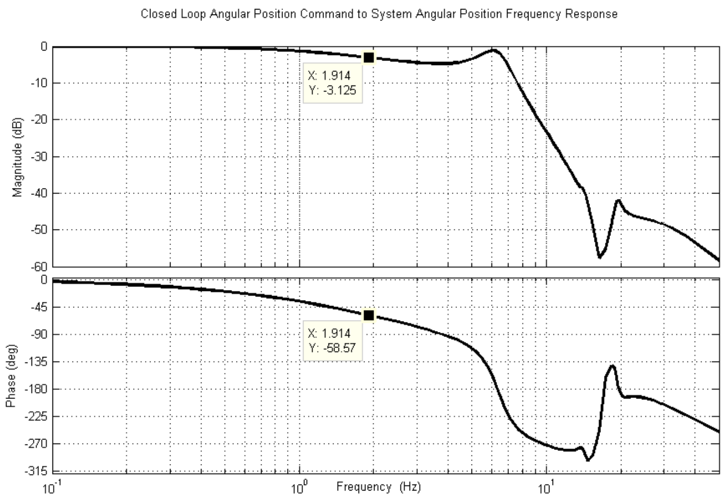

Figure 5.18: Closed loop frequency response function(FRF) between desired position and actual position of the system

5.3 Simulation Results

In order to evaluate the behaviour of the proposed controller, a continuous-time system model is constructed in the enlightenment of the explained analysis and estimations by using MATLAB Simulink. For a better approximation, all the other structures like filters, controllers and observers are constructed in discrete-time as they are also implemented within the digital processor of the real system . A fixed-step solver with step size of 0.001 seconds is used for the simulations and this step size is equal to the sampling time of the real system. At the beginning of each sub-section, first the required on-line tuning procedures will be explained and then performance evaluations will be made. Simulation results start with the comparison of the PBSMC and PID, which is already available on the system, for both inner and outer loops. Then the effects of non-linearities will be shown and performance of the proposed enhancement methods offered for the compensation of these non-linearities will be discussed. The simulation results section will be concluded by simulation results about disturbance rejection capability which is directly related with the stabilization performance.

5.3.1 Comparison of PID and PBSMC

In order to compare the performance of the already available controller on the real system and proposed controller approach to be mounted on the system, two cascaded controller structures are constructed by using conventional output-limited PID controllers with anti-wind up extension and PBSMCs. For a better comparison of the controller structures independent of variations due to parameter tuning, the parameters of the PID controllers and PID part of the PBSMCs are chosen identical and equal to the values calculated in Section 5.3 . Three-mass model with additional notch filter substructure is used in the simulations as the controlled system. First, comparisons are conducted for controllers in the inner speed loop and then similar simulations are repeated for the controllers in the outer position loop to verify the advantages of PBSMC in both loops of the cascaded structure. In the rest of the chapter, conventional PID or conventional force-limited PID controller expressions are also used to denote total force-limited PID controller with anti-wind up extension. This type of PID controller is chosen for the performance comparison since it is the controller structure used for the control of the current actual system.

5.3.1.1 Comparison of PID and PBSMC for Inner Speed Loop

In order to compare the conventional force-limited PID controller and PBSMC, first, force limits of the controllers and SMC parameters of the PBSMC need to be adjusted. Force limits for both controllers are chosen the same and equal to 19800 Nm which is the force limit of the real system. This force limit is guaranteed by a saturation block added at the output of the controller in the conventional PID and in PBSMC this constraint is satisfied directly by just adjusting the controller gain(T) parameter of the PBSMC.

The time constant(H) parameter of the SMC in the PBSMC controller is specifying the global dynamics of the controller which corresponds to the controller response characteristics when large errors occur. So, in order to decide on H parameter of the PBSMC, step response characteristics of the controller for different values of H are investigated. Results obtained in the simulations for 10 deg/s step desired speed signal and for five different H parameter values can be seen in Fig.5.19.

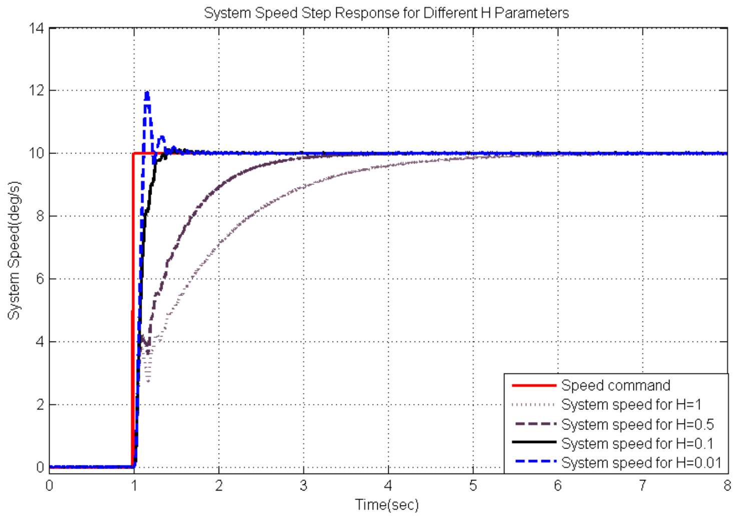

Figure 5.19: Step response characteristics of the inner PBSMC for different values of SMC time constant(H)

Fig.5.19 shows that there is a contradiction between overshoot suppression and settling time for different H values. With the increase of the H parameter, the system response becomes slower and settling time increase while providing a better overshoot suppression. On the other hand, with the reduction in the H parameter, effect of SMC in the PBSMC decrease and overshoots arise although settling time becomes smaller. So, H is chosen as 0.1 which provides optimal equilibrium between overshoot suppression and settling time performance.

After the parameters of the controllers are specified, different scenarios are simulated to compare the performance of the conventional PID with force limit and PBSMC. First, step desired speed signals are applied and the resulting system speeds are investigated to compare the response characteristics of the controller structures when big speed errors occur in the system. Step desired speed signals with 10 deg/s, 20 deg/s and 5 deg/s are given to the system in order to see the effect of error amplitudes on the tracking performance. Results obtained in these three tests can be found in Fig.5.20, Fig.5.21 and Fig.5.22.

As it can be seen from Fig.5.20 and Fig.5.21 that system speed responses with overshoots about 3.4 deg/s and 2.99 deg/s for 10 deg/s and 20 deg/s step speed inputs are

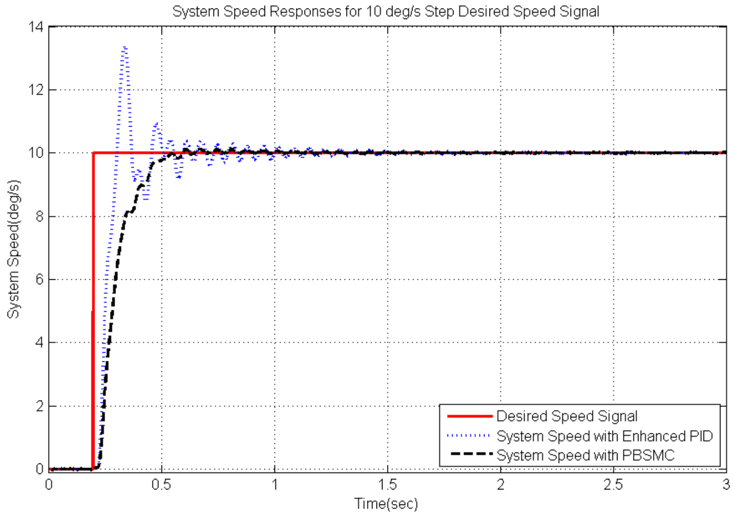

Figure 5.20: Response characteristics of PID and PBSMC for 10 deg/s step desired speed signal

obtained by PID controller. On the other hand, PBSMC provides overshoot-free system speed responses with settling time performance at least as good as PID controller. However, with the decrease in the amplitude of the error as in Fig.5.22 for step input of 5 deg/s, overshoots starts to appear in the system speed despite of the PBSMC. Such overshoots appear due to the fact that SMC in the PBSMC supporting global dynamics is losing its effectiveness with the decrease in the error and PBSMC starts to behave as a pure PID controller which is stated and explained in Chapter 3, Section 3.2.

Torque signals created by PID and PBSMC are also investigated to understand the reason of such differences in the performances and evaluate the possible problems such as chattering, in the implementation of PBSMC to the real system. Torque signals created by the controllers for 10 deg/s step desired speed signals are given in Fig.5.23.

As it can be seen from Fig.5.23, while PID controller is saturated and stuck to the maximum torque limit (19800 Nm), the SMC controller in the PBSMC handles possible saturations better and it does not stuck in the maximum torque limit as much as PID response does which prevents overshooting in the system speed. Also, as it is expected, there are no additional oscillations in the torque signal created by PBSMC

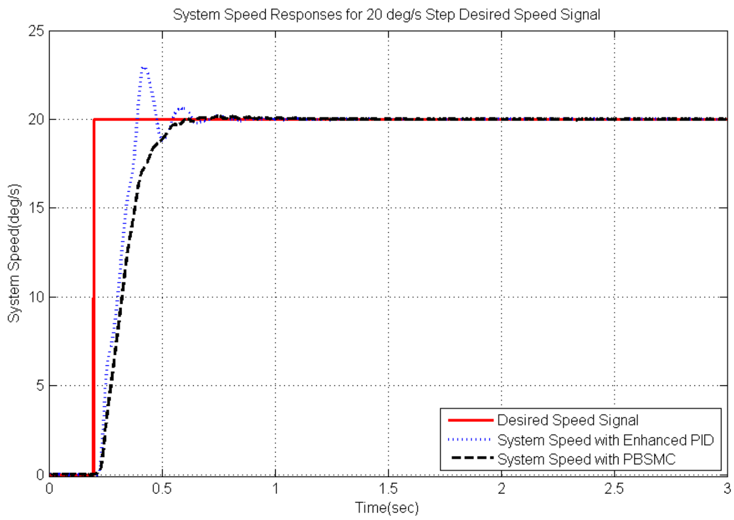

Figure 5.21: Response characteristics of PID and PBSMC for 20 deg/s step desired speed signal

due to chattering problem of SMC which makes the implementation of PBSMC possible in real systems. Noise type of oscillations in both PID's and PBSMC's torque signals are resulted from the gyroscope noise.

After that we showed clear advantages of the PBSMC in global dynamics, its performance in local dynamics are then simulated and evaluated. The aim of this simulation is to prove the claim in Chapter 3 that PBSMC is acting just like conventional PID for small errors and SMC in PBSMC does not have any negative effect on local dynamics. For this simulation 1 deg/s sinusoidal desired speed signal with frequency of 0.5 Hz is given to the controllers. The resulting system speed can be seen in Fig.5.24 and its zoomed in version in Fig.5.25.

As it can be seen from Fig.5.24 and Fig.5.24, system speeds obtained by PID controller and PBSMC are so close to each other that it is very hard to identify the difference even from the zoomed version. That excessively small difference is due to the one sample delay resulted from implementation in discrete-time. However, if the amplitude or frequency of the input sinusoidal wave is increased enough to cause torque saturations, again behaviours of the PID and PBSMC starts to differ from each other and SMC in the PBSMC becomes active. In order to generate such a saturation in the torque demand, a sinusoidal desired speed waveform with 15 deg/s amplitude and 2

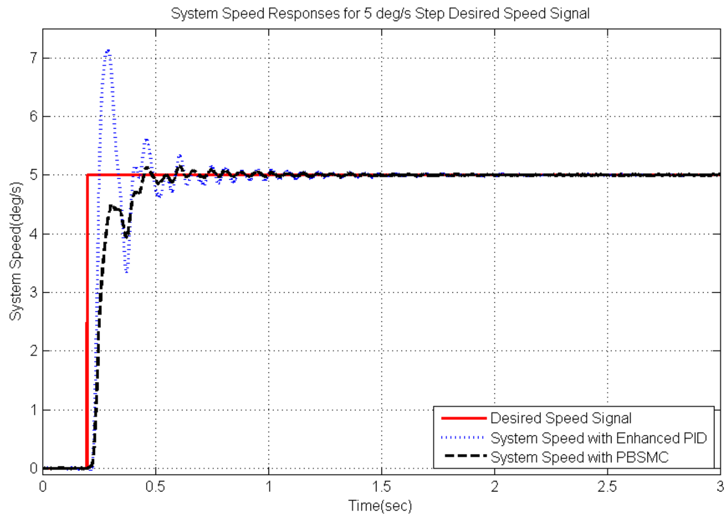

Figure 5.22: Response characteristics of PID and PBSMC for 5 deg/s step desired speed signal

Hz frequency is applied to the system. System speeds and torque signals created by PID and PBMSC for such desired speed signal are shown in Fig.5.26 and Fig.5.27.

System speeds and torque signals created by controllers seen in Fig.5.26 and Fig.5.27 clearly exhibits that PBSMC can handle the torque saturation situations much better than PID and avoids overshoots even for sinusoidal type of desired speed signals and unexpected oscillations are successfully damped. For example, oscillations appeared in the speed of the system with PID controller are resulted from the motion of the first inertia in the model. This correlation can be detected from the correspondence between frequencies of the oscillations in the system speed and the first inertia's motion. Motion of the first inertia for the same scenario are shown in Fig.5.28 for comparison.

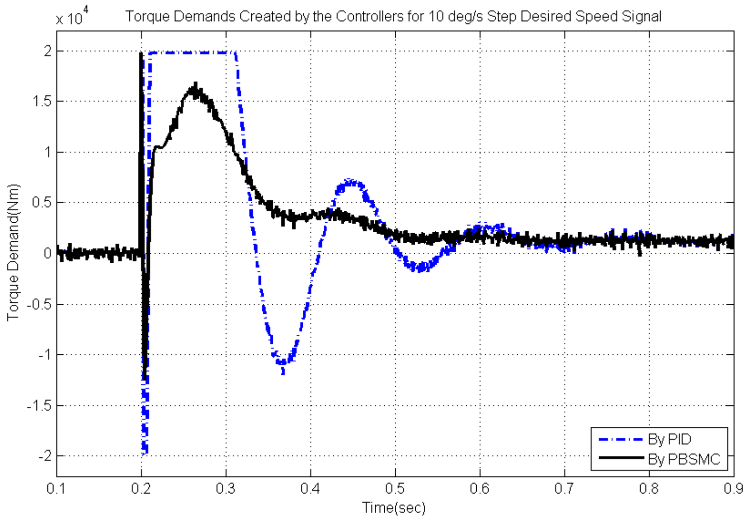

Figure 5.23: Torque demand signals created by PID and PBSMC for 10 deg/s step desired speed signal

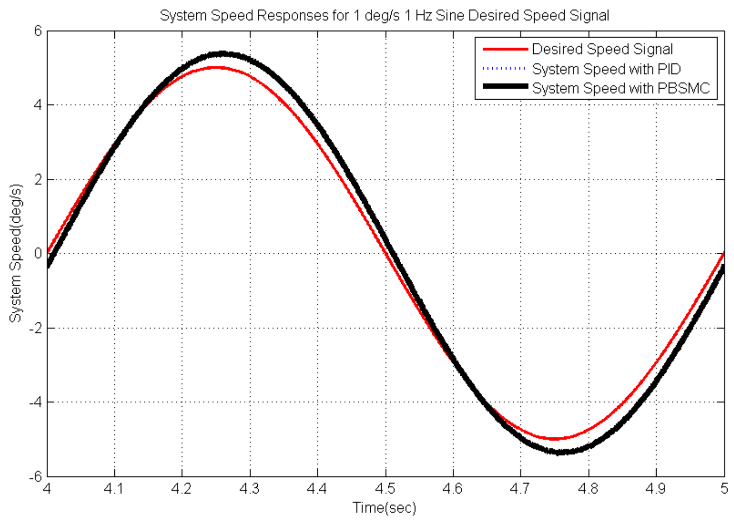

Figure 5.24: Response characteristics of PID and PBSMC for 1 deg/s 1 Hz sine desired speed signal

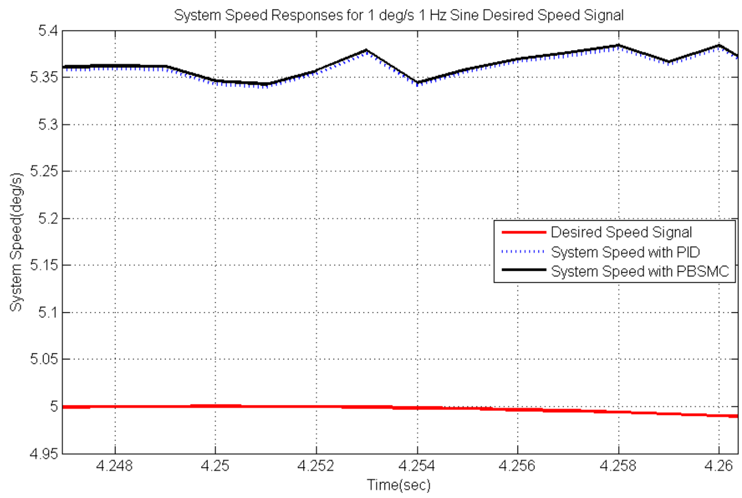

Figure 5.25: Response characteristics of PID and PBSMC for 1 deg/s 1 Hz sine desired speed signal, zoomed to a peak of the sine

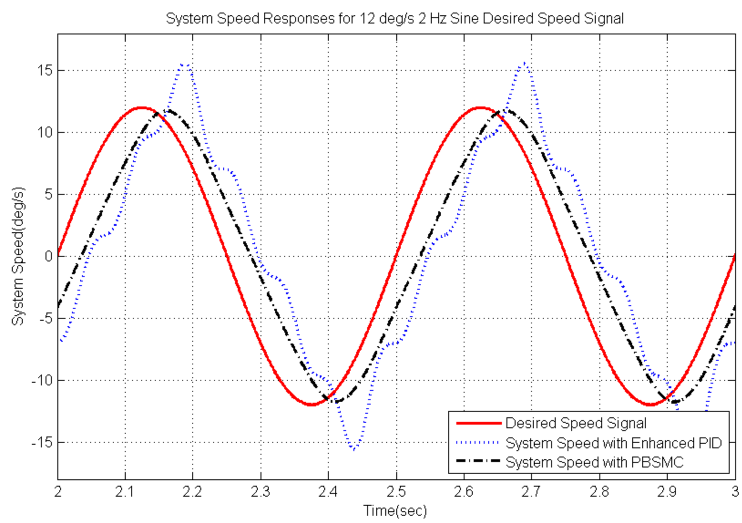

Figure 5.26: Response characteristics of PID and PBSMC for 12 deg/s 2 Hz sine desired speed signal

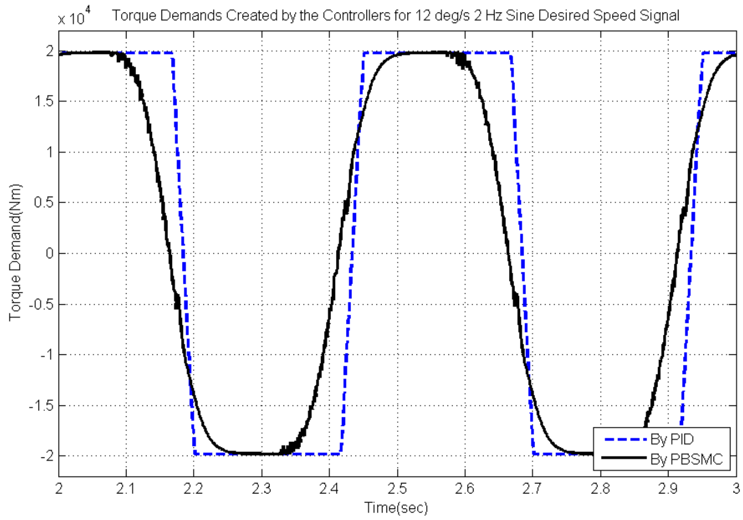

Figure 5.27: Torque demand signals created by PID and PBSMC for 12 deg/s 2 Hz sine desired speed signal

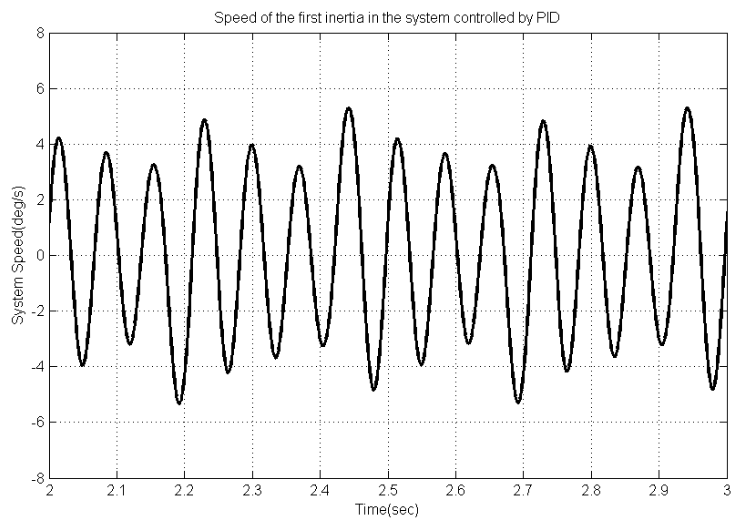

Figure 5.28: Speed of the first inertia in the system controlled by PID for 12 deg/s 2 Hz sine desired speed signal

5.3.1.2 Comparison of Cascaded PID and PBSMC for Position Loop

Similar simulations carried out for the inner loop are also repeated for the outer loop, in order to compare the performance of cascaded PBSMCs with conventional cascaded PID controllers in position control. Detailed explanations given in the previous section will not be repeated for the outer loop simulations to avoid useless duplications. The comparisons yielding to same discussions will only be mentioned. First, speed limits of the controllers and SMC parameters of the PBSMC need to be adjusted. Speed limits for both controllers are chosen identical and equal to 30 deg/s which is the speed limit of the real system. This speed limit is guaranteed by a saturation block added at the output of the controller in conventional PID and in PBSMC this constraint is satisfied by just adjusting the controller gain(T) parameter of the PBSMC.

In order to decide on the H parameter of the outer PBSMC, step response characteristics of the controller for different values of H are investigated as it is made for the PBSMC in the inner loop. Results obtained in the simulations for 10 degs step desired position signal for five different H parameters can be seen in Fig.5.29.

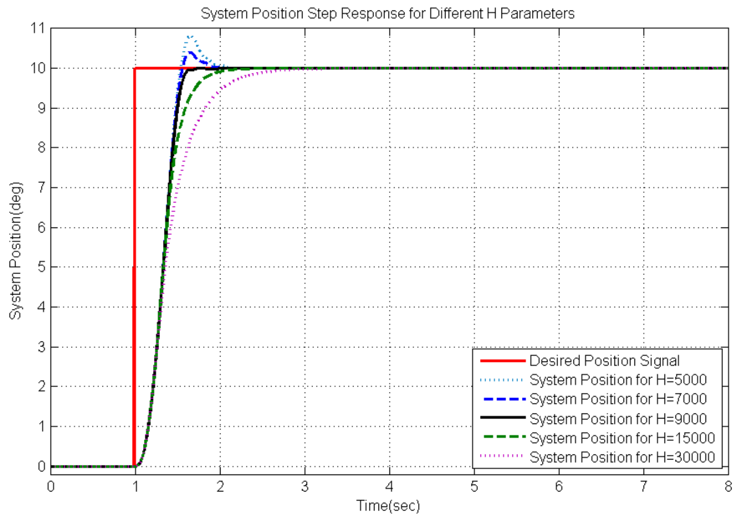

Figure 5.29: Step response characteristics of the position PBSMC for different values of SMC time constant(H)

Simulation results given in Fig.5.29 show that with the increase of the H parameter the system response becomes over-damped and settling time increase while providing better overshoot suppression. On the other hand, with the reduction in the H parameter, the effect of SMC in the PBSMC decrease and tends to increase the occurrence of the overshoots as in the PBSMC used for speed control. So, H is chosen as 9000 which provides optimal equilibrium between overshoot suppression and settling time performance.

After tuning the parameters of the controllers, different scenarios are simulated to compare the performance of the cascaded PID and the proposed cascaded PBSMC structure. First, step desired position signals are applied and resultant system positions are investigated to compare the response characteristics of controller structures when big position errors occur in the system. Step desired speed signals with 10 degs, 40 degs and 2 degs amplitudes are applied to the system in order to see the effect of error amplitudes on the tracking performance. Results obtained in these three tests can be found in Fig.5.30, Fig.5.31 and Fig.5.32.

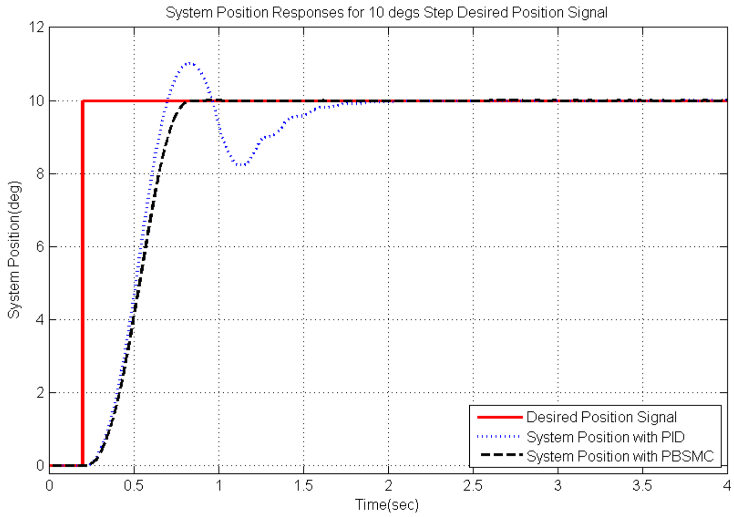

Figure 5.30: Response characteristics of cascaded PID and PBSMC for 10 degs step desired position signal

As it can be seen from Fig.5.30, Fig.5.31 and Fig.5.32; cascaded PID controller provides system position responses with overshoots about 1.7 degs, 2.1 degs and 2.85 degs for 10 degs, 40 degs and 5 degs step desired position inputs. On the other hand, PBSMC provides overshoot-free system position responses with settling time performance at least as good as PID controller as in the inner speed loop. The only difference between the inner position loop and the outer speed loop results is that cascaded

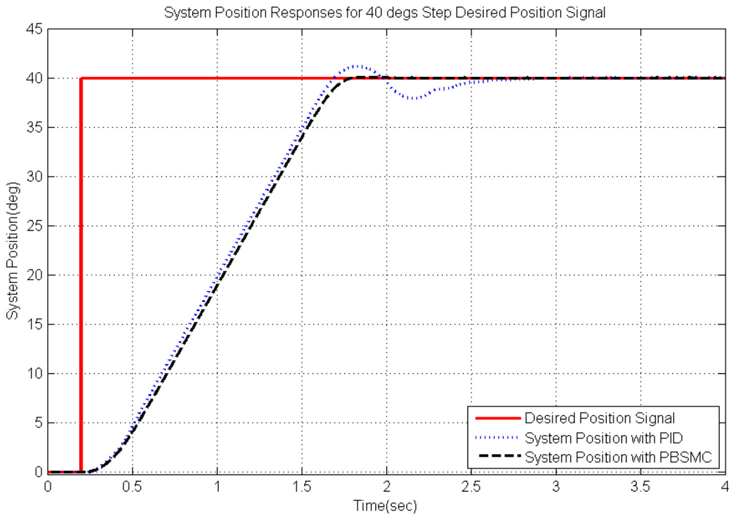

Figure 5.31: Response characteristics of cascaded PID and PBSMC for 40 degs step desired position signal

PBSMC continues its superiority over cascaded PID for much smaller amplitudes of the step input. Although SMC in the outer PBSMC looses its effect with the decrease in the amplitude of the step desired position signal as expected, SMC in the inner loop stays active and prolongs the superiority of the PBSMC for much smaller step inputs up to a certain point.

Torque signals created by two cascaded controller structures and desired speed signals created by the outer controllers are also investigated to understand the reason of such differences in the performance and also to detect the effect of the SMCs in the inner and the outer PBSMCs. Torque and speed signals created by controllers for 10 degs step desired position signal are given in Fig.5.33, while the signals created for 2 degs step desired position signal are as given in Fig.5.34.

As it can be seen in the signals given in Fig.5.33 for 10 degs step desired position signal; PID controllers saturate and get stuck to the maximum torque(19800 Nm) and speed (30 deg/s) limits respectively. On the other hand, SMCs in the inner and outer PBSMCs handles torque and speed saturations better and avoids possible overshoots in the system position. Different from Fig.5.33, measurements given in Fig.5.34 show that speed saturation does not occur at the tracking of the 2 degs step desired position signal due to the smaller amplitude and the outer PBSMC just acts like a PID. How-

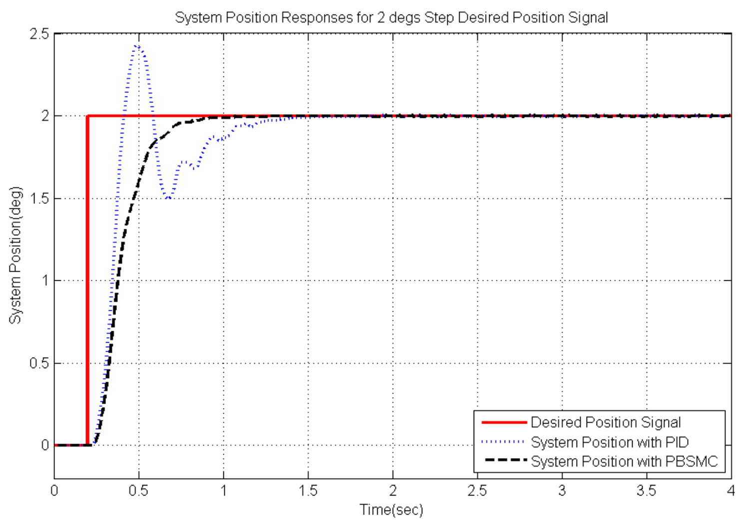

Figure 5.32: Response characteristics of cascaded PID and PBSMC for 2 degs step desired position signal

ever, even 2 degs step desired position signal results in saturations in the torque signal and activates the SMC dynamics in the inner PBSMC. So the SMC in the inner loop stays active and maintains the superiority of the cascaded PBSMC over cascaded PID even for smaller step inputs up to a point, although SMC in the outer PBSMC looses its effectiveness with the decrease in the amplitude of the step desired position signal as expected.

After the advantages of cascaded PBSMC in the step response characteristics, its impact on local dynamics of the controller is evaluated by a simulation. The aim of this simulation is to prove the claim in Chapter 3 that cascaded PBSMC is acting just like a cascaded conventional PID for small errors and SMC in PBSMC does not have any negative effect on local dynamics of the controller. For this simulation 5 degs sinusoidal desired position signal with frequency of 0.1 Hz is applied to the controller. The resultant system speed is obtained as in Fig.5.35 and its zoomed in version is shown in Fig.5.36.

As it can be seen from Fig.5.35 and Fig.5.36, system positions obtained by cascaded PID controller and PBSMC are so close to each other that it is very hard to identify the difference even from the zoomed in version, as it was also the case for inner loop controllers. Such little difference between the cascaded controllers is resulted from

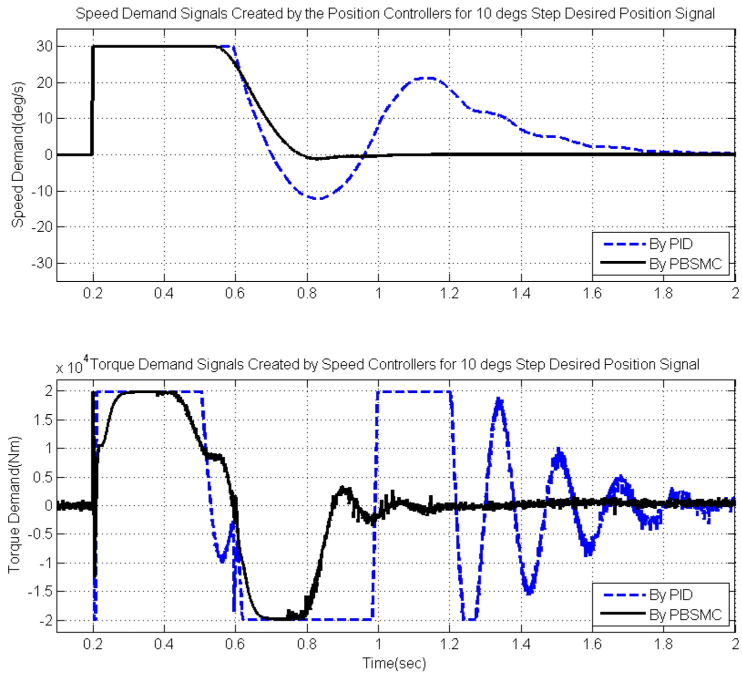

Figure 5.33: Torque and speed demand signals created by cascaded PID and PBSMC for 10 degs step desired position signal case

the one sample delay due to implementation in discrete-time and does not have any significance.

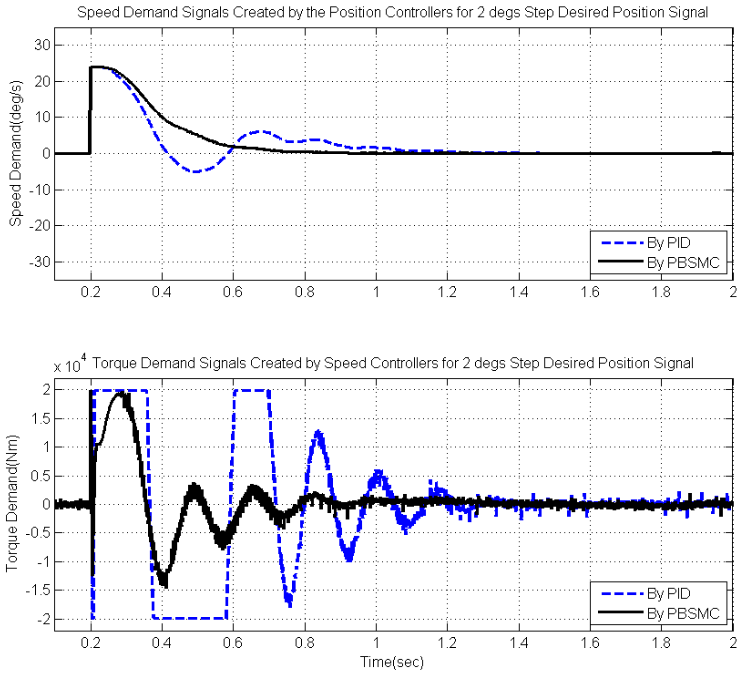

Figure 5.34: Torque and speed demand signals created by cascaded PID and PBSMC for 2 degs step desired position signal case

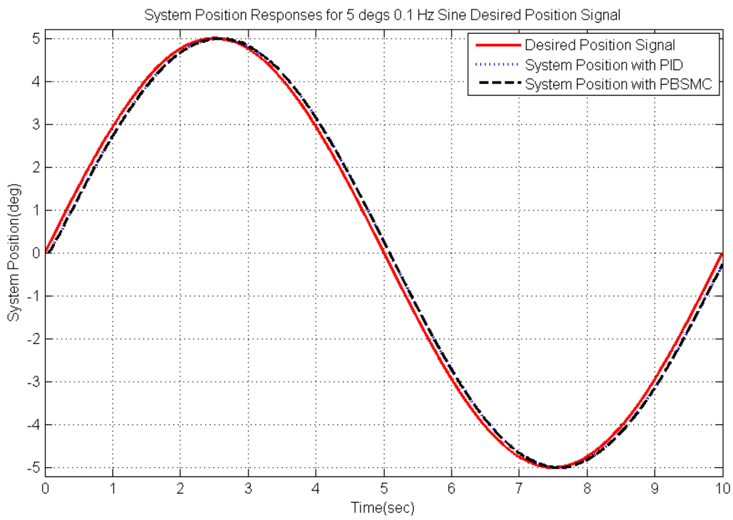

Figure 5.35: Response characteristics of cascaded PID and PBSMC for 5 degs 0.1 Hz sine desired position signal

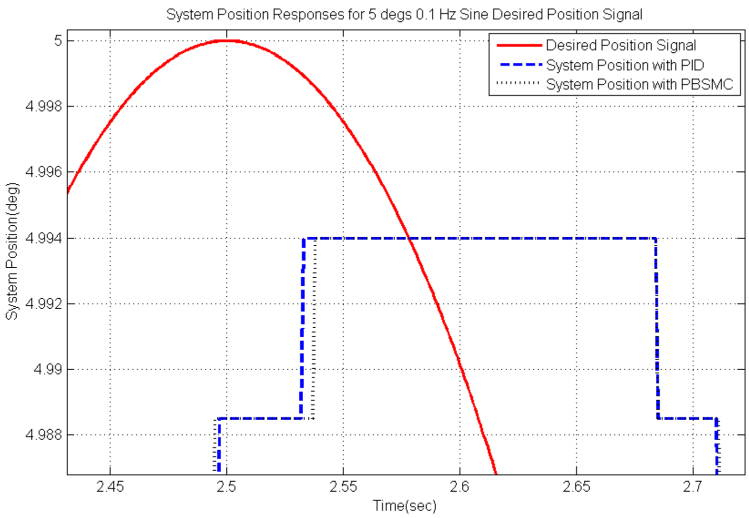

Figure 5.36: Response characteristics of cascaded PID and PBSMC for 5 degs 0.1 Hz sine desired position signal, zoomed to a peak of the sine

5.3.2 Effects of Non-Linearities In the System and Their Compensation

For the simulations in this part, non-linearities identified in Section 5.1.2 are inserted to the three-mass linear system model with additional notch filter used in the previous section and their effects will be investigated first. Then, the disturbance observer structure constructed for the compensation of these non-linearities is added to the inner PBSMC and its contribitions will be evaluated. And finally, the Kalman filter enhancement for disturbance observer will be implemented and its effects in the performance of the observer will be analysed.

5.3.2.1 Effects of Non-Linearities In the System

Non-linearities are active in all scenarios in which the system is running; however, their effects on the system becomes much more powerful and important at lower angular speeds and especially upon changes in the direction of motion leading to zero-crossings. In order to simulate the effects of these non-linearities namely friction and backlash, two separate system models are constructed and the responses of these systems to a sinusoidal desired speed signal with 1 deg/s amplitude and 0.25 Hz frequency are compared. One of these models is just the three-mass linear system model with additional notch filter while the other model also includes the friction and backlash components explained and derived in Section 3.1.2. The inner PBSMC structure obtained in the previous sections is used for the control of angular speed in both system models. System speeds obtained from simulations running for both models can be seen in Fig.5.37 and its zoomed version to zero-crossing is given in Fig.5.38 for better identification.

When the tracking performance of the controllers shown in Fig.5.37 and Fig.5.38 are compared, it can obviously be said that additional backlash and friction distort controller behaviour significantly especially at the zero-crossings. During the stabilization, the aim is to hold the system stationary with respect to earth so that zero-crossings occur very frequently and the system angular speed is low in general.Thus, non-linearities become adversely very effective during stabilization and disturbs the stabilization performance substantially.

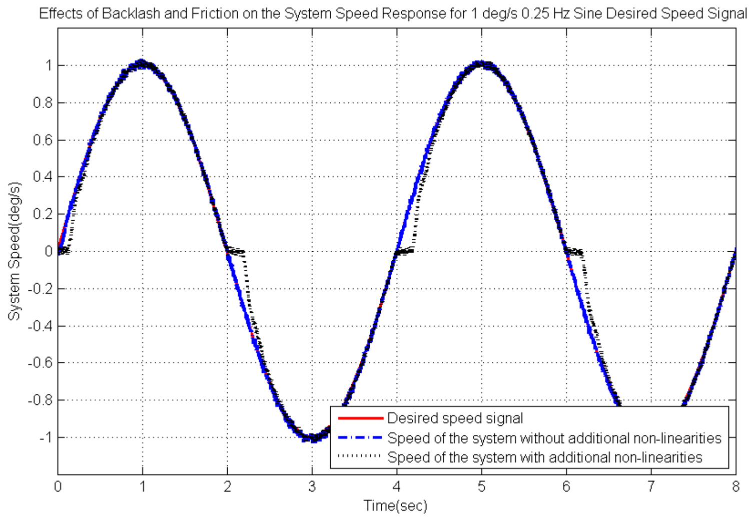

Figure 5.37: Effects of friction and backlash on the system speed for 1 deg/s 0.25 Hz sine desired speed signal

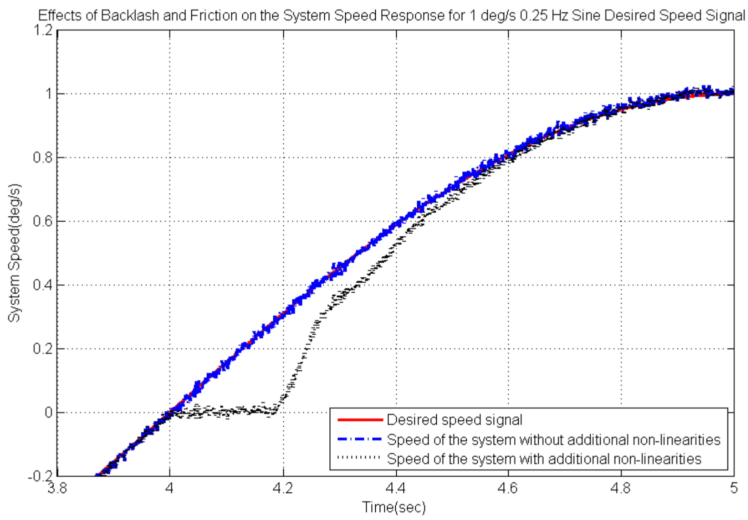

Figure 5.38: Effects of friction and backlash on the system speed for 1 deg/s 0.25 Hz sine desired speed signal, zoomed in to a zero-crossing

5.3.2.2 Disturbance Observer for The Compensation of the Non-linearities

In order to compensate the negative effects of the non-linearities explained in the previous section and improve the stabilization performance, a single state disturbance observer is added to the controller as it is explained in Chapter 4. Such a disturbance observer has two parameters; one is the estimate of system inertia which is calculated directly from the tests made on the real system as in Section 5.1.1, and the other parameter is the observer gain which needs to be tuned experimentally. Observer gain is directly designating the bandwidth of the disturbance observer and needs to be as high as possible to improve the performance of the structure. However, after a certain level, the increase in the gain starts to disturb the main controller performance due to possible estimation errors in the system inertia and amplified gyroscope noise coupled to the torque demand signal. For deciding on the suitable observer gain, a sinusoidal desired speed signal with 1 deg/s amplitude and 0.25 Hz frequency is applied to the system and disturbance estimations of the observer for different observer gains are investigated. Disturbance estimations of the observer for three different values of observer gain can be seen in Fig.5.39.

According to the results given in Fig.5.39, the amplitude of the gyroscope noise coupled to the system increase with the increment in the observer gain, as expected. So, by taking the trade-off between coupled noise and observer bandwidth into consideration, observer gain in the proposed controller is chosen as 3×10^6 because the ratio between the gain and amount of the noise coupled to the system begins to creep up gradually after that level. The effect of the gain in the observer bandwidth will be investigated in disturbance rejection capability section.

After deciding on the observer gain, the disturbance observer's enhancement performance is evaluated through simulations. Two controller structures, one with disturbance observer and the other without any compensator, are constructed and a sinusoidal desired speed signal with 1 deg/s amplitude and 0.25 Hz frequency is applied to the system to observe the improvements. Simulation results for the systems with and without disturbance observer are given in Fig.5.40 and in Fig.5.41 a zooming into a zero-crossing is shown.

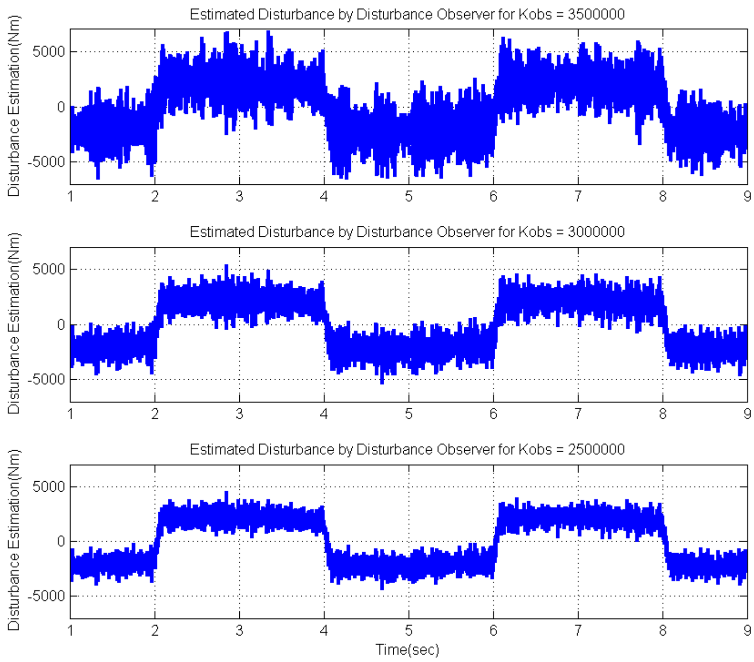

Figure 5.39: Effect of observer gain on the disturbance estimations of the disturbance observer

As it can be seen from Fig.5.40 and Fig.5.41, the system recovers from the impacts of backlash and friction quicker with the additional disturbance observer despite the small overshoots seen in the system speed. Such a contribution of the disturbance observer makes it a very desirable enhancement in a controller structure designed for stabilization since such an improvement in zero-crossing will result in a better stabilization performance. Contributions of disturbance observer to disturbance rejection capability of the controller will be investigated in the following section.

In addition to the analysis about tuning the observer gain and its compensation performance, its robustness against possible errors in the estimate of system inertia is investigated through simulations. Such errors can be resulted from possible faults made in measuring the inertia of the real system or possible inertia variations during the operation due to changes in gun elevation angle or changes in the number of ammunition hold in the turret. To analyse the sensitivity of the observer for such errors in inertia estimation, performance test of disturbance observer are repeated with inertias estimated as 10000 kgm^2 above and below the original inertia(31730 kgm^2) of the system and results are compared. Results obtained from these simulations are

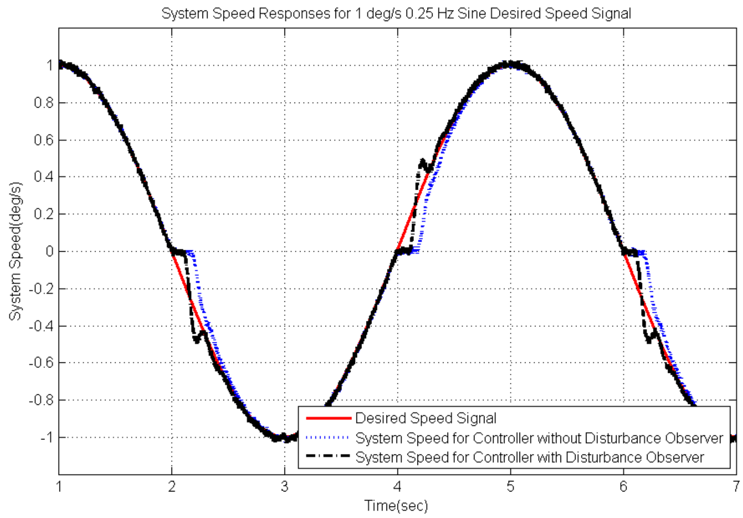

Figure 5.40: Performance of the disturbance observer in compensating friction and backlash

gathered in Fig.5.42.

From the results given in Fig.5.42, it can be said that if lower inertia estimates are used in the disturbance observer then overshoots in the zero-crossing increase while higher inertia estimates increase the settling time of the observer. However; result of variations in the estimated inertia are not fatal and not that much effective in the performance of the disturbance observer despite the high error rates: 10000 kgm^2 which corresponds to 33 percent error, tested in the simulations. So, it can be said that single state disturbance observer is insensitive to possible estimation errors due to its closed loop structure and such an insensitivity makes it a very desirable compensator for the application platform of the thesis.

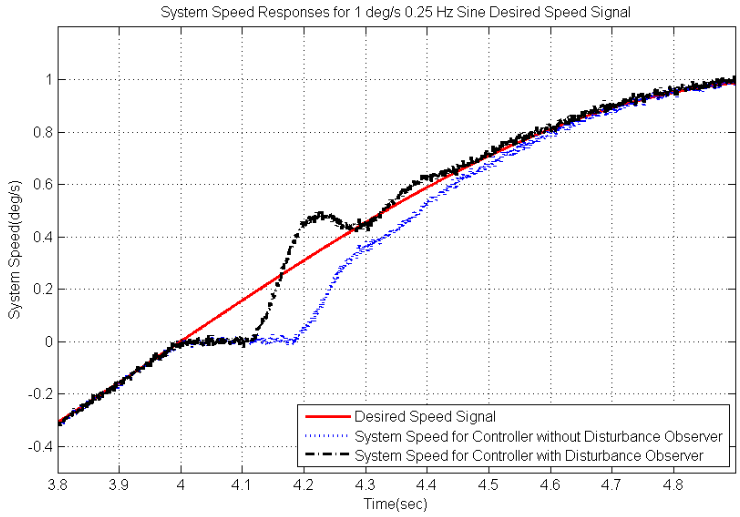

Figure 5.41: Performance of the disturbance observer in compensating friction and backlash, zoomed in to a zero-crossing

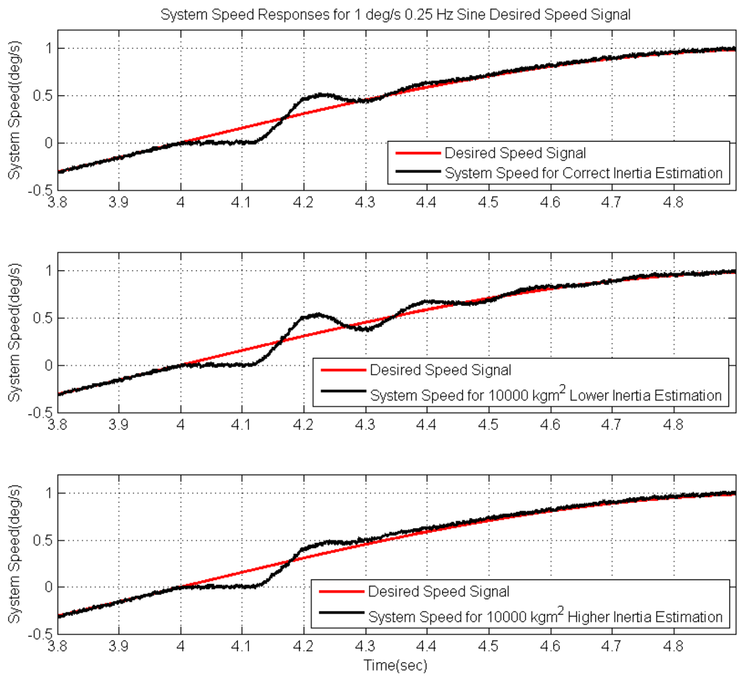

Figure 5.42: Sensitivity of the disturbance observer against the errors in the inertia estimation

5.3.2.3 Additional Kalman Filter

To reduce the noise coupling problem of the disturbance observer, a Kalman filter is integrated to the input path of the observer structures. The measurement noise covariance parameters of the Kalman filter are determined by analysing the sensor measurements taken from the real system in Section 5.1.3. However, deciding on the modelling noise covariance of the filter is not that easy by analysis so simulations are made for on-line tuning. A sinusoidal desired speed signal with 1 deg/s amplitude and 1 Hz frequency is applied to the system and system speed measurement is used as the input signal of the Kalman filter with the measurements obtained from encoder and feed-forward gyroscope. In these tests, noise component of the feed-forward gyroscope measurements is active and mean value of the base motion is set to zero. In order to determine the optimal modelling noise covariance, filtered measurements are obtained for different covariance values and compared with the system speed measurement for two different frequencies, namely 0.5 Hz and 10 Hz. Filtered measurements obtained through simulations are given in Fig.5.43 and Fig.5.44.

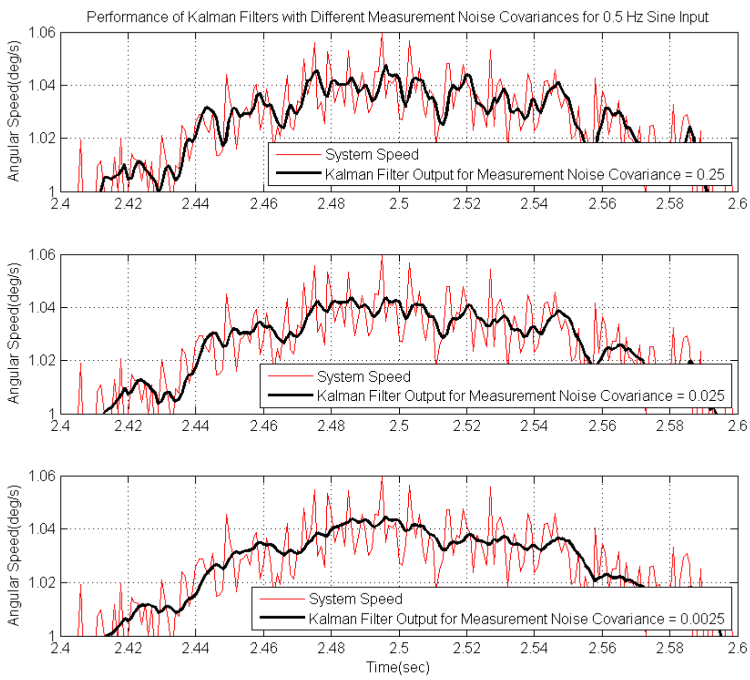

Figure 5.43: Performance of Kalman filters with different measurement covariances for 0.5 Hz sinusoidal input

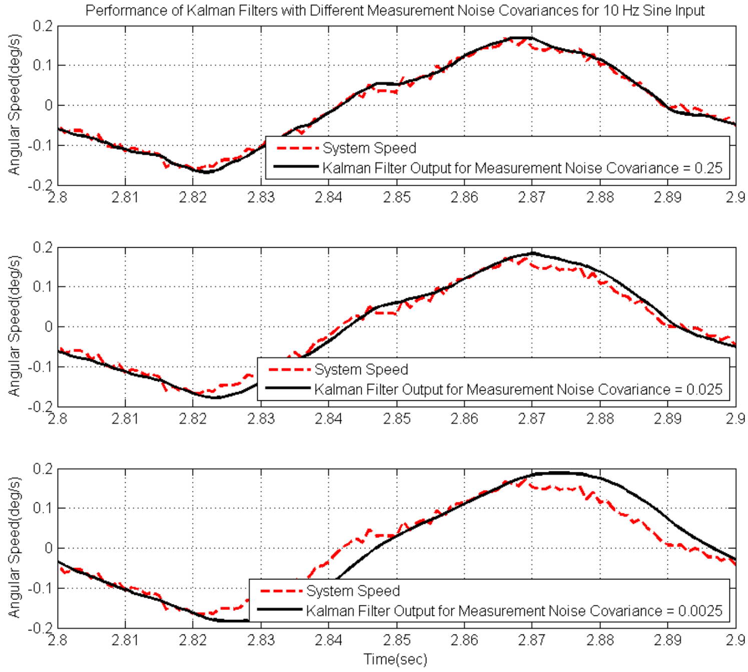

Figure 5.44: Performance of Kalman filters with different measurement covariances for 10 Hz sinusoidal input

The purpose of simulations made with 0.5 Hz sinusoidal input is to measure the rate of increase in the noise suppression performance with the decrease in the modelling noise covariance. On the other hand, by simulations made with 10 Hz sinusoidal input, the effect of modelling noise covariance upon estimation performance of high frequency signals are evaluated. 10 Hz is chosen as the upper limit frequency for these simulations since the system bandwidth does not exceed such frequencies and non-linearities are not that much effective at higher frequencies. From the results in Fig.5.43 and Fig.5.44, modelling noise covariance of the Kalman filter is determined as 0.025 in order to maintain the balance between noise suppression and estimation performances.

After deciding on the parameters and finalizing the Kalman filter design, simulations about its effect on the disturbance observer performance is conducted. With the addition of the Kalman filter, noise in the estimations of the disturbance observer needs to be suppressed according to the expectations. To investigate the existence of such a suppression, a sinusoidal desired speed signal with 1 deg/s amplitude and 0.25 Hz frequency is given to the system and disturbance estimations of the observers with and without Kalman filter are compared. Disturbance estimations of the observers can be seen in Fig.5.45.

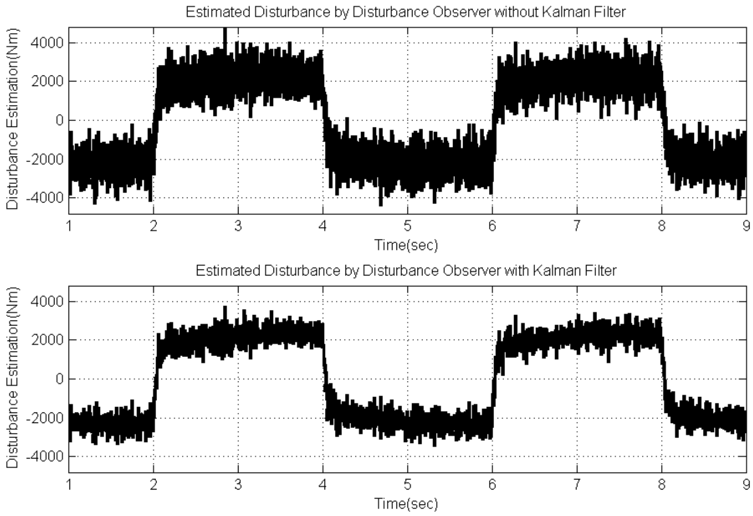

Figure 5.45: Effect of the Kalman filter on the observer's disturbance estimations

From the disturbance estimations given in Fig.5.45, it can be said that the amount of gyroscope noise coupled to the estimations are decreased about 1.8 times with the additional Kalman filter. This reduction ratio can be increased by decreasing the modelling noise covariance parameter of the Kalman filter but side-effects explained in the previous paragraph should be taken into account. Also, such a reduction rate is sufficient for the system model used in the simulations because amount of gyroscope noise coupled to the torque signal created by the cascaded PBSMC is similar to the noise in estimations. So, additional suppression would not reduce the noise in the total torque signal significantly. Simulations about the effects of gyroscope noise on the system speed are not made with the constructed model since these effects are closely related with the relationship between the torque signal created by the controller and the actual torque provided by the motors and transmitted to the system. However, the modelling of such a relationship is out of the scope of the thesis and such analysis will be made directly by the experiments carried on the real system.

5.3.3 Disturbance Rejection Capability

Disturbance rejection capability of the proposed controller is very important especially for a better stabilization performance. In this subsection, disturbance torques with different structures will be applied to the system model to simulate the possible scenarios during the operation of the real system. During these simulations, constant zero desired speed signals will be given to the system and speed of the system will be observed. Throughout the simulations, performance of the proposed controller will be compared to the conventional force-limited PID controller with anti-wind up extension.

First, sinusoidal disturbance torques with 5000 Nm amplitude are applied to the model to simulate the effects of the common base motion on the real system. Simulations are repeated for sinusoidal inputs with 0.25 Hz, 1 Hz and 5 Hz frequencies. Resultant speeds measured at the output of the system models incorporating PID and enhanced PBSMC can be seen in Fig.5.46, Fig.5.47 and Fig.5.48.

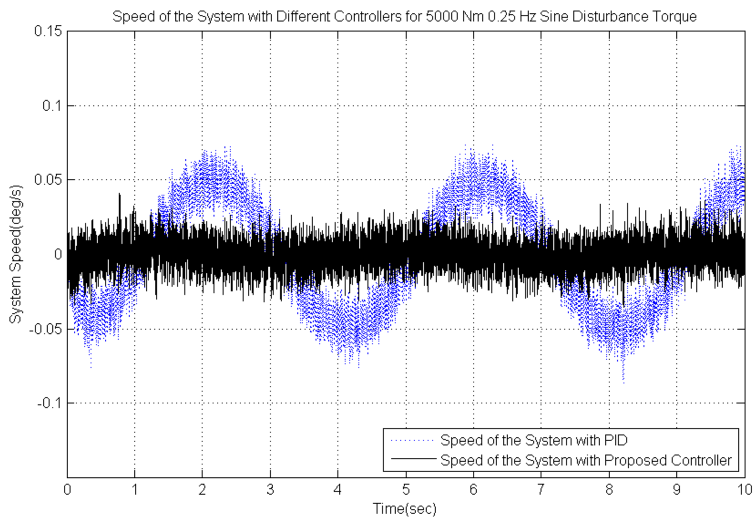

Figure 5.46: Disturbance rejection capability of the controllers for 0.25 Hz sine disturbance torque

The results given in Fig.5.46, Fig.5.47 and Fig.5.48 show that the proposed controller structure provides a much better disturbance rejection performance compared to the PID. Such a better performance of the proposed controller results from the additional disturbance observer enhancement available in the proposed architecture. The superi-

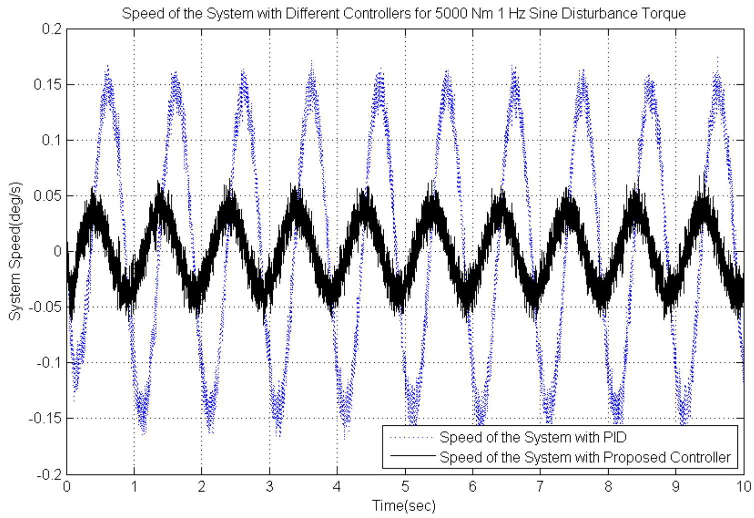

Figure 5.47: Disturbance rejection capability of the controllers for 1 Hz sine disturbance torque

ority of the proposed controller over PID decreases with the increase in the frequency of the disturbance torque just due to bandwidth limitation of the disturbance observer, which is also expected theoretically.

In addition to sinusoidal disturbances, step disturbance torques with amplitudes above the available torque limit (19800 Nm) of the system is applied to the system to simulate the response of the system to sharper disturbance patterns like shocks. These step disturbance torques are applied to the system model with two controller structures for 200 milliseconds and their amplitude is 25000 Nm. Resultant system model speeds measured during the simulations are given in Fig.5.49. In the simulations the step disturbance starts at 0.2^{nd} second and ends at 0.4^{th} second.

As it can be seen from the simulation results given in Fig.5.49, our proposed solution has a disturbance rejection performance for shock type of disturbances is also greater than the currently used PID controller. However, different from the sinusoidal disturbance case, SMC part of the PBSMC also plays an important role in rejecting the step disturbance with amplitudes over the torque limit in addition to the disturbance observer. With the contribution of the SMC in PBSMC, our proposed controller handles the torque saturation due to high disturbance better than the conventional PID controller, and helps to improve the total system disturbance rejection performance.

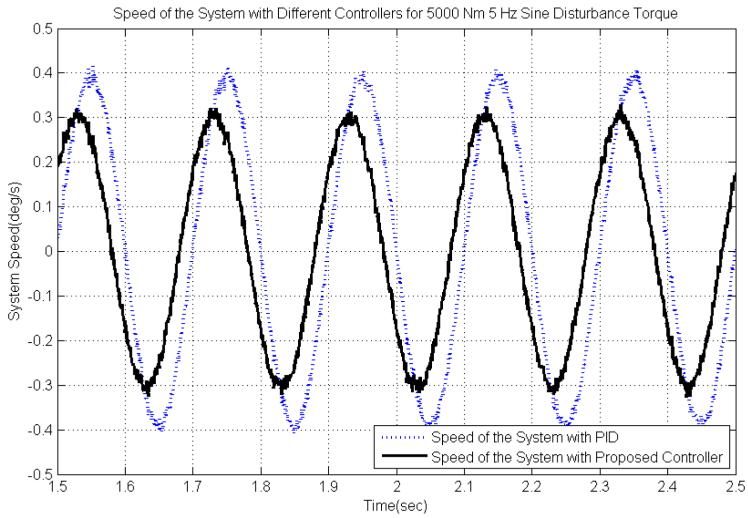

Figure 5.48: Disturbance rejection capability of the controllers for 5 Hz sine disturbance torque

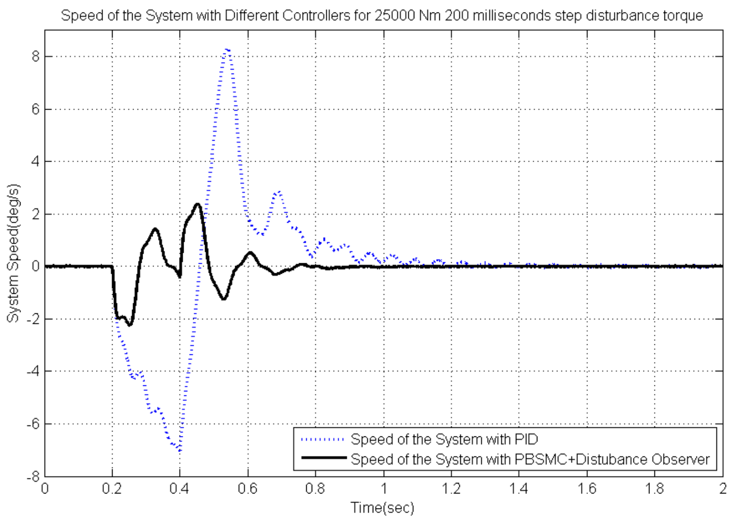

Figure 5.49: Disturbance rejection capability of the controllers for 25000 Nm 200 milliseconds step disturbance torque

CHAPTER 6

HARDWARE EXPERIMENTAL RESULTS AND DISCUSSIONS

Experiments made on the real system are the most important part of this thesis work since they form the validation of our novelty when operating in a real system. All the studies and simulations explained in the previous chapters are conducted as preparative works towards the test results given in this chapter. After the success of our proposed controller structure verified by simulation results, the proposed controller is integrated to the real system for running the real time experiments.

In these experiments, our proposed controller is realized in MATLAB Simulink and then converted to C code to be implemented in the DSP of a gun-turret platform prototype. This chapter starts with off-line tuning of the possible parameters used in the porposed controller. Then results obtained throughout the experiments are given. First, the PBSMC or main controller sub-structure of the proposed controller is compared with the enhanced PID controller currently used for the control of the hardware. After verifying the advantages of the PBSMC, the effects of dominant non-linearities in the system and effectiveness of the disturbance observer with additional Kalman Filter offered as a compensation is tested by experiments. This chapter is finalized by results of the disturbance rejection capability experiments made on the 6-DOF motion simulator.

6.1 Off-line Tuning of the Possible Parameters

Before starting the experiments on the real system, some parameters of the proposed controller are determined by off-line tuning procedures. First of all, the SMC control gain of the inner PBSMC is designated as 19800 Nm which is the torque limit of the real system and the SMC control gain of the outer PBSMC is designated as 30 deg/s which is the speed limit of the real system. Also measurement covariances of the Kalman Filter have already been determined by analysing the raw measurements taken from the sensors before the simulations and the modelling noise covariance is found by on-line tuning methods with required simulations in the previous Chapter. These covariance values of the Kalman filter are directly used in the experiments. Lastly, the PID parameters of the inner and outer PBSMC are determined by frequency domain analysis using Bode plots as it is done for the proposed control used in the simulations.

Frequency domain tuning procedure for PID parameters of the PBSMCs starts with the acquisitons of the plant response or open loop frequency response function(FRF) of the real system between torque input and corresponding angular system velocity. These experiments are also made for the modelling of the system, details of which are explained in Chapter 5 and resultant plant responses for different amplitudes of the sinusoidal torque input are given in Fig.5.2. The plant response of the real system given in Fig.5.2 is used in the off-line tuning of the PID parameters.

When the plant response of the real system in Fig.5.2 is investigated, the gain margin limitation due the first resonance can be seen. Due to the limited gain margin, controller gains cannot be increased enough not to disturb the stability of the system so a very limited controller performance can be obtained. To remove such a limitation on gain margin due to resonance, a notch filter is integrated to the controller to suppress the first resonance of the system. Different from the simulations, in the controller proposed for the control of the real system, a single notch filter is used rather than double notch sub-structure since the amplitude of the second resonance is smaller and does not limit the gain margin as much as in the system model used for simulations. The center frequency of the notch filter is designated as 14.25 Hz which corresponds to the first resonance frequency as expected. Damping ratio of the notch filter is determined as 0.035 to suppress the first resonance and flatten the plant response. The asymmetric gain value is assigned as 1 so notch filter in the proposed controller is used as symmetric. The resultant enhanced plant response obtained after the addition of the single franklin notch filter can be seen in Fig.6.1.

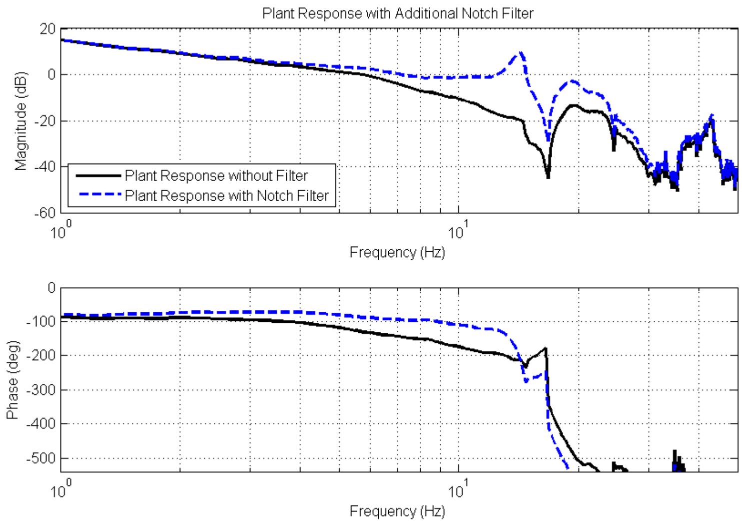

Figure 6.1: Plant response of the real system with the additional notch filter

According to the enhanced plant response of the real system in Fig.6.1, the PID parameters of the inner PBSMC are determined with the same way as in the simulations. Gains of the controller are increased as much as possible until the open loop response with the controller exceeds the gain and phase margin limits for the stability of the system. Safety limits for gain and phase margins are again taken as 6 dB and 30 degrees to ensure the stability of the system. By taking these principles into account, the proportional gain of the inner PBSMC is determined as 1.7 while the integral gain is adjusted to 8.5 and the derivative gain is not used since it amplifies the feedback sensor noise coupled to the actual system velocity due to the derivation operation which is highly undesirable. The resultant open loop frequency response function(FRF) between the desired speed signal and the actual speed of the system for these PID parameters is given in Fig.6.2.

Using the open loop frequency response function(FRF) given in Fig.6.2, the closed loop FRF between the desired speed signal and the actual speed of the system can be calculated as in Fig.6.3. The bandwidth (3-dB cut-off frequency) of the inner speed loop can also be estimated as 10.25 Hz.

The plant response for the outer controller can be defined as the closed loop frequency response function between the desired speed signal and the actual position of the system whose schematic representation is given in Fig.5.13 and is derived by using

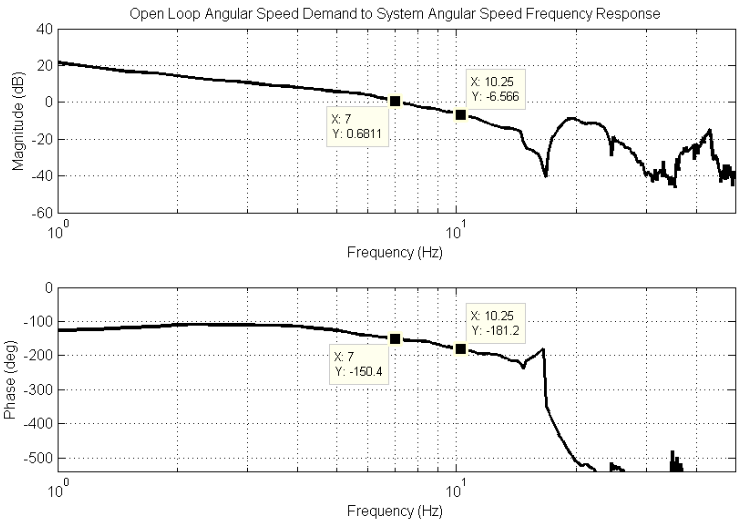

Figure 6.2: Open loop frequency response function(FRF) between the desired speed signal and the actual speed of the system

the closed loop response estimate of the inner loop. The plant response derived from the closed loop response estimate of the inner loop is as given in Fig.6.4.

The PID parameters of the outer PBSMC are determined using the estimate plant response given in Fig.6.2 and the same off-line tuning procedure in frequency domain explained for the PID parameters of the inner PBSMC. As a result, the proportional gain of the outer PBSMC is determined as 9.5 while the integral and derivative gains of the PBSMC are not used. Similar to the inner loop, derivative gain is not used since it amplifies the encoder quantization error coupled to the actual system position due to the derivation operation which is highly undesirable. Integral gain is omitted in addition to the derivative gain in the outer PBSMC because even a small amount of integral gain disturbs the phase margin conditions in low frequencies. The resultant open loop frequency response function(FRF) between the desired position signal and the actual position of the system for these PID parameters is given in Fig.6.5.

By using the open loop frequency response function(FRF) for the outer loop given in Fig.6.5, closed loop FRF between the desired position signal and the actual position of the system can be calculated as in Fig.6.6. The bandwidth (3-dB cut-off frequency) of the outer position loop can also be estimated as 1.75 Hz.

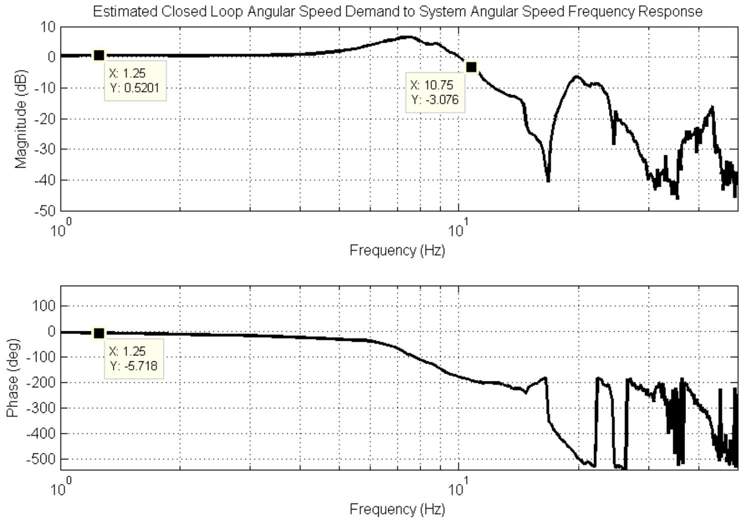

Figure 6.3: Estimate closed loop frequency response function(FRF) between the desired speed signal and the actual speed of the system with inner PBSMC

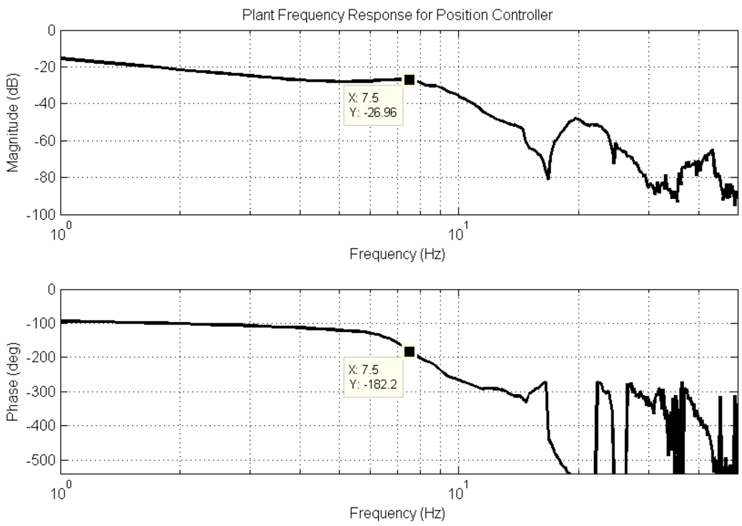

Figure 6.4: Estimate plant response for the outer loop in frequency domain

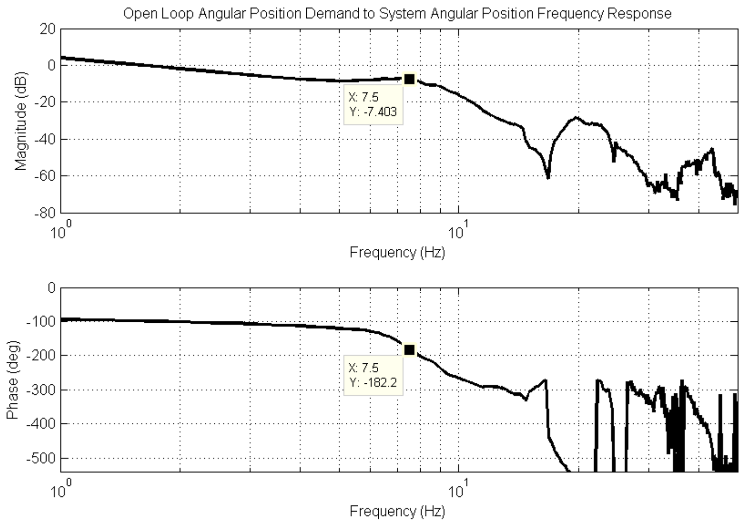

Figure 6.5: Open loop frequency response function(FRF) between the desired position signal and the actual position of the system with the cascaded PBSMC

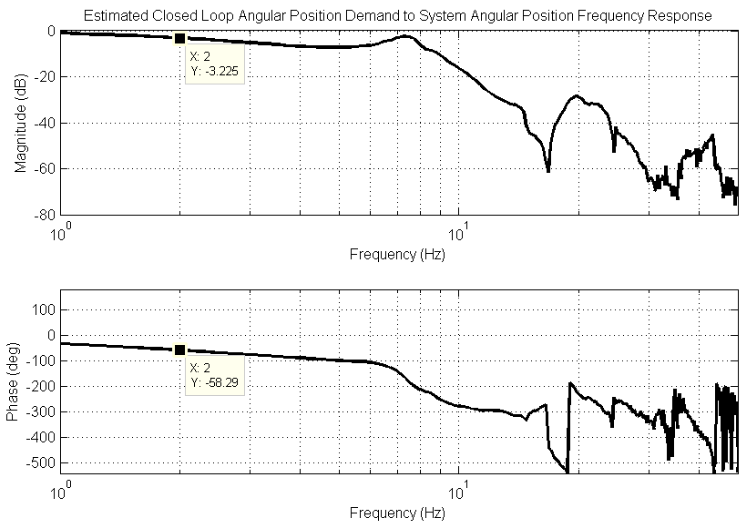

Figure 6.6: Estimate closed loop frequency response function(FRF) between the desired position signal and the actual position of the system with the cascaded PBSMC

6.2 Experimental Results

After completing the off-line tuning of relevant parameters, experiments are conducted on the hardware system to evaluate the performance of the proposed controller structure as a solution of the tracking and stabilization problems. Within each subsection, first the required on-line tuning procedures are carried out and then related experiments are conducted. Each sub-structure of the proposed controller is tuned and validated separately during the experiments. In the test of each sub-structure, that sub-structure is tested for its different parameter sets or compared with its alternatives while other sub-structures are also implemented and tuned optimally if otherwise not stated. Experiments start with the comparison of the PBMSC structures offered in the proposed controller and the enhanced PID controllers already in use in the system. After proving the superiority of the PBSMC structures, effects of the dominant non-linearities and compensation performance of the proposed disturbance observer structure with Kalman filter addition is evaluated with the experiments. The section is finalized with the tests made for observing the improvements in the disturbance rejection capability with the proposed controller architecture compared to the older enhanced PID controller.

6.2.1 Comparison of PID and PBSMC

In this section, the inner PBSMC used for speed control and the cascaded PBSMC structure used for position control are compared with their already used enhanced PID equivalents. Enhanced PID controllers already used in the tests and implemented throughout the comparative experiments are composed of a conventional PID controller, a saturation block at its output as a limiter between predefined boundaries and an anti-wind up structure which restricts the increment in the magnitude of the integrated error if the output reaches the saturation limit. The same notch filters as in simulations are used to enhance frequency response of the real system and parameters of the enhanced PID controller are chosen identical with the PID parameters of the PBSMC for better comparison of the controller structures, independent of the variations due to parameter tuning. For the rest of this chapter, the "enhanced PID" expression is used to denote this whole integrated controller.

6.2.1.1 Comparison of PID and PBSMC for Inner Loop

As it is claimed in the explanations about PBSMC and validated by simulations, PB-SMC used in the inner loop is expected to provide an overdamped response for big error signals such as under step desired speed inputs and to have the same response characteristics as PID's for small error signals such as in tracking sinusoidal desired speed signal. So experiments made for the comparison of the enhanced PID and PBSMC are mainly focused on these two points.

PID parameters of the PBSMC and parameters of PID are determined off-line while the torque constant of the PBSMC and saturation boundaries of the enhanced PID are designated by torque limits of the system itself. So on-line tuning test are made only for deciding the time constant parameter(H) of the PBSMC, as it is the case in simulations. In order to decide on the H parameter of the PBSMC, the step response characteristics of the controller for different values of H are investigated and step desired speed signals with the amplitude of 10 deg/s are given to the system. Resultant system speeds for five different H parameters can be seen in Fig.6.7.

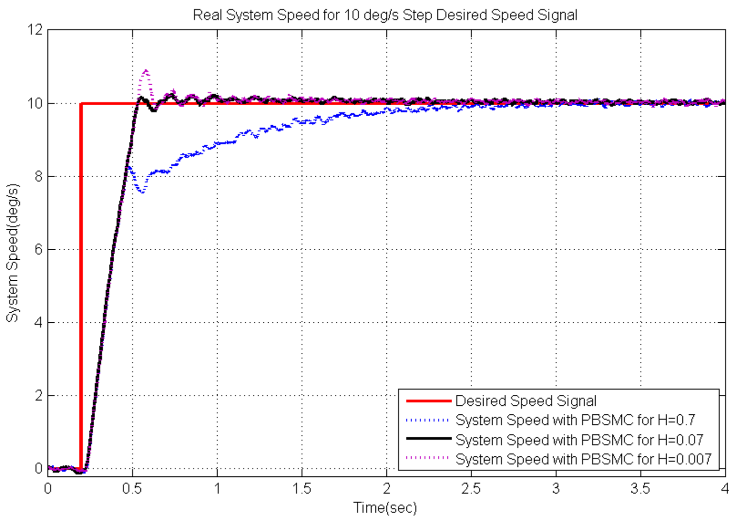

Figure 6.7: Step response characteristics of the inner PBSMC for different values of SMC time constant(H)

As it can be seen in the Fig.6.7, results obtained from the real system are compatible with the simulations results. A better overshoot suppression is obtained but system response becomes slower with the increase of H; however, SMC effect in the PBSMC decreases and overshoots arise with the reduction in the H. So, the choice of H needs a compensation and is chosen as 0.07 for the inner PBSMC used in the real system to sustain the optimality between overshoot suppression and settling time performance.

After finalizing the parameter tuning procedure for the controllers, first, comparative experiments are made to observe the step response characteristics of the controllers, to compare their responses under big error signal situations. For these experiments, step desired speed signals with the amplitude of 10 deg/s, 20 deg/s and 5 deg/s are applied to the system in order to see the effect of error amplitude on the tracking performance. Real system speeds obtained in these experiments are given in Fig.6.8, Fig.6.9 and Fig.6.10.

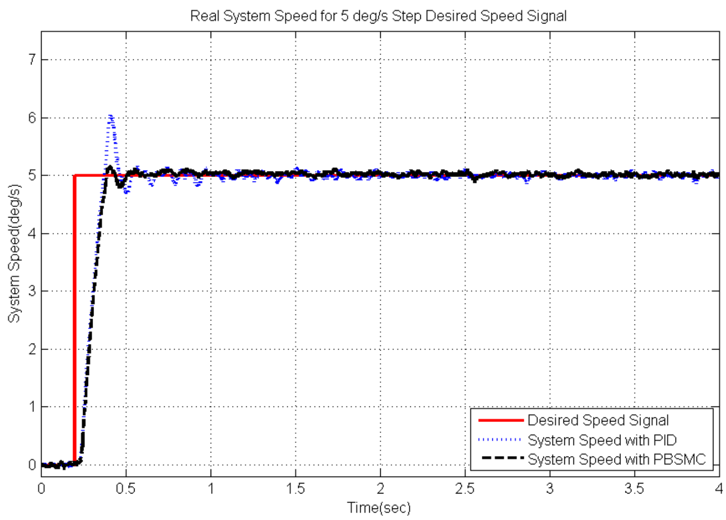

Figure 6.8: Response characteristics of PID and PBSMC for 5 deg/s step desired speed signal

As it can be seen from Fig.6.8 and Fig.6.9, system speed responses with overshoots about 1.04 deg/s and 0.99 deg/s for 5 deg/s and 10 deg/s step desired speed signal inputs are obtained by PID controller. On the other hand, PBSMC provides overshoot-free system speed responses with settling time performance at least as good as the PID controller for the same desired speed signals. However, when the amplitude of the step desired speed signal is decreased to smaller values like 1 deg/s as in Fig.6.10, overshoots can arise in the speed of the system even with PBSMC as observed in the simulation results also. Such overshoots are normal and expected due to the characteristics of the PBSMC, since the SMC in controller looses its effectiveness for

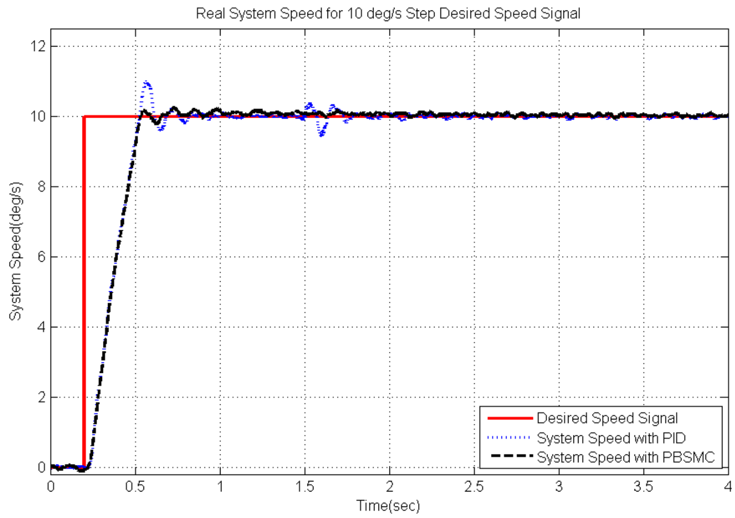

Figure 6.9: Response characteristics of PID and PBSMC for 10 deg/s step desired speed signal

smaller speed errors and PBSMSC starts to behave like a PID controller.

Torque signals created by enhanced PID and PBSMC are also investigated to understand the reason of differences in the step tracking performance as it is investigated in the simulations. Torque signals created by the controllers for 10 deg/s step desired speed signal is given in Fig.6.11.

Torque signals given in Fig.6.11 are compatible with the measurements taken in the simulations; while PID controller is saturated and get stuck to the the maximum torque limit (19800 Nm), the SMC controller in the PBSMC handles possible saturations better and PBSMC does not get stuck at the maximum torque limit as much as in the case of a PID which prevents probable overshoots in the system speed. Noise type of oscillations can be seen in the torque signals created by both controllers as in the simulations and are due to the gyroscope noise.

After that the superiority of the PBSMC control over PID is verified for big error situations(global dynamics), behaviours of the controllers in small error situations(local dynamics) are tested where a 3 deg/s sinusoidal desired speed signal with frequency of 0.5 Hz is applied to both controllers. The resultant system speeds are given in Fig.6.12 and its zoomed version in Fig.6.13.

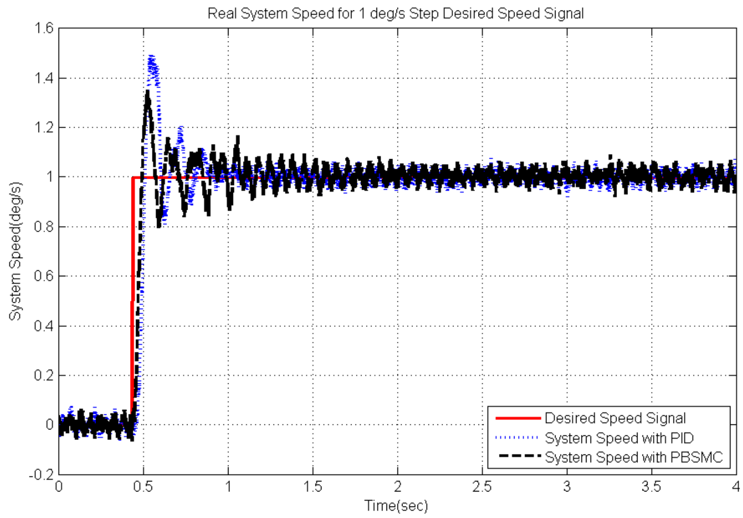

Figure 6.10: Response characteristics of PID and PBSMC for 1 deg/s step desired speed signal

As it can be seen from the Fig.6.13 and Fig.6.14, system speeds obtained by PBSMC and PID are very close to each other and are very similar to the results obtained in simulations. According to these results, it can be said that SMC in PBSMC does not cause any degradation in the tracking performance for the small error situations and so the claim about the local dynamics of the PBSMC is proven with experiments. In simulations it is also shown that if the amplitude and frequency of the sinusoidal desired speed signal is increased to a point enough to cause torque saturations, then behaviours of PID and PBSMC again differs due to the activation of the SMC in the PBSMC. In order to realize such a scenario in the real system, 3 deg/s sinusoidal desired speed signal with frequency of 0.5 Hz is given to both controllers. Resultant system speeds and torque demands created by the controllers are given in Fig.6.14 and Fig.6.15.

Results in Fig.6.14 and Fig.6.15 are also parallel with the simulation results and show that PBSMC can handle the torque saturation situations better than that of PID and provides better performance even for sinusoidal desired speed inputs with high frequency and amplitude, as they can also trigger the global dynamics and cause saturations in the torque signal. The only difference between simulation results and real system speeds resides in the amplitude of oscillations in the speed of the system with PID controller and it is most probably due to the difference between the model and

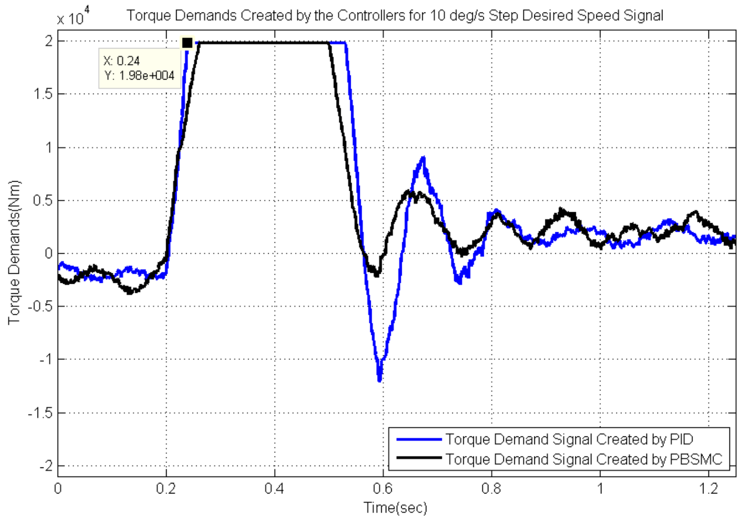

Figure 6.11: Torque demand signals created by PID and PBSMC for 10 deg/s step desired speed signal

the real system especially in damping coefficients.

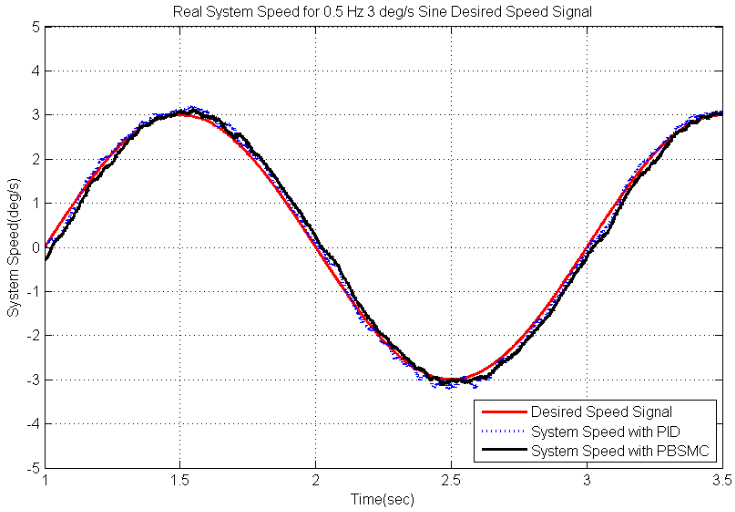

Figure 6.12: Response characteristics of PID and PBSMC for 3 deg/s 0.5 Hz sinusoidal desired speed signal

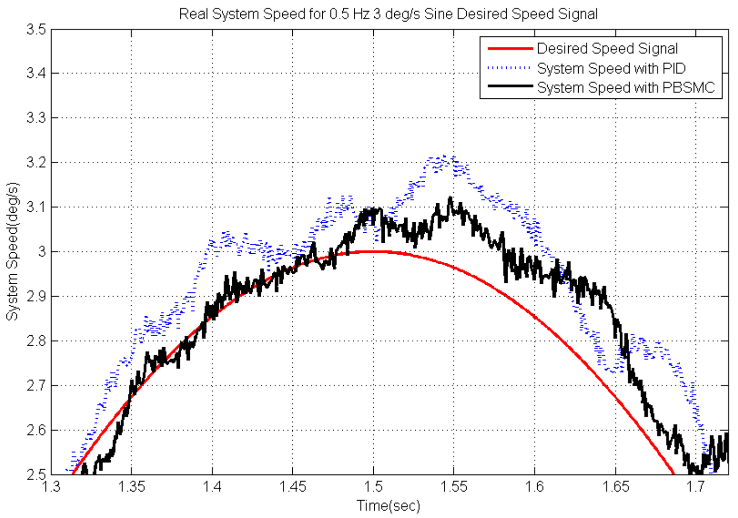

Figure 6.13: Response characteristics of PID and PBSMC for 3 deg/s 0.5 Hz sinusoidal desired speed signal, zoomed to a peak of the sine

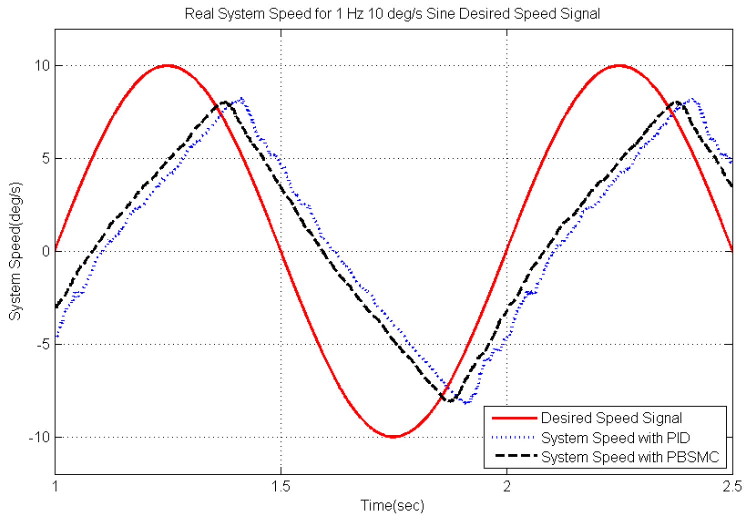

Figure 6.14: Response characteristics of PID and PBSMC for 10 deg/s 1 Hz sinusoidal desired speed signal

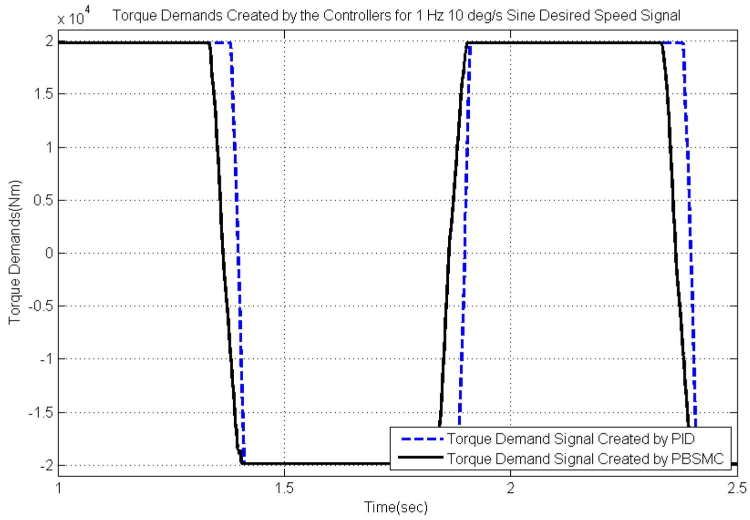

Figure 6.15: Torque demand signals created by PID and PBSMC for 10 deg/s 1 Hz sinusoidal desired speed signal

6.2.1.2 Comparison of Cascaded PID and PBSMC for Outer Loop

Similar experiments conducted for the inner speed loop are repeated for the outer position loop in order to verify the simulation results together with validation of claims about the characteristics of the cascaded PBSMC in the real system. As for the inner loop, experiments are initiated with parameter tuning. Boundary of the saturation block at the output of the outer PID and the control gain(T) of the SMC in the outer PBSMC are chosen to be the same and equal to 30 deg/s which is the speed limit of the system. H parameter of the SMC in the outer PBSMC is determined by on-line tuning through experiment on the real system as usual.

In order to determine the H parameter, step desired position signals with amplitude of 10 degs are applied to the system. Resultant system speeds measured from the real system for each H value are given in Fig.6.16.

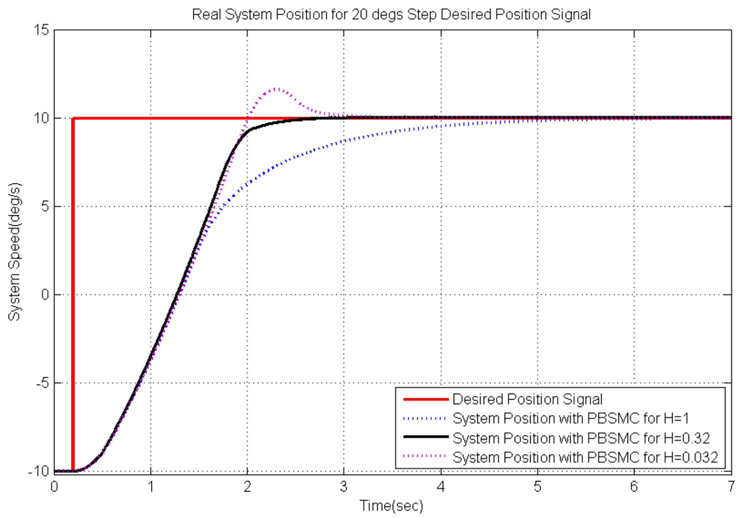

Figure 6.16: Step response characteristics of the position PBSMC for different values of SMC time constant(H)

Results given in Fig.6.16 also show similar characteristics as in the simulations made for the tuning of the H parameter. A better overshoot suppression is obtained but system response becomes slower with the increase of the H. On the other hand, effectiveness of SMC in the PBSMC decreases and overshoots arise with the reduction in the H as expected. So, H is chosen as 0.32 for the outer PBSMC used in the real system to compensate better between overshoot suppression and settling time performance in the position loop.

After finalizing the tuning procedure of the outer controllers, global dynamics of the cascaded PID controller and cascaded PBSMC are analysed by observing their step response characteristics through experiments. For these experiments, step desired position signals with amplitude of 40 degs, 20 degs and 5 degs are given to the system in order to see the effect of the position error amplitude on the tracking performance. Real system positions measured in these three experiments are given in Fig.6.17, Fig.6.18 and Fig.6.19.

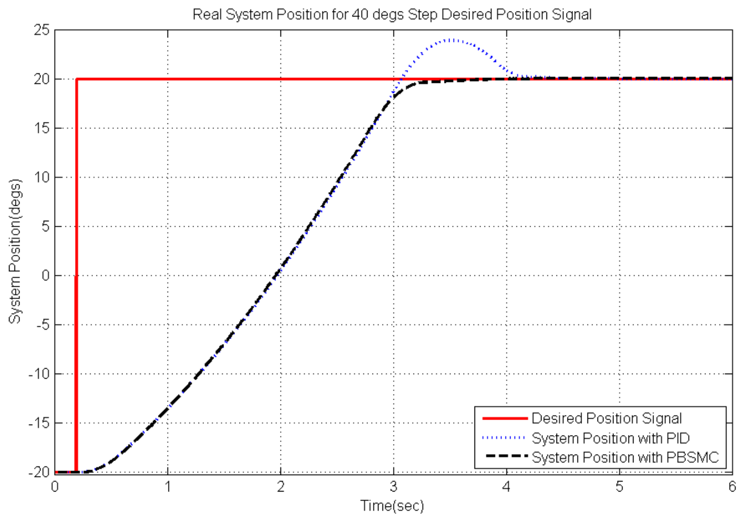

Figure 6.17: Response characteristics of cascaded PID and PBSMC for 40 degs step desired position signal

Results given in Fig.6.17, Fig.6.18 and Fig.6.19 show that cascaded PID controller provides system position responses with overshoots about 2.203 degs, 3.89 degs and 0.625 degs for 20 degs, 40 degs and 7 degs step desired position inputs. On the other hand, PBSMC provides overshoot-free system position responses with settling time performance at least as good as the PID controller as in the experiments conducted for the inner speed loop. Such a superior performance of the cascaded PBSMC is due to the saturation handling capability of both SMCs in the inner and outer PBSMC. In order to investigate the effects of these SMCs in the inner and outer PBSMCs , torque signals created by the inner PBSMC and speed demand signals created by the outer PBSMC are compared with the demand signals created by the corresponding inner and outer enhanced PID controllers. Torque and speed demand signals created

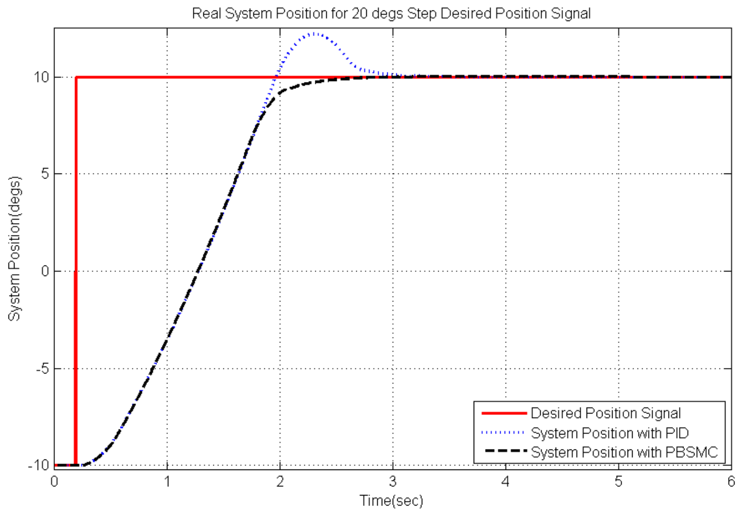

Figure 6.18: Response characteristics of cascaded PID and PBSMC for 20 degs step desired position signal

by the inner and outer controllers for 10 degs step desired position signals are given in Fig.6.20.

As it can be seen in the demand signals given in Fig.6.20 for 20 degs step desired position signal; PID controllers are saturated and get stuck to the maximum torque(19800 Nm) and speed (30 deg/s) limits respectively. On the other hand, SMCs in the inner and outer PBSMCs provide a better torque and speed saturation handling which avoids the possible overshoots and oscillations in the system response. In order to distinguish the effects of the inner-outer PBSMCs seperately and to support the cascaded PBSMC choice in the proposed controller architecture, another set of experiments are conducted by two other alternative cascaded controller structures. In the first configuration PID is used as the position controller and PBSMC is used as the speed controller (PID+PBSMC), while PBSMC is used for position control and PID is used as the speed controller in the second configuration (PBSMC+PID). Step position tracking performance of these two alternative configurations are compared with the proposed cascaded PBSMC structure. Torque and speed signals created by the inner and the outer controllers in each configuration are also compared with the signals created by the controllers in the proposed(PBSMC+PBSMC) structure. A 10 degs step desired position signal is applied to the system to evaluate the performance of the three different cascaded controller architecture; resultant system position mea-

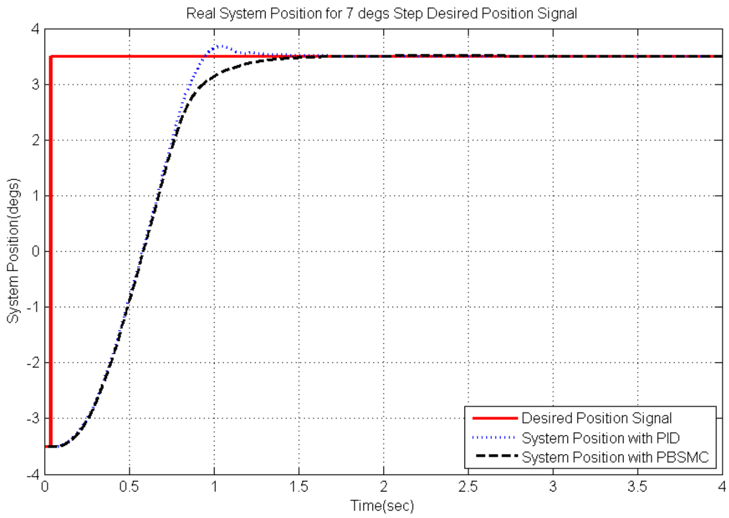

Figure 6.19: Response characteristics of cascaded PID and PBSMC for 7 degs step desired position signal

surements are given in Fig.6.21, and its zoomed version in Fig.6.22.

The resultant system positions in Fig.6.21 and Fig.6.22 show that the best position tracking performance is provided by the proposed cascaded PBSMC(PBSMC+PBSMC) configuration as expected and stated. PID+PBSMC configuration obviously differs from the other two alternatives with its high overshoot and acts similar to the pure cascaded PID. On the other hand, PBSMC+PID configuration seems to behave similar to the proposed cascaded PBSMC except for the small overshoot before reaching 10 degs which also cause an increase in the settling time. However, during the tests a coarse irregularity can be easily seen in the behaviour of the system with PBSMC+PID configuration when it is compared with the smoothness in the proposed cascaded PBSMC's response. So, torque and speed demand signals created by the inner and outer controllers in each alternative configuration is also compared with the signals created by the controllers in the proposed PBSMC structure.Demand signals measured for 10 degs step desired position signal are given in Fig.6.23.

As it can be seen from the demand signals given in Fig.6.23, the speed and torque signals in PID+PBSMC configuration directly differs from the other two configurations as a reflection of its response characteristics due to the PID in the outer loop. On the other hand, speed demand signals created by PBSMC+PID configuration and our

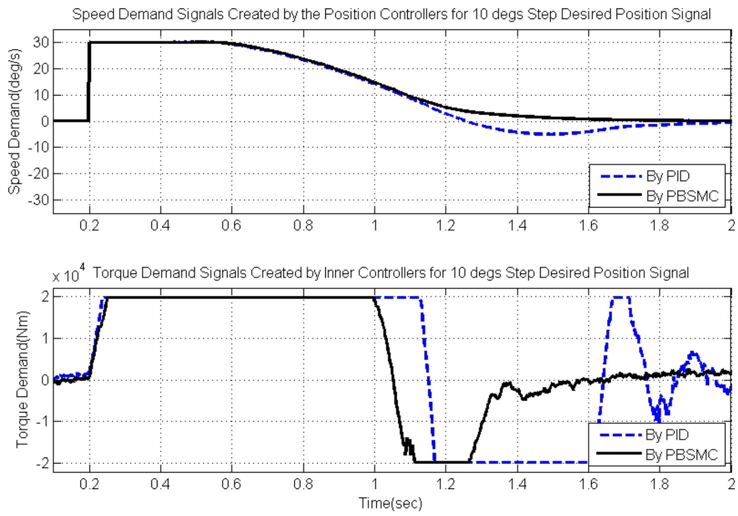

Figure 6.20: Torque and speed demand signals created by cascaded PID and PBSMC for 20 degs step desired position signal

proposed cascaded PBSMC are similar like in their response characteristics as both of them have PBSMC at the outer loop. However, torque demand signals in Fig.6.23 unveils the difference between these two controller structures. While our proposed cascaded PBSMC yields smooth torque signals, PBSMC+PID controller configuration produces torque signals with large oscillations. Such large oscillations in the torque demand signal clearly explains roughness in the motion of the PID-PBSMC controller. So, both PBSMCs in the inner and outer loop of the proposed controller are required and are important for higher performance and smoother plant reactions.

After the verification of the advantages provided by the cascaded PBSMC in global dynamics of the position loop, experiments conducted for the comparison of the cascaded PID and PBSMC are finalized by tests made for small error situations occurring in the position control. For these tests, 10 degs sinusoidal desired position signal with frequency of 0.1 Hz is applied to the cascaded controllers. Resultant system speeds are as given in Fig.6.24 and its zoomed version in Fig.6.25.

As it can be seen from Fig.6.24 and Fig.6.25, system positions obtained by cascaded PID controller and PBSMC are very close to each other and it is very hard to identify the difference even from the zoomed version, as it was also the case in simulations and experiments made for the inner speed loop. According to all of these experiments

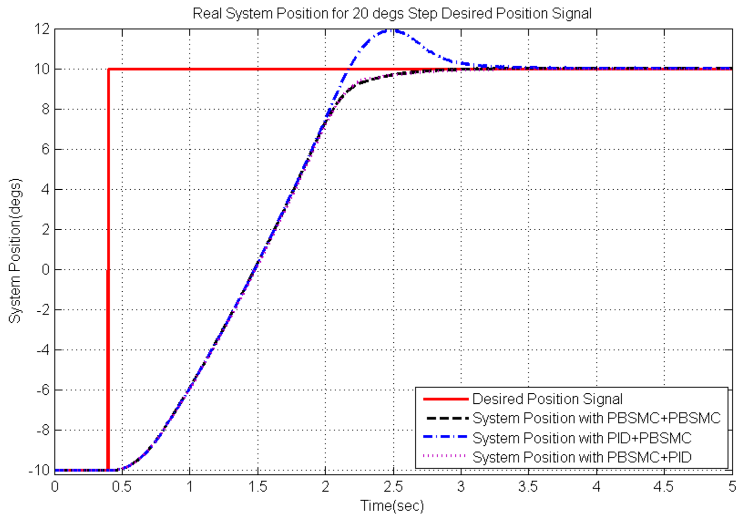

Figure 6.21: Response characteristics of alternative cascaded controller configurations for 20 degs step desired position signal

and simulation results obtained for inner and outer loops, it can be obviously said that PBSMC is acting just like a cascaded conventional PID for small errors and SMC in PBSMC does not have any negative effect on local dynamics of the controller.

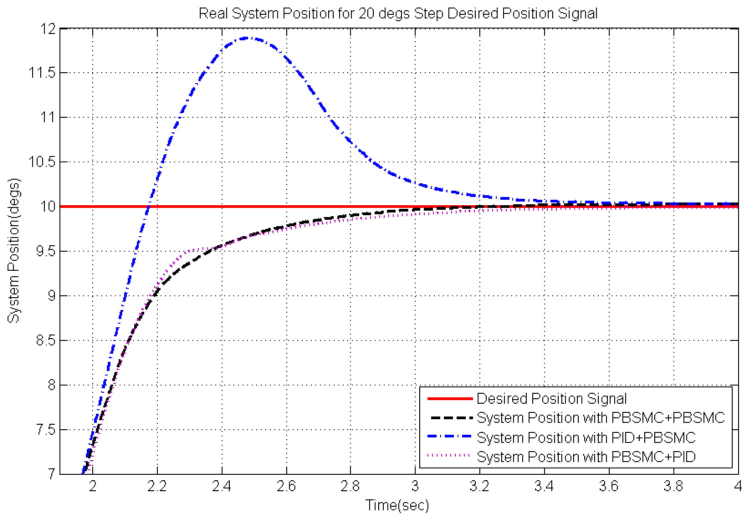

Figure 6.22: Response characteristics of alternative cascaded controller configurations for 20 degs step desired position signal, zoomed into critical region

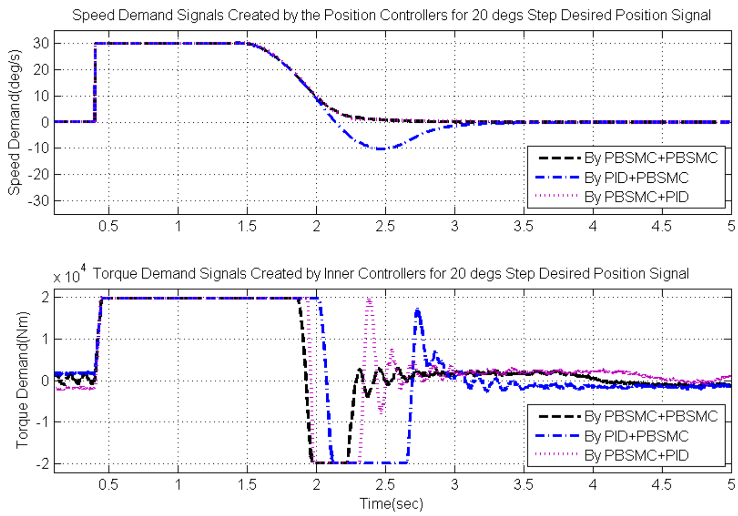

Figure 6.23: Torque and speed demand signals created in alternative configurations for 20 degs step desired position signal

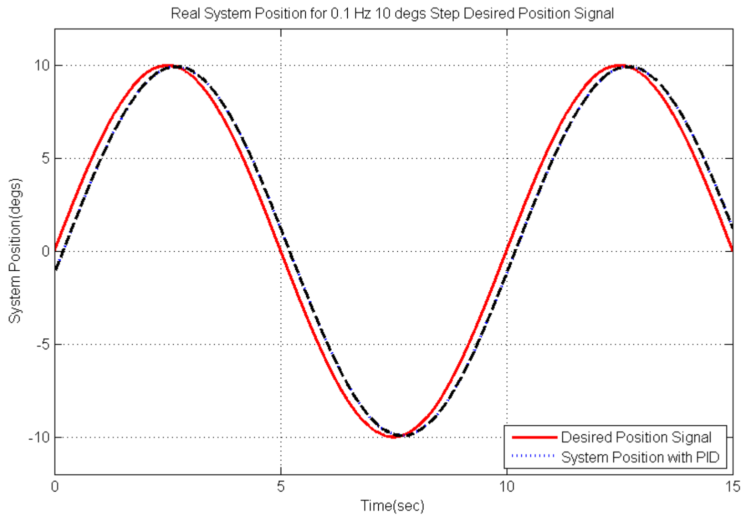

Figure 6.24: Response characteristics of cascaded PID and PBSMC for 10 degs 0.1 Hz sinusoidal desired position signal

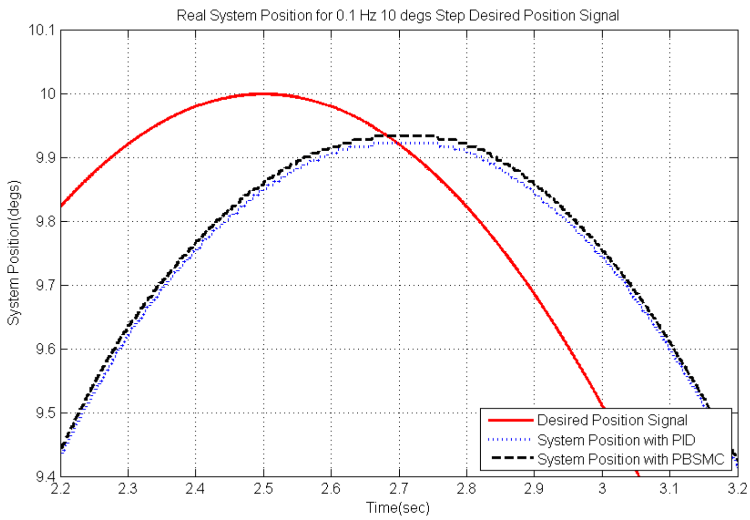

Figure 6.25: Response characteristics of cascaded PID and PBSMC for 10 degs 0.1 Hz sinusoidal desired position signal, zoomed into a peak of the sine

6.2.2 Effects of Non-Linearities In the System and Their Compensation

After deciding on the cascaded PBSMC as the main controller; the necessity of the disturbance observer and the additional Kalman filter, their properties and performance improvements provided by these sub-structures are evaluated with experiments made on the real system, preserving the structure and parameters of the main controller. First of all, effects of the non-linearities on the tracking performance of the controller is observed by removing the disturbance observer and Kalman filter enhancements from the controller structure. Then, the disturbance observer is inserted to the controller, to test its characteristics and to verify the improvements in the tracking performance brought by this additional observer structure. The section is finalized with the implementation of the Kalman filter and experiments made to evaluate its estimation performance and its contributions to the performance of disturbance observer enhancement.

6.2.2.1 Effects of Non-Linearities In the System

Friction and backlash are added to the system model to represent the non-linearities in the system and simulations are made to observe the effects of these non-linearities in the tracking of a desired position signal. In this sub-section these simulations are verified by detecting the effect of non-linearities in the system by experiments directly made on the real system. As it is stated and supported with simulations, effects of the non-linearities in the system are much more dominant in the tracking performance for lower desired velocities and especially at zero-crossings of the velocity. So, in order to identify the effects of non-linearities in desired speed tracking with PBSMC, a sinusoidal desired speed signal with 1 deg/s amplitude and 0.25 Hz frequency is given to the system. The resultant angular velocity of the system obtained with a pure cascaded PBSMC controller is as given in Fig.6.26 and in Fig.6.27 it zoomed version at vicinity of a zero-crossing for better identification.

The resultant system speed given in Fig.6.26 and Fig.6.27 is similar to the results obtained in the simulations and shows that speed tracking performance of the controller is distorted significantly by non-linearities. When stabilization is taken into account,

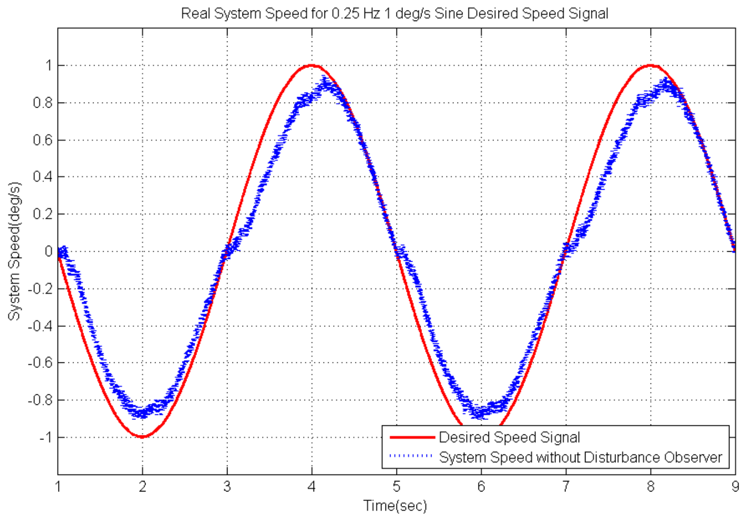

Figure 6.26: Effects of non-linearities on the system speed for 1 deg/s 0.25 Hz sinusoidal desired speed signal

the system is generally moving with low speeds and zero-crossings occur very frequently since the aim is to hold the angular velocity at zero. So, such non-linearities are very critical in the stabilization performance and need to be compensated for the sake of the stabilization accuracy provided by the controller. Therefore, the main controller is enhanced with an additional disturbance observer structure.

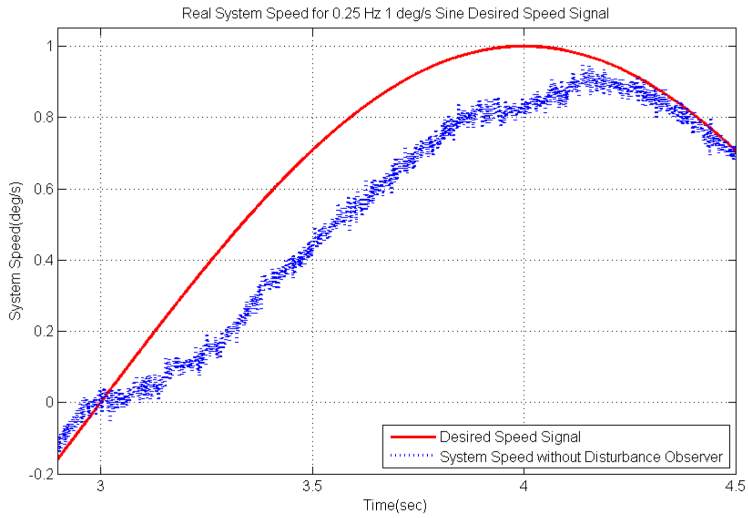

Figure 6.27: Effects of non-linearities on the system speed for 1 deg/s 0.25 Hz sinusoidal desired speed signal, zoomed into a zero-crossing

6.2.2.2 Disturbance Observer for The Compensation of the Non-linearities

A single-state observer proposed in Chapter 4 is added to the controller structure to compensate the negative effects of non-linearities and to improve the tracking and stabilization performance. As in the previous applications, experiments start with the tuning procedure of the parameters of the disturbance observer. Estimated inertia parameter used in the observer is directly found by the experiments made on the system as explained in the modelling part in Chapter 5, Section 5.1. On the other hand, the observer gain parameter is determined by on-line tuning. Different from the method used in the simulations, noise coupled to the system speed is directly evaluated for determining the optimal observer gain instead of observing noise in the torque signal created by the disturbance observer. For the on-line tuning of the observer gain, zero desired position signal is given to the system and noise in the system speed is measured for different gains. Amount of noise coupled to the system speed for different observer gain values can be seen in Fig.6.28.

Increase in the amplitude of the noise coupled to system speeds in Fig.6.28 for higher values of the observer gain is an expected result and this situation is in parallel with the mathematical analysis in Section 4.3 and with the simulation results in Section 5.3. Experiment results are given for different values of observer gain up to 2500000

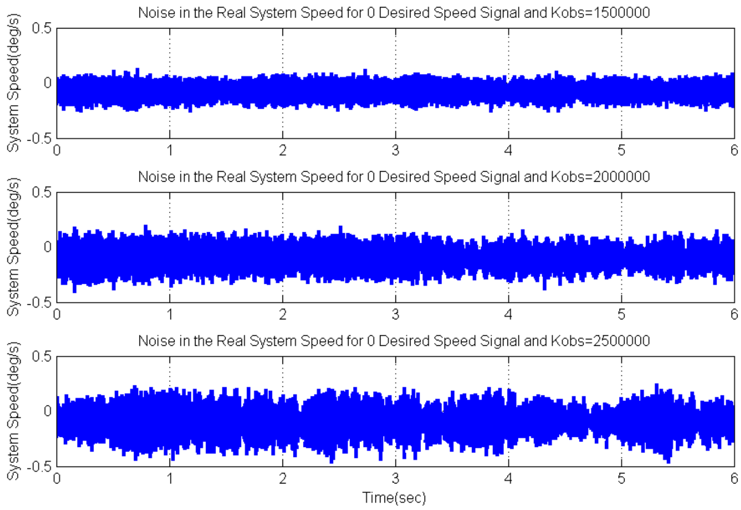

Figure 6.28: Effect of the observer gain on the noise coupled to the system speed

because noise in the system speed grows up rapidly due to vibration and system becomes unstable for higher observer gains. In order to maximize the bandwidth of the disturbance observer, observer gain is chosen as 2500000 which is the highest gain value reached without disturbing stability of the system. Observer gain tuning issue will be revisited in the experiments made for the Kalman filter after its implementation in Section 6.2.2.3.

After specifying the parameters of the disturbance observer, its contribution to tracking performance is tested by applying the sinusoidal wave with lower amplitude and frequency to the controllers with and without disturbance observer. For this tests a sinusoidal desired speed signal with 1 deg/s amplitude and 0.25 Hz frequency is used and angular speeds measured from the real system are depicted in Fig.6.29 and in Fig.6.30 its zoomed version in the vicinity of a zero-crossing is given for better identification of the difference.

As it can be seen form the resultant system speeds given in Fig.6.29 and Fig.6.30, implementation of the disturbance observer greatly improves the tracking performance of the controller by compensating non-linear effects especially at the zero-crossing as it was the case found in simulations. Such an improvement in the zero-crossings not only enhances the tracking performance but also increase stability performance naturally. Such improvements are discussed in next section after finalizing the proposed

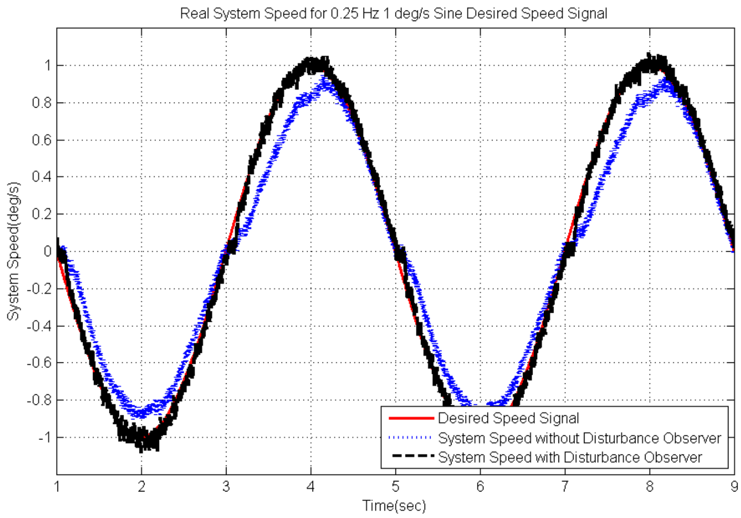

Figure 6.29: Performance of the disturbance observer in compensating friction and backlash

controller design with the addition of the Kalman filter.

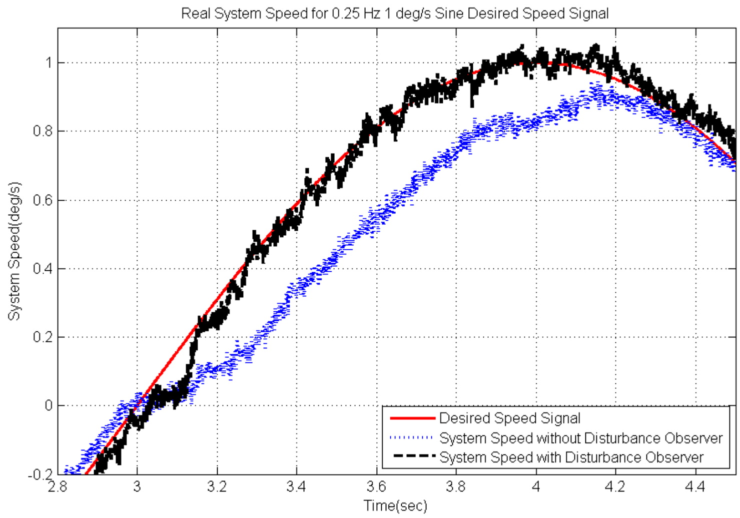

Figure 6.30: Performance of the disturbance observer in compensating friction and backlash, zoomed into a zero-crossing

6.2.2.3 Additional Kalman Filter

As explained in the previous chapters, Kalman filter is added to the disturbance observer in order to reduce the noise coupling problem by filtering the noise in the gyroscope measurements fed to the observer. Measurement noise covariances of Kalman filter are already tuned by the analysis made for the simulations and modelling noise covariance is determined by on-line tuning made by simulations. Same measurement covariance values are used for the Kalman filter implemented for the experiments since these values are derived directly from real sensor measurements and modelling noise covariance value is determined as 0.01 by using the same on-line tuning procedure explained in the simulations. In order to test the estimation performance of the tuned Kalman filter two sinusoidal desired speed signals with different frequencies are given to the system and Kalman filter system speed estimations are compared with the original gyroscope measurements. First of all, a sinusoidal desired speed signal with 1 deg/s amplitude and 0.25 Hz frequency is applied to the system in order to observe the noise suppression performance of the Kalman filter. Resultant gyroscope measurement and Kalman speed estimation are as given in Fig.6.31 and in Fig.6.32 its zoomed version in the vicinity of a peak of the sinusoidal wave is shown for better identification of the noise suppression performance.

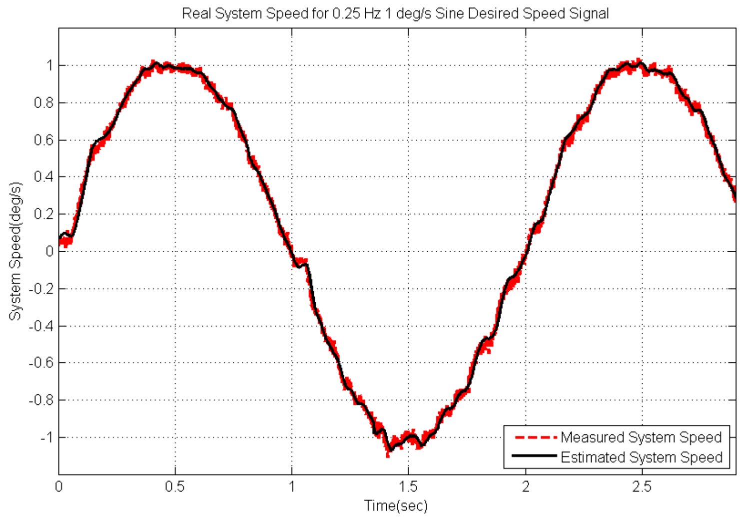

Figure 6.31: Estimation performance of the tuned Kalman filter for low frequency sinusoidal angular speed of the system

Another experiment is also conducted to evaluate the estimation performance of the Kalman filter for higher frequency system speeds. In this experiment, a sinusoidal desired speed signal with 1 deg/s amplitude and 5 Hz frequency is applied to the system and again Kalman estimation is compared with the real gyroscope measurement. Estimated and measured system speeds in this experiment are given in Fig.6.33.

Estimated and measured speeds in Fig.6.31 and Fig.6.32 show that Kalman filter has a very good estimation performance for low frequency signals and greatly reduces the noise in the angular speed measurements with its noise suppression capability. When the results in Fig.6.33 are analysed, it can be said that estimated angular velocity has higher peaks compared to the original measurements taken from the gyroscope. However, such differences are not significant in the performance of the disturbance observer since they are small and the disturbance observer is loosing its power with the increase in the frequency. Also such differences can be ignored as they occur generally at the peaks of the sinusoidal waves and peaks are less important compared to zero-crossings.

Due to the advantages of the Kalman filter explained in the previous paragraph, such a structure is added to the disturbance observer and improvements in the performance of the disturbance observer are shown with experiments on the real system. In these

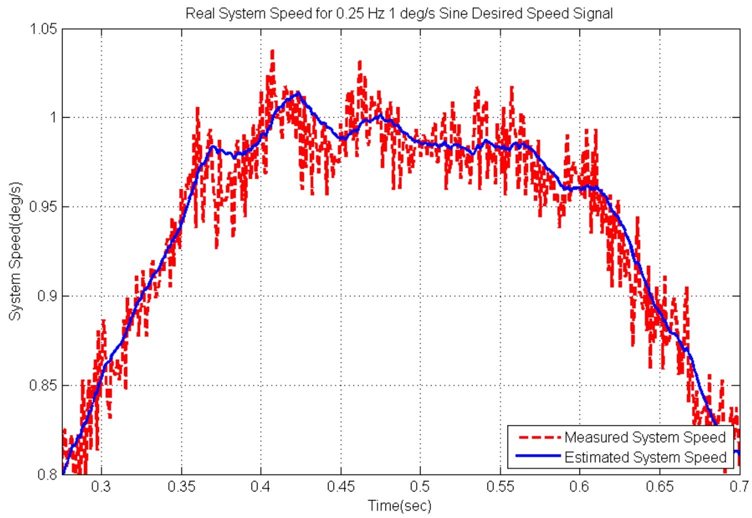

Figure 6.32: Estimation performance of the tuned Kalman filter for low frequency sinusoidal angular speed of the system, zoomed into a peak of sine

experiments, zero desired position signal is applied to the system and noise in the torque signals created by the disturbance observers with and without Kalman filter are measured. Disturbance observer gains in both controllers are adjusted to 2500000 for an accurate comparison. The resultant torque signals created by disturbance observers are given in Fig.6.34.

Torque signals in Fig.6.34 show that noise generated by the disturbance observer is greatly reduced with the addition of a Kalman filter. With the implementation of the Kalman filter and the reduction in the noise coupling, the observer gain is increased up to 3700000 and such an increment does not cause any problem in the stability of the system which is not possible without the additional Kalman filter.

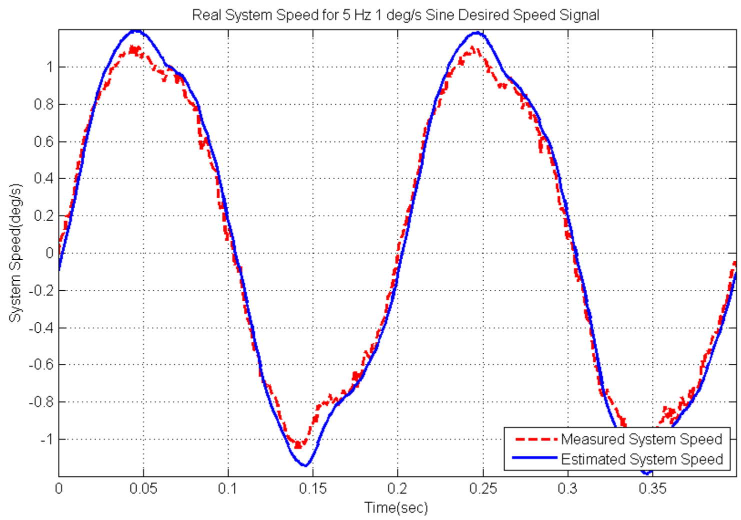

Figure 6.33: Estimation performance of the tuned Kalman filter for sinusoidal angular speed of the system with higher frequency

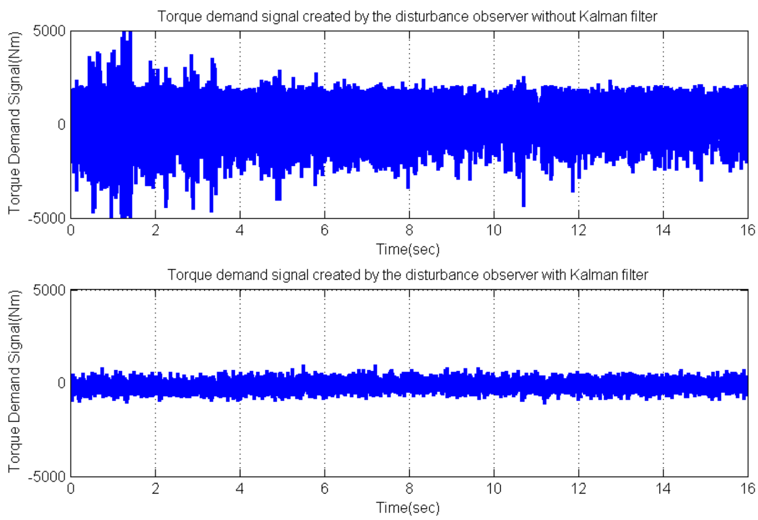

Figure 6.34: Noise in the torque demand signals created by the disturbance observers with and without Kalman filter addition

6.2.3 Disturbance Rejection Capability

Improvement of the disturbance rejection capability underlying stabilization performance is one of the main purposes of this thesis work since it is very critical for the efficient usage of a mobile gun-turret platform. Simulations are made to compare the stabilization performance of the proposed controller architecture and that of the enhanced cascaded PID structure already in use for the control of the gun-turret prototype. However, disturbances in the real system are omnipresent and are mainly caused by the motion of the base so it is very difficult to simulate the interactions between moving base and turret due to the complex dynamics of the coupling between base and the system. Therefore, simulation results provide a valuable evaluation medium about the performance of the proposed controller; however, its performance still needs to be tested by experiments with the real system and real base motion disturbance to be sure about its advantages. In this section, results of such experiments conducted on the real system with real base motion are given and analysed. For these tests, the prototype gun turret platform is mounted on a 6-degree of freedom Stewart platform explained in Chapter 3 and different sinusoidal base motions are created by applying sinusoidal accelerations. Such experiments are repeated for both configurations involving either our proposed controller or the enhanced cascaded PID controller for comparison. Sinusoidal accelerations created by the Stewart platform in the experiments have the amplitude of 1 rad/s^2 and their frequencies are varying from 0.25 Hz to 4 Hz. Such disturbances with different frequencies are applied to the system in order to observe the disturbance rejection bandwidth of the controllers. Such sinusoidal accelerations defined for the Stewart platform result in sinusoidal angular velocities in the base with the same frequency and these resultant base motions are measured by the feed-forward gyroscope mounted on the Stewart platform. The angular speed of the base, the angular speed of the turret with the enhanced cascaded PID and that of the turret equipped with the proposed controller are given when the system is under the influence of disturbance with the frequency of 0.25 Hz in Fig.6.35, with the frequency of 1 Hz in Fig.6.36 and with the frequency of 4 Hz in Fig.6.37. Although measurements in the experiments are taken for longer periods of time, 4 seconds intervals of these measurements are given in Fig.6.35, Fig.6.36 and Fig.6.37 for a better observation of the patterns in the angular velocity of the systems with the enhanced

PID controller and the proposed controller. Also initial time in all graphs are decided by observing the feed-forward gyroscope measurements of the corresponding experiment and the beginning of sinusoidal waves in the base motion are selected as the initial time again for a better comparison of the resultant system speed patterns and for better analysis of the correlation between the base motion and the oscillations in the real system speeds.

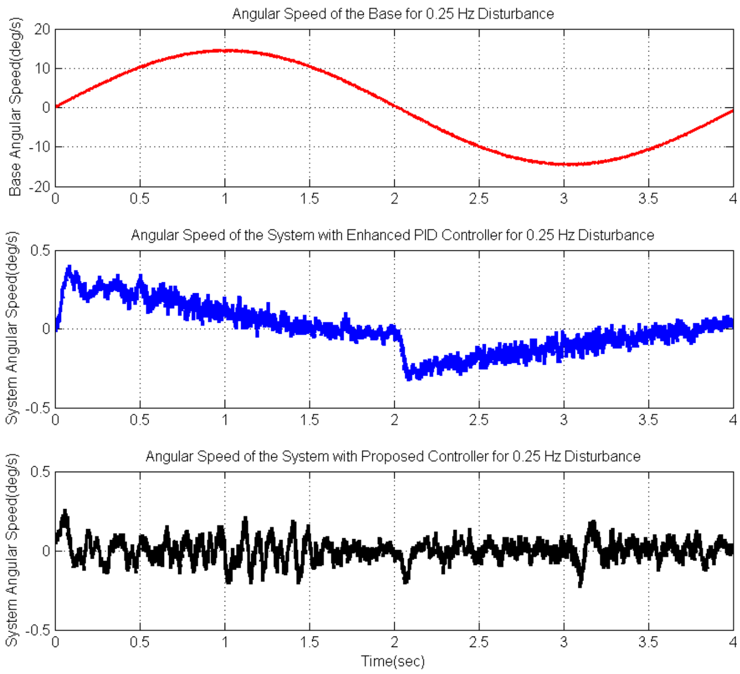

Figure 6.35: Stabilization performance of the controllers for 0.25 Hz disturbance

Amplitudes and patterns of the oscillations in Fig.6.35, Fig.6.36 and Fig.6.37 show the superiority of the proposed controller over the enhanced cascaded PID structure in stabilization even under the influence of disturbance with frequency of 4 Hz. By fusing results given in the figures together with the outcomes of the previous experiments made with different sub-structures of the proposed controller, it can be said that superiority of the proposed controller is enhanced with the implementation of the disturbance observer coupled to a Kalman filter addition since SMC in the PBSMC is not active in small error situations as in stabilization. So the decrement in the difference between the performance of the controllers with the increase in the disturbance can be associated with the bandwidth of the disturbance observer. Stabilization performance

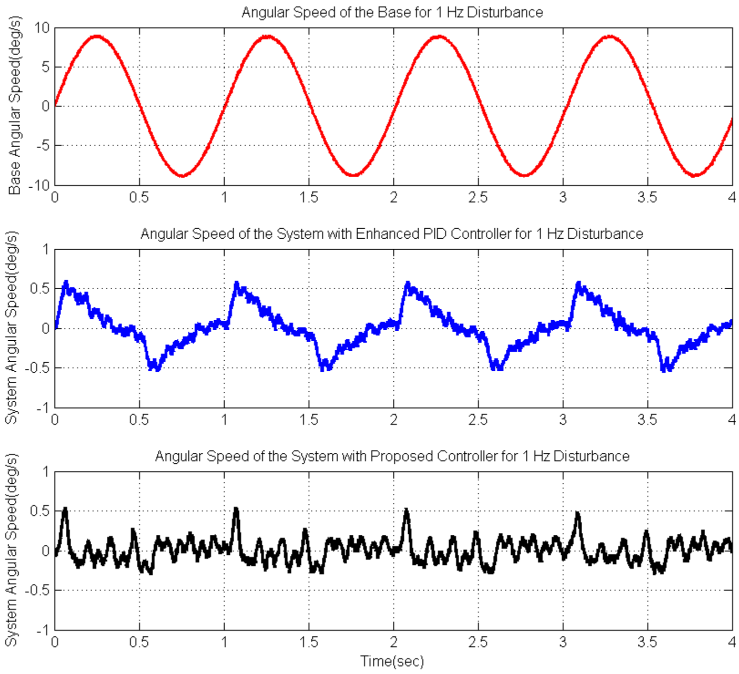

Figure 6.36: Stabilization performance of the controllers for 1 Hz disturbance

of both controllers is also decreased for disturbances with higher frequencies, and this decrement can be linked to the disturbance rejection bandwidth of the cascaded PID and that of the main controller in the proposed architecture. Another interesting point in the experiment results is the correlation between the peaks of the oscillations in the system speed and the zero-crossings of the base. Such a correlation between these two situations is proving the importance of the system behaviour in the zero-crossings for the stabilization performance as stated in the comments about the enhancements of the disturbance observer.

Experiments for disturbance rejection performance comparison of the enhanced cascaded PID and proposed controller are repeated for some other frequencies between 0.25 Hz and 4 Hz. However, instead of giving figures for all frequencies, stabilization performance of the controllers are compared analytically by using the stabilization accuracy metric used for representing the performance. Procedure of the stabilization accuracy calculation from a gyroscope measurement of the system under the effect of a disturbance can be summarized by the following steps:

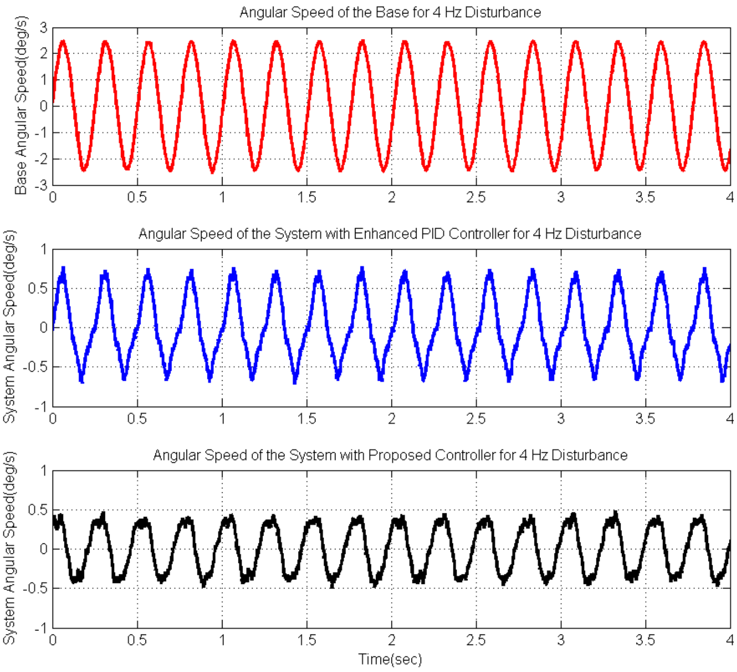

Figure 6.37: Stabilization performance of the controllers for 4 Hz disturbance

- First of all, gyroscope measurement's unit is converted to mrad/s and the converted data is integrated by taking sampling frequency into account. With this integration, angular displacement of the turret with respect to ground is obtained in mrads.

- Due to the offset drift of the gyroscope, a drift with a constant slope can be seen in the angular displacement data obtained by integration. In order to compensate such a drift in angular displacement before calculating the stabilization accuracy, a line equation with the same slope as the angular displacement is derived and the drift in the angular displacement is obtained by using this equation and time data collected through the experiment.

- By subtracting the drift obtained in the second step from the original displacement data obtained from measurements in the first step, a drift-free angular displacement is obtained.

- At the end, stabilization accuracy is calculated as the 1σ standart deviation of the drift-free angular displacement data obtained in the third step. As the angular displacement is calculated in mrads, unit of the stabilization accuracy is also mrads.

Stabilization accuracy rates of the enhanced cascaded PID controller and proposed controller for different frequencies of the disturbances are summarized in Table 6.1. As the sinusoidal accelerations with constant amplitudes are generated by the Stewart platform, deviation in the position of the base with respect to a fixed reference is decreasing with the increase in the frequency of the disturbance. Due to such variations in the amplitude of the deviations in the base position, evaluating the disturbance rejection performance of a controller for different disturbance frequencies by using only the stabilization accuracy of that controller can be misleading. So, the stabilization accuracy for the locked turret case is also given in the table in order to represent the amplitude of the deviations in the base position.

Table6.1: Stabilization accuracies obtained with different configurations of the system for different disturbance frequencies

Disturbance Frequency	**Stabilization Accuracy of Locked System (mrad)**	**Stabilization Accuracy with Enhanced PID Controller (mrad)**	**Stabilization Accuracy with Proposed Controller (mrad)**
0.25 Hz	114.584	1.559	0.106
0.5 Hz	58.550	1.094	0.158
0.75 Hz	29.718	0.8346	0.182
1 Hz	17.479	0.686	0.170
2 Hz	4.603	0.3921	0.219
3 Hz	2.090	0.386	0.226
4 Hz	1.189	0.285	0.197

First of all, the stabilization accuracies given in Table 6.1 obviously shows that our proposed controller is superior to the enhanced PID in stabilization performance for all the disturbances with different frequencies tested in the experiments. Despite the drop in the performance difference between enhanced PID and proposed controller with the increase in the disturbance frequency, the proposed controller provides approximately 1.5 times better stabilization performance even for 4 Hz as it can be also seen in Fig.6.37. The effect of the frequency on the controller's disturbance rejection performance can also be viewed separately from the results in Table 6.1. In order to evaluate the effect of disturbance frequency on the stabilization performance of each controller, stabilization accuracies with locked actuators and with controllers should be taken into account together to come up with more accurate comments. As it can be seen from Table 6.1, stabilization accuracies with locked actuators drop more rapidly compared to the stabilization accuracies with controllers. Such a relation between the drops directly points out the limited disturbance rejection bandwidth of the controllers and supporting the theoretical assertions about the disturbance rejection characteristics of the controllers made from their frequency domain analysis.

CHAPTER 7

CONCLUSION AND FUTURE WORK

7.1 Conclusion

The objective of this thesis work is the development of a complete controller architecture to stabilize a gun-turret platform and make it track the desired position or speed signals sent from an upper-level controller. The main motivation behind such a design is to provide a high stabilization and tracking performance despite the non-linearities resulting from the nature of the controlled system, non-ideal sensor measurements and external disturbances caused by the motion of the system and varying operation conditions of the armoured land vehicle.

From the control point of view, the controller to be developed needs to be robust against non-linearities and provide high tracking performance with low overshoot and settling time. It should also have an effective disturbance rejection capability to cope with the external disturbances mainly due to the motion of the base. Besides these performance requirements, the controller should require minimum computation power and memory during its operation as it is implemented on DSP chips available in the servo controller hardware on the gun-turret platform.

Going beyond available controller architectures existing in the literature and satisfying some of the requirements aforementioned, we propose a cascaded proxy-based sliding mode controller(PBSMC), designed as the main controller of our control architecture. PBSMC is a combination of sliding mode and PID control ideas which eliminates the chattering problem in real-time applications of the sliding mode control and solves the performance trade-off between local and global dynamics of PID control for different parameter sets. We also add a reduced order disturbance observer to the main controller for the compensation of the non-linearities so as to improve its disturbance rejection capability. Moreover, this disturbance observer is enhanced with an additional Kalman filter to be able to improve its gain and consequently its performance, with less additional sensor noise coupled to the torque applied to the system.

Both model-based and non-model based methods are used in the literature for the compensation of the non-linearities. However, due to the variations in system characteristics with its life time and due to dependencies to operation conditions, a non-model based reduced order observer is implemented for compensating the non-linearities in the gun-turret platform. It combines the torque applied to the system with a single inertia system model for estimating the ideal angular speed of the system and compares this estimation with the speed feedback obtained from the real system in order to calculate additional torques resulting from non-linearities and external disturbances acting on the system. This calculated disturbance torque is directly added to the torque demand signal created by the main controller to eliminate the effect of such non-linearities and external disturbances. Luenberger type of observer is used to estimate the disturbance torque and its closed loop structure renders the observer robust against possible errors in the estimated system model and the variations in the system or environment. Such a disturbance observer also improves the disturbance rejection capability of the main controller due the calculated disturbance torque also including the effects of external disturbances.

Angular speed measurements provided by the feedback gyroscope is used by the disturbance observer to calculate disturbance torque. So, noise in the gyroscope measurements is directly coupled to the calculated torque and becomes effective if the observer gain exceeds a limit. Therefore, this noise in the measurements needs to be suppressed in order to be able to increase the observer gain and to obtain a better performance from the observer. For this purpose, a Kalman filter is also added to the disturbance observer which fuses feed-back gyroscope measurements with encoder and feed-forward gyroscope measurements for providing an angular velocity with less noise.

Our proposed controller architecture is tested with both simulations and experiments conducted on the real system. Its performance is compared to a cascaded output-limited PID controller with anti-wind up enhancement which is already designed and used for the control of the real system. A three-mass model is used in the simulations to represent the real system behaviours. Friction, backlash and sensor noise models are also added to the simulation model and all the parameters in the model are tuned according to data collected from the real system for a better representation of system characteristics.

In the simulations, tracking performance of the PBSMC is compared to PID-based method as speed controller at first. Different step desired speed signals are given to the controllers and overshoots are observed at the speed of the system controlled by PID-based controller while PBSMC provides overshoot-free system speed without any deterioration in the settling time. Sinusoidal desired speed signals are also given to the controllers to observe the tracking performance of both methods and we show that both controllers have very similar local dynamics. Similar step and sinusoidal commands are also given as desired position signals to the cascaded PBSMC and PID-based controller. Superiority of the cascaded PBSMC in over-shoot suppression without any degradation in the local dynamics is also demonstrated in position control.

Effects of non-linearities in the system speed are also observed in the simulations especially in the zero-crossings by applying sinusoidal desired speed signals with small amplitude and low frequency. When the disturbance observer in the proposed controller architecture is activated, we show that these distortions in the zero-crossings due to non-linearities are reduced and tracking performance of the controller is increased. Performance of the disturbance observer for faulty inertia estimates are tested and its robustness against parameter variations or errors in inertia estimate is verified. Disturbance torques calculated by disturbance observers with and without Kalman filter are also investigated which proves the contribution of the Kalman filter in suppressing the sensor noise coupled to the system speed.

Simulations are finalized with disturbance rejection performance comparisons between proposed controller architecture and the PID-based controller already used in the real system. For this aim different disturbance torques are applied to the system model and disturbance rejection capability of the controllers are observed. Sinusoidal disturbance torques with different frequencies are applied to the system model to simulate the effect of base motion in the real system. Our proposed controller is demonstrated to provide much better stabilization performance in lower frequencies and the difference between controller performances is seen to decrease with the increase in the frequency of the disturbance as expected. Step disturbance torques with amplitudes above the available torque limit of the system are also applied to the system to simulate the response of the controllers to sharper disturbance patterns like shocks. The superiority of our proposed controller is also proven for such impulsive disturbances with the better saturation handling capability provided by PBSMC used for speed control.

In the experiments, the proposed controller architecture and PID-based controller are implemented in the DSP on the real system and similar tests are repeated to verify the results obtained in the simulations. First, the superiorities of the PBSMC and the cascaded PBSMC over PID and cascaded PID-based controllers in tracking are verified. The effect of non-linearities on the tracking performance, their compensation with the disturbance observer, robustness of the disturbance observer against faults in inertia estimate and contribution of the Kalman filter in the performance of the disturbance observer are also checked in the real-system as it was the case for simulations.

Different from simulations, comparative experiments are carried out on their disturbance rejection capability and stabilization performance by creating controlled accelerations as the base motion with the help of a Stewart platform rather than injecting disturbance torques directly to the system. Such an experiment conducted with the help of the Stewart platform is directly reflecting performance of the system in real operation scenarios. Although the method is different in the experiments, results are very similar to the simulations and our proposed controller provides much better stabilization performance especially for the base motion with lower frequency while its superiority degrades with the increase in the frequency of the base motion created by the Stewart platform.

To sum up, an effective controller is designed within the balance of this thesis for the control of the gun-turret platform. Tracking and stabilization performance are the two of the most important measures for the success of a controller and our proposed controller is better than the previous PID-based controller in both measures without losing robustness or adding much complexity. Superiority of the proposed controller and function of the each component used in it are proved with simulations and experiments.

7.2 Future Work

The proposed control is offered as a solution for the control of a specific gun-turret platform prototype designed for armoured land vehicles; however, it can be used in other platform control applications and would be beneficial especially for the applications with dominant non-linearities and effective external disturbances. We planned to implement the proposed controller architecture for similar stabilized gun-turret platforms designed for naval applications and to platforms with different armaments like radars or rocket launchers. These different applications will contribute to the validation of the controller and will improve its reliability. Independent from disturbance observer, single cascaded PBSMC structure can also be tried in all applications instead of cascaded PID to be able to tune the local and global dynamics of the controller separately.

Many enhancements can also be tried on the proposed controller. A feed-forward path can be added to the controller to improve its tracking and stabilization performance. System model used in the disturbance observer can be upgraded and performance of the disturbance observer with higher degree models can be tested. Kalman filter structure can be also improved with new estimation models or with additional sensors such as accelerometers. Adaptive tuning of the cascaded PBSMC parameters can be studied to improve the robustness of the controller. However, sensitivity, robustness and complexity of the controller should be always taken into account and needs to be tested during all these enhancements.

REFERENCES

[1] M. Nordin and P.-O. Gutman. Controlling mechanical systems with backlash—a survey. *Automatica*, 38(10):1633–1649, 2002.

[2] V. Lampaert, J. Swevers, and F. Al-Bender. Comparison of model and non-model based friction compensation techniques in the neighbourhood of pre-sliding friction. In *American Control Conference, 2004. Proceedings of the 2004*, volume 2, pages 1121–1126. IEEE, 2004.

[3] R. Kikuuwe, S. Yasukouchi, H. Fujimoto, and M. Yamamoto. Proxy-based sliding mode control: a safer extension of pid position control. *Robotics, IEEE Transactions on*, 26(4):670–683, 2010.

[4] R. Kikuuwe and H. Fujimoto. Proxy-based sliding mode control for accurate and safe position control. In *Robotics and Automation, 2006. ICRA 2006. Proceedings 2006 IEEE International Conference on*, pages 25–30. IEEE, 2006.

[5] R. Kikuuwe, T. Yamamoto, and H. Fujimoto. Velocity-bounding stiff position controller. In *Intelligent Robots and Systems, 2006 IEEE/RSJ International Conference on*, pages 3050–3055. IEEE, 2006.

[6] J. Hilkert and B. Pautler. A reduced-order disturbance observer applied to inertially stabilized line-of-sight control. In *SPIE Defense, Security, and Sensing*, pages 80520H–80520H. International Society for Optics and Photonics, 2011.

[7] H. Özgür, E. Aydan, and E. İsmet. Proxy-based sliding mode stabilization of a two-axis gimbaled platform. In *Proceedings of the World Congress on Engineering and Computer Science*, 2011.

[8] P. Trewhitt. *Armored Fighting Vehicles: 300 of the World's Greatest Military Vehicles*. Sterling Publishing Company, 2001.

[9] Wikipedia. Lanchester 4x2 armoured car — wikipedia, the free encyclopedia, 2013. [Online; accessed 25-June-2014].

[10] Wikipedia. Rolls-royce armoured car — wikipedia, the free encyclopedia, 2014. [Online; accessed 25-June-2014].

[11] Wikipedia. Renault ft — wikipedia, the free encyclopedia, 2014. [Online; accessed 25-June-2014].

[12] P. J. Kennedy and R. L. Kennedy. Direct versus indirect line of sight (los) stabilization. *Control Systems Technology, IEEE Transactions on*, 11(1):3–15, 2003.

[13] M. K. Masten. Inertially stabilized platforms for optical imaging systems. *Control Systems, IEEE*, 28(1):47–64, 2008.

[14] Y. F. Xu, Z. Y. Zhang, K. Li, and M. K. He. Study of control algorithm for indirect stabilized optical seeker. *Applied Mechanics and Materials*, 44:4053–4057, 2011.

[15] R. M. Ogorkiewicz. *Technology of tanks*, volume 1. Jane's Information Group, 1991.

[16] M. Nordin, J. Galic', and P.-O. Gutman. New models for backlash and gear play. *International Journal of Adaptive Control and Signal Processing*, 11(1):49–63, 1997.

[17] R. Dhaouadi, K. Kubo, and M. Tobise. Analysis and compensation of speed drive systems with torsional loads. *Industry Applications, IEEE Transactions on*, 30(3):760–766, 1994.

[18] Z. Yumrukcal. Dynamic modeling of backlash dynamics in high performance motion platform. Master's thesis, Middle East Technical University, 2013.

[19] L. Walha, T. Fakhfakh, and M. Haddar. Nonlinear dynamics of a two-stage gear system with mesh stiffness fluctuation, bearing flexibility and backlash. *Mechanism and Machine Theory*, 44(5):1058–1069, 2009.

[20] H. Olsson, K. J. Åström, C. Canudas de Wit, M. Gäfvert, and P. Lischinsky. Friction models and friction compensation. *European journal of control*, 4(3):176–195, 1998.

[21] J. Swevers, F. Al-Bender, C. G. Ganseman, and T. Projogo. An integrated friction model structure with improved presliding behavior for accurate friction compensation. *Automatic Control, IEEE Transactions on*, 45(4):675–686, 2000.

[22] C. C. De Wit, H. Olsson, K. J. Astrom, and P. Lischinsky. A new model for control of systems with friction. *Automatic Control, IEEE Transactions on*, 40(3):419–425, 1995.

[23] G. Kumar, P. Y. Tiwari, V. Marcopoli, and M. V. Kothare. A study of a gun-turret assembly in an armored tank using model predictive control. In *American Control Conference, 2009. ACC'09.*, pages 4848–4853. IEEE, 2009.

[24] M. Cychowski, R. Jaskiewicz, and K. Szabat. Model predictive control of an elastic three-mass drive system with torque constraints. In *Industrial Technology (ICIT), 2010 IEEE International Conference on*, pages 379–385. IEEE, 2010.

[25] M. Athans. A tutorial on the lqg/ltr method. In *American Control Conference, 1986*, pages 1289–1296. IEEE, 1986.

[26] K.-J. Seong, H.-G. Kang, B.-Y. Yeo, and H.-P. Lee. The stabilization loop design for a two-axis gimbal system using lqg/ltr controller. In *SICE-ICASE, 2006.*

International Joint Conference, pages 755–759. IEEE, 2006.

[27] G. Stein and M. Athans. The lqg/ltr procedure for multivariable feedback control design. *Automatic Control, IEEE Transactions on*, 32(2):105–114, 1987.

[28] S. Skogestad and I. Postlethwaite. *Multivariable feedback control: analysis and design*, volume 2. Wiley New York, 2007.

[29] N. K. Gupta. Frequency-shaped cost functionals-extension of linear-quadratic-gaussian design methods. *Journal of Guidance, Control, and dynamics*, 3(6):529–535, 1980.

[30] M.-Y. Shieh and T.-H. S. Li. Design and implementation of integrated fuzzy logic controller for a servomotor system. *Mechatronics*, 8(3):217–240, 1998.

[31] A. I. Al-Odienat and A. A. Al-Lawama. The advantages of pid fuzzy controllers over the conventional types. *American Journal of Applied Sciences*, 5(6), 2008.

[32] J. Velagic and A. Aksamovic. Fuzzy logic system for position control and current stabilization of a robot manipulator. In *Computer as a Tool, 2005. EUROCON 2005. The International Conference on*, volume 1, pages 334–337. IEEE, 2005.

[33] H. A. Malki, H. Li, and G. Chen. New design and stability analysis of fuzzy proportional-derivative control systems. *Fuzzy Systems, IEEE Transactions on*, 2(4):245–254, 1994.

[34] J. C. Spall and J. A. Cristion. A neural network controller for systems with unmodeled dynamics with applications to wastewater treatment. *Systems, Man, and Cybernetics, Part B: Cybernetics, IEEE Transactions on*, 27(3):369–375, 1997.

[35] K. S. Narendra and K. Parthasarathy. Identification and control of dynamical systems using neural networks. *Neural Networks, IEEE Transactions on*, 1(1):4–27, 1990.

[36] T. Pajchrowski and K. Zawirski. Application of artificial neural network to robust speed control of servodrive. *Industrial Electronics, IEEE Transactions on*, 54(1):200–207, 2007.

[37] C. L. Giles, D. Chen, G.-Z. Sun, H.-H. Chen, Y.-C. Lee, and M. W. Goudreau. Constructive learning of recurrent neural networks: Limitations of recurrent cascade correlation and a simple solution. *Neural Networks, IEEE Transactions on*, 6(4):829–836, 1995.

[38] J. Schumann, P. Gupta, and S. Nelson. On verification & validation of neural network based controllers. In *Proceedings, International Conference on Engineering Applications of Neural Networks*. Citeseer, 2003.

[39] R. Xu and U. Ozguner. Sliding mode control of a quadrotor helicopter. In *Decision and Control, 2006 45th IEEE Conference on*, pages 4957–4962. IEEE, 2006.

[40] Y. Niu, D. WC Ho, and J. Lam. Robust integral sliding mode control for uncertain stochastic systems with time-varying delay. *Automatica*, 41(5):873–880, 2005.

[41] B. Smith, W. Schrenk, W. Gass, and Y. Shtessel. Sliding mode control in a two-axis gimbal system. In *Aerospace Conference, 1999. Proceedings. 1999 IEEE*, volume 5, pages 457–470. IEEE, 1999.

[42] H. Lee and V. I. Utkin. Chattering suppression methods in sliding mode control systems. *Annual Reviews in Control*, 31(2):179–188, 2007.

[43] P. Kachroo and M. Tomizuka. Integral action for chattering reduction and error convergence in sliding mode control. In *American Control Conference, 1992*, pages 867–870. IEEE, 1992.

[44] H. Lee. *Chattering suppression in sliding mode control system.* PhD thesis, The Ohio State University, 2007.

[45] C. Knospe. Pid control. *IEEE Control Systems Magazine*, 26(1):30–31, 2006.

[46] W. Ji, Q. Li, B. Xu, J.-J. Tu, and D.-A. Zhao. Cascade servo control for los stabilization of opto-electronic tracking platform—design and self-tuning. In *Information and Automation, 2009. ICIA'09. International Conference on*, pages 1034–1039. IEEE, 2009.

[47] A. Pisano, A. Davila, L. Fridman, and E. Usai. Cascade control of pm dc drives via second-order sliding-mode technique. *Industrial Electronics, IEEE Transactions on*, 55(11):3846–3854, 2008.

[48] T. Blanchett, G. Kember, and R. Dubay. Pid gain scheduling using fuzzy logic. *ISA transactions*, 39(3):317–325, 2000.

[49] T.-Y. Kuc and W.-G. Han. An adaptive pid learning control of robot manipulators. *Automatica*, 36(5):717–725, 2000.

[50] D. J. Purdy. Main battle bank stabilisation ratio enhancement using hull rate feedforward. *Journal of Battlefield Technology*, 1(2):5–9, 1998.

[51] C. J. Kempf and S. Kobayashi. Disturbance observer and feedforward design for a high-speed direct-drive positioning table. *Control Systems Technology, IEEE Transactions on*, 7(5):513–526, 1999.

[52] Y. F. Xu, Z. Y. Zhang, K. Li, and M. K. He. Study of control algorithm for indirect stabilized optical seeker. *Applied Mechanics and Materials*, 44:4053–4057, 2011.

[53] M. R. Mataušek and T. B. Šekara. Pid controller frequency-domain tuning for stable, integrating and unstable processes, including dead-time. *Journal of Process Control*, 21(1):17–27, 2011.

[54] O. Yaniv and M. Nagurka. Design of pid controllers satisfying gain margin and sensitivity constraints on a set of plants. *Automatica*, 40(1):111–116, 2004.

[55] T. Hägglund. Signal filtering in pid control. In *IFAC Conference on Advances in PID Control, Brescia, Italy*, 2012.

[56] P. Schmidt and T. Rehm. Notch filter tuning for resonant frequency reduction in dual inertia systems. In *Industry Applications Conference, 1999. Thirty-Fourth IAS Annual Meeting. Conference Record of the 1999 IEEE*, volume 3, pages 1730–1734. IEEE, 1999.

[57] R. Dhaouadi, K. Kubo, and M. Tobise. Analysis and compensation of speed drive systems with torsional loads. *Industry Applications, IEEE Transactions on*, 30(3):760–766, 1994.

[58] M. Nordin and P.-O. Gutman. Nonlinear speed control of elastic systems with backlash. In *Decision and Control, 2000. Proceedings of the 39th IEEE Conference on*, volume 4, pages 4060–4065. IEEE, 2000.

[59] D. Gebler and J. Holtz. Identification and compensation of gear backlash without output position sensor in high-precision servo systems. In *Industrial Electronics Society, 1998. IECON'98. Proceedings of the 24th Annual Conference of the IEEE*, volume 2, pages 662–666. IEEE, 1998.

[60] J. O. Jang, M. K. Son, and H. T. Chung. Friction and output backlash compensation of systems using neural network and fuzzy logic. In *American Control Conference, 2004. Proceedings of the 2004*, volume 2, pages 1758–1763. IEEE, 2004.

[61] S. E. Modeling and compensation of friction in high performance motion platforms. Master's thesis, Middle East Technical University, 2013.

[62] F. Al-Bender, V. Lampaert, and J. Swevers. A novel generic model at asperity level for dry friction force dynamics. *Tribology Letters*, 16(1-2):81–93, 2004.

[63] L. Freidovich, A. Robertsson, A. Shiriaev, and R. Johansson. Lugre-model-based friction compensation. *Control Systems Technology, IEEE Transactions on*, 18(1):194–200, 2010.

[64] L. Lu, B. Yao, Q. Wang, and Z. Chen. Adaptive robust control of linear motor systems with dynamic friction compensation using modified lugre model. In *Advanced Intelligent Mechatronics, 2008. AIM 2008. IEEE/ASME International Conference on*, pages 961–966. IEEE, 2008.

[65] Y. Zhu and P. R. Pagilla. Static and dynamic friction compensation in trajectory tracking control of robots. In *Robotics and Automation, 2002. Proceedings. ICRA'02. IEEE International Conference on*, volume 3, pages 2644–2649. IEEE, 2002.

[66] V. Lampaert. *Modelling and control of dry sliding friction in mechanical systems*. PhD thesis, Katholieke University of Leuven, 2003.

[67] G. Morel, K. Iagnemma, and S. Dubowsky. The precise control of manipulators with high joint-friction using base force/torque sensing. *Automatica*, 36(7):931–941, 2000.

[68] L. Le Tien, A. Albu-Schaaffer, A. De Luca, and G. Hirzinger. Friction observer and compensation for control of robots with joint torque measurement. In *Intelligent Robots and Systems, 2008. IROS 2008. IEEE/RSJ International Conference on*, pages 3789–3795. IEEE, 2008.

[69] A. A. Pervozvanski and C. Canudas-de Wit. Asymptotic analysis of the dither effect in systems with friction. *Automatica*, 38(1):105–113, 2002.

[70] N. E. Leonard and P. S. Krishnaprasad. Adaptive friction compensation for bi-directional low-velocity position tracking. In *Decision and Control, 1992., Proceedings of the 31st IEEE Conference on*, pages 267–273. IEEE, 1992.

[71] A. Voda and L. Ravanbod-Shirazi. High performance position tracking with friction compensation for an electro-pneumatical actuator. *Journal of Control Engineering and Applied Informatics*, 6(2):15–33, 2004.

[72] S. Huang and K. K. Tan. Intelligent friction modeling and compensation using neural network approximations. *Industrial Electronics, IEEE Transactions on*, 59(8):3342–3349, 2012.

[73] H. Du and S. S. Nair. Low velocity friction compensation. *Control Systems, IEEE*, 18(2):61–69, 1998.

[74] R. R. Selmic, V. V. Phoha, and F. L. Lewis. Intelligent compensation of actuator nonlinearities. In *Decision and Control, 2003. Proceedings. 42nd IEEE Conference on*, volume 4, pages 4327–4332. IEEE, 2003.

[75] R. R. Selmic and F. L. Lewis. Neural-network approximation of piecewise continuous functions: application to friction compensation. *Neural Networks, IEEE Transactions on*, 13(3):745–751, 2002.

[76] L. R. Ray, A. Ramasubramanian, and J. Townsend. Adaptive friction compensation using extended kalman–bucy filter friction estimation. *Control Engineering Practice*, 9(2):169–179, 2001.

[77] A. Ramasubramanian and L. R. Ray. Comparison of ekbf-based and classical friction compensation. *Journal of Dynamic Systems, Measurement, and Control*, 129(2):236–242, 2007.

[78] N. Mallon, N. van de Wouw, D. Putra, and H. Nijmeijer. Friction compensation in a controlled one-link robot using a reduced-order observer. *Control Systems Technology, IEEE Transactions on*, 14(2):374–383, 2006.

[79] B. Lee. Review of the present status of optical fiber sensors. *Optical Fiber Technology*, 9(2):57–79, 2003.

[80] O. J. Woodman. An introduction to inertial navigation. *University of Cambridge, Computer Laboratory, Tech. Rep. UCAMCL-TR-696*, 14:15, 2007.

[81] J. Skaloud, A. Bruton, and K. Schwarz. Detection and filtering of short-term ($1/f\gamma$) noise in inertial sensors. *Navigation*, 46(2):97–107, 1999.

[82] Y. Pu, N. Jiangfan, and L. Xiao. The design of a kind of multi-wavelet signal

filtering algorithm and its application to precision optical tracking servo system. *Journal of Chemical & Pharmaceutical Research*, 5(9), 2013.

[83] M. Ben, W. J. Wei, W. J. Tong, and Z. X. Mei. Mems gyro denoising based on second generation wavelet transform. In *Pervasive Computing Signal Processing and Applications (PCSPA), 2010 First International Conference on*, pages 255–258. IEEE, 2010.

[84] M. C. Algrain and D. E. Ehlers. Suppression of gyroscope noise effects in pointing and tracking systems. In *SPIE's International Symposium on Optical Engineering and Photonics in Aerospace Sensing*, pages 402–413. International Society for Optics and Photonics, 1994.

[85] R. Peesapati, S. L. Sabat, K. Karthik, J. Nayak, and N. Giribabu. Efficient hybrid kalman filter for denoising fiber optic gyroscope signal. *Optik-International Journal for Light and Electron Optics*, 124(20):4549–4556, 2013.

[86] H. Chang, L. Xue, W. Qin, G. Yuan, and W. Yuan. An integrated mems gyroscope array with higher accuracy output. *Sensors*, 8(4):2886–2899, 2008.

[87] C. Kownacki. Optimization approach to adapt kalman filters for the real-time application of accelerometer and gyroscope signals' filtering. *Digital Signal Processing*, 21(1):131–140, 2011.

[88] D. Simon. *Optimal state estimation: Kalman, H infinity, and nonlinear approaches*. John Wiley & Sons, 2006.

[89] J. Kim, Y. Kim, and S. Kim. An accurate localization for mobile robot using extended kalman filter and sensor fusion. In *Neural Networks, 2008. IJCNN 2008.(IEEE World Congress on Computational Intelligence). IEEE International Joint Conference on*, pages 2928–2933. IEEE, 2008.

[90] J. Bijker and W. Steyn. Kalman filter configurations for a low-cost loosely integrated inertial navigation system on an airship. *Control Engineering Practice*, 16(12):1509–1518, 2008.

[91] M. L. Anjum, J. Park, W. Hwang, H.-i. Kwon, J.-h. Kim, C. Lee, K.-s. Kim, and D.-i. Cho. Sensor data fusion using unscented kalman filter for accurate localization of mobile robots. In *Control Automation and Systems (ICCAS), 2010 International Conference on*, pages 947–952. IEEE, 2010.

[92] E.-H. Shin and N. El-Sheimy. An unscented kalman filter for in-motion alignment of low-cost imus. In *Position Location and Navigation Symposium, 2004. PLANS 2004*, pages 273–279. IEEE, 2004.

[93] J. Walters-Williams and Y. Li. Comparison of extended and unscented kalman filters applied to eeg signals. In *Complex Medical Engineering (CME), 2010 IEEE/ICME International Conference on*, pages 45–51. IEEE, 2010.

[94] R. Van Der Merwe, E. A. Wan, S. Julier, et al. Sigma-point kalman filters for nonlinear estimation and sensor-fusion: Applications to integrated navigation. In *Proceedings of the AIAA Guidance, Navigation & Control Conference*, pages

16–19. AIAA, 2004.

[95] Y. Duan and K. Jin. Digital controller design for switchmode power converters. In *Applied Power Electronics Conference and Exposition, 1999. APEC'99. Fourteenth Annual*, volume 2, pages 967–973. IEEE, 1999.

[96] E. Ari and E. Kocaoglan. Yuksek basarimli stabilize bir platformun kontrolü. In *Otomatik Kontrol Turk Milli Komitesi Ulusal Toplantisi Bildiri Kitabi*, pages 874–879, 2012.

[97] Y. Nakayama, K. Fujikawa, and H. Kobayashi. A torque control method of three-inertia torsional system with backlash. In *Advanced Motion Control, 2000. Proceedings. 6th International Workshop on*, pages 193–198. IEEE, 2000.

[98] G. Zhang and J. Furusho. Vibration control of three-inertia system. In *Industrial Electronics Society, 1999. IECON'99 Proceedings. The 25th Annual Conference of the IEEE*, volume 3, pages 1045–1050. IEEE, 1999.